ISSP

ACTIVITY REPORT OF SYNCHROTRON RADIATION LABORATORY

2016

Activity Report2016

TABLE OF CONTENTS

1) CO$_2$ HYDROGENATION ON THE Zn-DEPOSITED Cu(997) SURFACE STUDIED BY AMBIENT-PRESSURE X-RAY PHOTOELECTRON SPECTROSCOPY

Takanori Koitaya, Susumu Yamamoto, Yuichiro Shiozawa, Yuki Yoshikura, Masahiro Hasegawa, Jiayi Tang, Kaori Takeuchi, Kozo Mukai, Shinya Yoshimoto, Iwao Matsuda, and Jun Yoshinobu

2) Operando photoelectron nano-spectroscopy of energy efficient devices, power generation devices and energy storage devices using 3D-Nano-ESCA

Masaharu Oshima and Naoka Nagamura

3) DEVELOPMENT OF A SOFT X-RAY PHASE MODULATOR TO MEASURE THE ELEMENT-SPECIFIC COMPLEX PERMITTIVITY

Y. Kubota, Y. Hirata, J. Miyawaki, S. Yamamoto, H. Akai, R. Hobara, Sh. Yamamoto, K. Yamamoto, T. Someya, K. Takubo, Y. Yokoyama, M. Araki, M. Taguchi,Y. Harada, H. Wadati, M. Tsunoda, R. Kinjo, A. Kagamihata, T. Seike, M. Takeuchi,T. Tanaka, S. Shin, and I. Matsuda

4) High energy resolution resonant soft x-ray inelastic scattering study of LaCoO$_3$ thin films

Yuichi Yokoyama, Yuichi Yamasaki, Munetaka Taguchi, Yasuyuki Hirata, Kou Takubo, Jun Miyawaki, Yoshihisa Harada, Daisuke Asakura, Jun Fujioka, Masao Nakamura, Hiroshi Daimon, Masashi Kawasaki, Yoshinori Tokura, Hiroki Wadati

5) PEUCULIAR INTERFACIAL DYNAMICS OF DIRAC ELECTRON SYSTEM

Hirokazu Fukidome, Takashi Someya, Susumu Yamamoto, Iwao Matsuda

6) DYNAMICS OF PHOTOEXCITED CARRIERS AT ORGANIC-OXIDE INTERFACE

Kenichi Ozawa, Susumu Yamamoto, Ro-Ya Liu, Yuto Natsui, Naoya Terashima, Hiroo Kato and Iwao Matsuda

7) TIME RESOLVED X-RAY MAGNETO CIRCULAR DICHROISM OF FePt AND RESONANT SOFT X-RAY SCATTERING OF $IrTe_2$

Kou Takubo, Kohei Yamamoto, Yasuyuki Hirata, Yuichi Yokoyama, and Hiroki Wadati

8) RESONANT INELASTIC X-RAY SCATTERING STUDY ON BI2223 SUPERCONDUCTORS

H. Wang, J. Miyawaki, K. Ishii, T. Tohyama, S. Adachi, T. Watanabe, S. Shin, and Y. Harada

9) INVESTIGATING THE ELECTRONIC STRUCTURE OF THE NITROGENASE ENZYME BY 2P3D RIXS

Benjamin E. Van Kuiken, Anselm W. Hahn, Serena DeBeer, Yi-Tao Cui, Jun Miyawaki, Yoshihisa Harada

10) ELECTRONIC STATES REVEAL THE FUNCTION OF WATER ENCAPSULATED IN NANO-SPACES: SOFT X-RAY ABSORPTION/EMISSION STUDY

K. Yamazoe, D. Murakami, J. Miyawaki, Y.-T. Cui, M. Tanaka and Y. Harada

11) Study on electronic structure of Prussian blue analogues controlled by molecular adsorption

Takanobu Inoue, Jun Miyawaki, Yi-Tao Cui, Hiroko Tokoro, Yusuke Nakagawa, Shin-ichi Okoshi, Yoshihisa Harada

12) CHARGE EXCITATIONS RELATED TO CHARGE ORDER IN HOLE-DOPED CUPRATE SUPERCONDUCTORS

Kenji Ishii, Shun Asano, Masaki Fujita, Shuichi Wakimoto, Jun Miyawaki, Yoshihsa Harada

13) Ni $L_{2,3}$-edge operando soft X-ray absorption spectroscopy of $LiNi_{0.5}Mn_{1.5}O_4$ cathode for Li-ion battery

Daisuke Asakura, Takaaki Sudayama, Hirofumi Matsuda, Jun Miyawaki, Yoshihisa Harada, and Eiji Hosono

14) MAGNETIC FIELD DEPENDENCE OF RESONANT INELASTIC SOFT X-RAY SCATTERING OF MN_2VAL HEUSLER ALLOY WITH HALF METAL-TYPE ELECTRONIC STATE

Rie Y. Umetsu, Hidenori Fujiwara, Jun Miyawaki, Kodai Nagai, Yasuhiro Nakatani and Shigemasa Suga

15) DUAL GATE GRAPHENE TRANSISTOR TO REALIZE PINCH-OFF FOR THE REALIZATION OF THZ OPERATION

Keiichi Omika, Masato Okada, Fuminori Mitsuhashi, Yasunori Tateno, Tsuyoshi Kouchi, Naoka Nagamura, Masato Kotsugi, Koji Horiba, Maki Suemitsu, Masaharu Oshima, Hirokazu Fukidome

16) High energy resolution resonant soft x-ray inelastic scattering study of $LaCoO_3$ thin films

Yuichi Yokoyama, Yuichi Yamasaki, Munetaka Taguchi, Yasuyuki Hirata, Kou Takubo, Jun Miyawaki, Yoshihisa Harada, Daisuke Asakura, Jun Fujioka, Masao Nakamura, Hiroshi Daimon, Masashi Kawasaki, Yoshinori Tokura, Hiroki Wadati

17) Angular dependences of Fe $L_{2,3}$-edge soft X-ray absorption spectra for $LiFePO_4$ thin-film cathode for Li-ion battery

Daisuke Asakura, Takaaki Sudayama, Jun Miyawaki, Yoshihisa Harada, Hirofumi Matsuda, and Eiji Hosono

18) OBSERVATION OF PHOTO-INDUCED VALENCE TRANSITION IN $EuNi_2(Si_{1-x}Ge_x)_2$ WITH TIME-RESOLVED X-RAY ABSORPTION SPECTROSCOPY

Yasuyuki Hirata, Yuichi Yokoyama, Kohei Yamamoto, Kou Takubo, Hiroki Wadati, Kojiro Mimura

19) ANALYSIS OF STRUCTURES AND ELECTRONIC STATES BY MICROSCOPIC HIGH ENERGY RESOLUTION PHOTOELECTRON DIFFRACTION

Hiroshi Daimon, Hiroki Momono, Yusuke Hashimoto, Shun Fukami, Yudai Higa, Xin Liang Tan, Hiroyuki Matsuda, Munetaka Taguchi

20) CARBONATE IONS STUDIED IN HIGH-RESOLUTION RIXS

Victor Ekholm, Minjie Dong, Johan Gråsjö, Jun Miyawaki, Yoshihisa Harada, Jan-Erik Rubensson

21) Unraveling the synergic effect between Ni and Mn during the water oxidation reaction of nickel and manganese-based oxides by 2p3d RIXS

M. al Samarai, A. Hahn, O. Rüdiger, J. Miyawaki, Y. Harada, S. DeBeer

22) Time-resolved X-ray photoemission study on the WSe_2 surfaces

Ro-Ya Liu, Kenichi Ozawa, Naoya Terashima, Yuto Natsui, Baojie Feng, Suguru Ito, Wei-Chuan Chen, Cheng-Maw Cheng, Susumu Yamamoto, Tai-Chang Chiang, Iwao Matsuda

Preface

The Synchrotron Radiation Laboratory (SRL) in Institute for Solid State Physics (ISSP) has been taking part in the Synchrotron Radiation Research Organization (SRRO) of the University of Tokyo since 2005 and operating a new beamline (BL07LSU) at the SPring-8 and experimental apparatuses in soft X-ray region. The beamline has a 27m-long polarization-controlled undulator and a monochromator covering the photon energy range from 250 eV to 2 keV, which was fully opened to users since 2009. The members of solid state spectroscopy group of SRL play an essential role to promote advanced materials sciences utilizing high brilliance SR from the new undulator. In FY 2010, they have succeeded to measure time-resolved photoelectron spectroscopy of the surface photovoltage in Si surface with the time-resolution of 30 ps by utilizing the time-structure of synchrotron radiation and an ultra-fast laser. In FYs 2011 and 2012, energy resolution of soft X-ray emission spectroscopy becomes 10,000 and the spatial resolution of the scanning photoelectron microscope (3D nano-ESCA) is better than 70 nm. In 2014, they succeeded to operate the undulator to use the circular and parallel polarization light. The first aims of BL07LSU have been achieved already. The SRL-ISSP and SRRO contribute the cuttingedge basic sciences and the applied sciences using synchrotron radiation.

June 2017

<div align="right">

Shin Shik
Director of SRL-ISSP

</div>

1. Status of Beamline BL07LSU at SPring-8

The University-of-Tokyo high-brilliance synchrotron soft X-ray outstation beamline BL07LSU at SPring-8 has been maintained by the permanent staff members with adjuncts for user operations. A scientific aim of the beamline is to promote advanced spectroscopy for solid state and soft (including bio) materials. There are currently three regular endstations: time-resolved soft X-ray spectroscopy (TR-SX spectroscopy), 3D-scanning photoelectron microscope (3D nano-ESCA) and ultrahigh resolution soft X-ray emission spectroscopy (HORNET), along with a free port station for users who bring their own experimental apparatus.

The beamline BL07LSU is equipped with a segmented cross-type undulator. In 2016, polarization control of soft X-rays was performed by using phase shifter among the undulator segments. Circularly and linearly polarized soft X-rays at full energy range (250 – 2000 eV) have been available by tuning the permanent magnet type phase shifter. Moreover, fast circular polarization switching at a rate of 10 Hz and 13 Hz has been achieved around four incident photon energies, 440 eV, 573 eV, 639 eV and 709 eV.

At the beamline endstations, various scientific researches were carried out by both the laboratory staffs and general users (G-type application). Below are brief introduction of recent activities at each station.

(1) Time-Resolved soft X-ray spectroscopy station (TR-SX spectroscopy)

The station is to perform time-resolved photoemission spectroscopy experiments by synchronizing the high-brilliant soft x-ray and the ultra-short laser pulses. A new type of the electron spectrometer, the two-dimensional angle-resolved time-of-flight (ARTOF) analyzer, has been used for the efficient time-resolved measurements and a low temperature manipulator (15 K) is installed for extensive experiments for users. In 2016, high repetition rate (208 kHz) laser was installed and successfully synchronized with synchrotron soft X-rays. As a result, about 200 times higher detection efficiency of the time-resolved photoemission was realized compared with the previous experiments using 1 kHz repetition rate laser. The new system was provided for general user experiments from the 2016B cycle.

One of the most significant results in 2016 is the observation of change in the lifetime of photo carriers on the WSe_2 surface by electron or hole doping induced by an adsorbed atom or molecule. Carrier dynamics of high quality graphene was also studied for future applications as a material for terahertz laser devices operated at room

temperature.

Optical response of $SrTiO_3$ in $SrRuO_3/SrTiO_3$ hetero structure highly modulated by the thickness of the $SrRuO_3$ layer was reported. Time resolved photoemission results on a semiconductor surface at high temperature (880 °C) was realized by a technical development of the beamline.

(2) 3D-scanning photoelectron microscope (3D nano-ESCA)

An originally developed system "3D-nano-ESCA", which is a combination of soft X-ray scanning photoelectron emission microscopy (SPEM) and an angle-resolved electron analyzer, is installed in this station. Users can use 3D-nano-ESCA for sub-100 nm range microscopic 2D mapping and depth profile of the chemical structure of functional materials and devices.

In 2016, operando nano-spectroscopy was performed for GaN-HEMT devices as collaboration with Sumitomo Electric Industries, Ltd. and Tohoku University as part of the NEDO academic-industrial alliance project. Almost 10 V shift of the Ga 3d level observed by application of a voltage between the gate and the drain of the transistor was successfully explained by the presence of interface state with a doping level of $10^{13}\,cm^{-2}$ at the AlGaN/GaN interface, which was found to be the origin of the current collapse effects in GaN-HEMT. Moreover, reduction of the interface state was observed as a reduction of the Ga 3d peak shift by an epitaxial growth of a 3 nm SiN capping layer on the GaN surface. Another operando experiments were performed on a cathode material $LiNi_{0.5}Mn_{1.5}O_4$ of a Li-ion battery as collaboration with AIST. Changes in the local electronic structure of $LiNi_{1.5}Mn_{0.5}O_4$ after charging/discharging were analyzed to elucidate detailed charge redistribution upon Li-ion exertion/insertion.

(3) Ultra high-resolution soft X-ray emission spectroscopy (HORNET)

The station is for soft X-ray emission (or resonant inelastic X-ray scattering: RIXS) spectroscopy measurements with ultra high-resolution ($E/\Delta E > 10^4$) and under various environmental conditions (gas, liquid and solid). In 2016, an original position-correction program was developed and successfully installed in the system to realize continuous horizontal rotation of the spectrometer for angle (momentum) resolved experiments without losing scattered soft X-rays. In order to satisfy the increasing needs for humidity controlled experiments new liquid flow-through cell system with precise control of humidity and temperature was also installed. The number of applications to the HORNET station is still increasing. In 2016, 14 user experiments were accepted and performed. 12 applications among them are evenly shared by strongly correlated

materials and catalytic materials. The other two are solution chemistry. Intriguing results were obtained for the analyses of water; one is encapsulated water in polyelectrolyte brushes, and the other is water at the interface of diblock copolymer. In both cases RIXS spectra revealed quite different hydrogen bond structure of water from the bulk, successfully explaining functions of those polymer interfaces such as antifouling property and biocompatibility. As the first application of an angle resolved experiment, the CDW diffraction peak in the elastic part and a dispersive charge excitation band in the inelastic part was observed at O K-edge XAS pre-edge resonant excitation of Bi2223.

(4) Free-port station

The station is equipped with a focusing mirror chamber, and users can connect their own experimental chambers. In 2016, the following experiments were performed: time resolved soft X-ray diffraction of $La_{0.33}Sr_{0.67}FeO_3$ thin film; time resolved XMCD of magnetic thin films such as FePt or CoPt; resonant magneto-optical Kerr effects using polarization switching of the undulator; ambient-pressure X-ray photoemission spectroscopy of an Pd alloy upon H_2 adsorption and humidity dependence of water structure around the surface of diblock copolymer; two-dimensional photoemission spectroscopy with a display-type ellipsoidal mesh analyzer (DELMA) to electronically distinguish two different iron sites in Fe_3O_4 and to observe strong anisotropy in O K-edge resonant photoemission of Bi2212 and to elucidate two boron sites in B-doped diamond.

References:

[1] K. Ozawa, S. Yamamoto, R. Yukawa, R. Liu, M. Emori, K. Inoue, T. Higuchi, H. Sakama, K. Mase, I. Matsuda, J. Phys. Chem. **120**, 29283, 2016.

[2] Y. Kubota, K. Murata, J. Miyawaki, K. Ozawa, M. C. Onbasli, T. Shirasawa, B. Feng, Sh. Yamamoto, R-Y. Liu, S. Yamamoto, S. K. Mahatha, P. Sheverdyaeva, P. Moras, C. A. Ross, S. Suga, Y. Harada, K. L. Wang and I. Matsuda, J. Phys. Cond. Matt. **29**, 055002, 2016.

[3] E. Sakai, N. Nagamura, J. Liu, T. Hisatomi, T. Yamada, K. Domen and M. Oshima, Nanoscale Commun. **8**, 18893, 2016

[4] Y.Kubota, Sh.Yamamoto, T.Someya, Y.Hirata, K.Takubo, M.Araki, M.Fujisawa, K.Yamamoto, Y.Yokoyama, M.Taguchi, S.Yamamoto, M.Tsunoda, H.Wadati, A.Shin, I.Matsuda, J. Electron Spectrosc. Relat. Phenom., *in press.*

[5] R. Yukawa, S. Yamamoto, K. Akikubo, K. Takeuchi, K. Ozawa, H. Kumigashira, I. Matsuda, Adv. Mater. Int. **3**, 1600527, 2016.

[6] S. Fatale, S. Moser, J. Miyawaki, Y. Harada, and M. Grioni, Phys. Rev. B **94**, 195131, 2016.

[7] R. Yukawa, K. Ozawa, S. Yamamoto, H. Iwasawa, K. Shimada, Eike F. Schwier, K. Yoshimatsu, H. Kumigashira, H. Namatame, M. Taniguchi, and I. Matsuda, Phys. Rev. B **94**, 165313, 2016.

[8] G. Oyama, H. Kiuchi, S. C. Chung, Y. Harada, A. Yamada, J. Phys. Chem. C **120**, 23323, 2016.

[9] S. Toyoda, K. Fukuda, K. Horiba, M. Oshima, K. Kumagai, Y. Kumagai, F. Oba, Y. Uchimoto, E. Matsubara, Chem. Mater. **28**, 5784, 2016.

[10] T. Nomura, Y. Harada, H. Niwa, K. Ishii, M. Ishikado, S. Shamoto, I. Jarrige, Phys. Rev. B **94**, 135134, 2016

[11] T. Fransson, Y. Harada, N. Kosugi, N.A. Besley, B. Winter, J.J. Rehr, L.G.M. Pettersson, A. Nilsson, Chem. Rev. **116**, 7551, 2016.

[12] B. M. de Boisse, G. Liu, J. Ma, S.-i. Nishimura, S. C. Chung, H. Kikuchi, Y. Harada, J. Kikkawa, Y. Kobayashi, M. Okubo, A. Yamada, Nat. Commun. **7**, 11397, 2016.

[13] H. Kiuchi, R. Shibuya, T. Kondo, J. Nakamura, H. Niwa, J. Miyawaki, M. Kawai, M. Oshima, Y. Harada, Nanosc. Res. Lett. **11**, 127, 2016.

[14] 朝倉大輔、細野英司、原田慈久, 表面科学 **37**, 66, 2016.

[15] Y. Nanba, T. Iwao, B. M. de Boisse, W. Zhao, E. Hosono, D. Asakura, H. Niwa, H. Kiuchi, J. Miyawaki, Y. Harada, Chem. Mater. **28**, 1058, 2016.

[16] 山本　達、松田　巌, 表面科学 **37**, 9, 2016.

[17] K. Akikubo, I. Matsuda, D. Schmaus, G. Marcaud, R. Y. Liu, M. G. Silly, F. Sirotti, M. D'Angelo, Thin Solid Films **603**, 149, 2016.

[18] K. Ozawa, S. Yamamoto, R. Yukawa, K. Akikubo, M. Emori, H. Sakama, I. Matsuda, Organic Electronics **31**, 98, 2016.

[19] T. Koitaya, S. Yamamoto, Y. Shiozawa, K. Takeuchi, R-Y. Liu, K. Mukai, S. Yamamoto, K. Akikubo, I. Matsuda, J. Yoshinobu, Top. Catal. **59**, 526, 2016.

Status of spin- and angle-resolved photoelectron spectroscopy with laser light at Laser and Synchrotron Research Laboratory

Spin- and angle-resolved photoelectron spectroscopy (SARPES) is a powerful technique to investigate the spin-dependent electronic states in solids. For example, we will look at the exchange splitting of ferromagnetic materials. Also, recently, we have been intensively studied strongly spin-orbit coupled materials, such as Rashba spin-split systems and topological insulators. We developed a SARPES apparatus with a vacuum-ultraviolet laser at Laser and Synchrotron Research Laboratory in the Institute for Solid State Physics, named LOBSTER (Laser-Optics-Based Spin-vecTor Experimental Research) machine. The LOBSTER machine is utilized to obtain precise information on spin-dependent electronic structures near the Fermi level in solids. We started a project to construct the LOBSTER machine from FY 2014 and joint researches at this station have started from FY 2015.

Figure 1 represents an overview of the LOBSTER machine. The apparatus consists of an analysis chamber, a sample-bank chamber connected to a load-lock chamber, and a molecular beam epitaxy (MBE) chamber, which are kept in an ultra-high vacuum (UHV) environment and are connected with

Fig. 1. Overview of the LOBSTER machine developed at the Laser and Synchrotron Research Laboratory at the Institute for Solid State Physics [1].

each other via UHV gate valves. The hemispherical electron analyzer is a custom-made ScientaOmicron DA30-L, modified to attach the very-low-energy-electron-diffraction type spin detectors. The electrons are excited by 6.994-eV photons, yielded by 6th harmonic of a Nd:YVO$_4$ quasi-continuous wave laser with repetition rate of 120 MHz. A helium discharge lamp (VG Scienta, VUV5000) is also available as a photon source. At the MBE chamber, samples can be heated by a direct current heating or electron bombardment. The surface evaluating and preparing instruments, such as evaporators, low energy electron diffraction, reflection high energy electron diffraction, sputter-gun and quartz microbalance, can be installed. At the carousel chamber, 16 samples can be stocked in the UHV environment.

Figure 2 shows Fermi edges taken from a gold (Au) thick film recorded with the ARPES and SARPES modes. The sample temperature was set to 9 K. The spectrum was taken with the analyzer pass energies of 1 and 2 eV for ARPES and SARPES modes, respectively. The sizes of an entrance slit and an exit aperture were set to 0.2 mm and 0.2×0.5 mm^2, respectively. The spectra were fitted with the Fermi distribution function. From the fitting, the energy resolutions were estimated to be 600 μeV for the ARPES mode and 1.7 meV for the SARPES mode. The new spectrometer can provide high-resolution spin-integrated and spin-resolved photoemission spectra in various types of solids, such as strongly correlated materials.

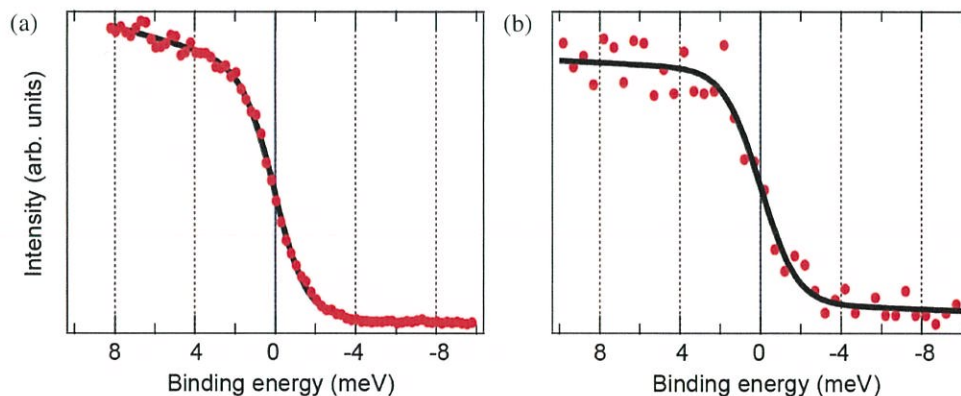Fig. 2 The Fermi edges (circle plots) of a gold thick film recorded in (a) ARPES mode and (b) SARPES mode. Solid curves represent fitting results with the Fermi–Dirac distribution function and a polynomial background [1].

Reference

[1] K. Yaji, A. Harasawa, K. Kuroda, S. Toyohisa, M. Nakayama, Y. Ishida, A. Fukushima, S. Watanabe, C.-T. Chen, F. Komori and S. Shin, Rev. Sci. Instrum. **87**, 053111 (2016).

3. Workshops & Meetings

ISSP workshop "Opening Interdisciplinary Fields of Material Science and Life Science"

Date: March 7, 2017
Place: Lecture Room (A632), 6th Floor, ISSP, the University of Tokyo

The Synchrotron Radiation Research Organization (SRRO) at The University of Tokyo has been at the forefront of the leading edge of synchrotron radiation science and technology over the last 10 years. On December 2016, the SRRO was renewed as an international base of excellence for the interdisciplinary field of synchrotron radiation science, aiming at the creation of a new discipline named "Electronic-structure-based life science," where multiscale/hierarchical complex structures involving the transport/reaction of atoms/ions in biomaterials and bioinspired materials have become a new subject in materials science.

In the 21st century, the development of synchrotron X-ray spectroscopy and diffraction techniques is quite remarkable and has realized "operando electronic structure analyses" for a variety of functional materials. With the forthcoming new synchrotron light source, we could even attain nanoscale focusing and various spectroscopies with a much higher energy resolution, permitting more precise and versatile measurements to probe the physical properties of materials. This workshop was held to effectively and promptly advance "Electronic-structure-based life science" by overviewing the future prospects of synchrotron science, visualizing the achievements and unknowns of protein science, and focusing on the development and analyses of bioinspired materials as one of the goals of the new discipline. Researchers from a broad range of scientific fields at the workshop intensively discussed the interface between materials science and life science, which will continue and contribute to maximize the synergy between materials science and bioscience.

ISSP, The University of Tokyo, Organizing committee of the ISSP workshop
Iwao MATSUDA, Yoshihisa HARADA, Shik SHIN
Fumio KOMORI, Hiroki WADATI

Program

10:20- **Introduction**
Iwao Matsuda (ISSP, the University of Tokyo)

10:25- **Opening Address**
Masashi Takigawa (ISSP, the University of Tokyo)

10:30- **Guest Address**
Masaki Takata (Tohoku University)

10:35- **Building a New Range of the State of the Art in Photon Science by SLiT-J**
Masaki Takata (Tohoku University)

11:05-   **Large-scale first-principles simulation for functional material research**
Osamu Sugino (ISSP, the University of Tokyo)

11:35-   **A Prospective of X-ray Phase Imaging**
Atsushi Momose (IMRAM, Tohoku Univ., JST-ERATO)

12:05-   **Lunch**

13:10-   **Iron-sulfur cluster biogenesis**
Takashi Fujishiro (Saitama University)

13:40-   **Molecular Mechanism of NO Reduction in Biological System**
Yoshitsugu Shiro (University of Hyogo/ RIKEN SPring-8 Center)

14:10-   **Current possibility of quantum chemical calculations for ion pump proteins**
Naoki Tsunekawa (IMCB, Univ. of Tokyo)

14:40-   **Mechanism of light-induced water-splitting in photosystem II of photosynthesis**
Jian-Ren Shen (Research Institute for Interdisciplinary Research)

15:10-   **Coffee Break**

15:25-   **Hierarchical Structures and Functions of Complex, Biological Interfaces**
Motomu Tanaka (Heidelberg University, Kyoto University)

15:55-   **Characterizing Self-Assembled Nanoparticles in Drug Delivery**
Kazuo Sakurai (University of Kitakyushu)

16:25-   **Biointerfaces explored by scanning probe microscopy and nanophotonics**
Tomohiro Hayashi (Tokyo Institute of Technology)

16:55-   **Nanostructured biointerface regulates protein adsorption and cell adhesion**
Madoka Takai (The University of Tokyo)

17:25-   **Closing Address**
Chikashi Toyoshima (The University of Tokyo)

3. Workshops & Meetings

ISSP workshop "*Origins of material functions elucidated by SPring-8 BL07LSU*"

Date: 2017/3/8(Wed)

Place: Lecture Room (A632), 6th Floor, ISSP, the University of Tokyo

Synchrotron radiation laboratory has a Harima branch to maintain and develop a high-brilliance soft X-ray beamline BL07LSU at SPring-8. There we are performing time-resolved, spatial-resolved and energy-resolved soft X-ray spectroscopy to study electronic states and their dynamics of new materials. In this workshop, recent research activities at our beamline were reported and we discussed our new experimental techniques which will reveal the origins of material functions. The speakers talked about their recent results from each end station (time-resolved spectroscopy, 3D nano-ESCA, emission spectroscopy, and so on). There were two invited talks; one is about soft X-ray nanofocusing with ultraprecise mirrors, and the other is about nano-metric spin textures observed by coherent soft X-ray scattering. There were a lot of discussions for each talk, and we successfully started to obtain a clear vision about how we can elucidate the origins of material functions such as magnetism, chemical reaction, and biological systems. We also encouraged the young generation in this research field by awarding the best poster prizes to two graduate students.

Program

10:00- **Opening Address**   Akio Kimura (Hiroshima University, VSX Users' Organization)

10:05- **Guest Address**   Ryotaro Tanaka (Japan Synchrotron Radiation Research Institute)

10:10- **Introduction**   Takahisa Arima (The University of Tokyo)

10:20- **Observation of nontrivial magnetic structures and spin dynamics by using polarization switching**

          Yasuyuki Hirata (ISSP, the University of Tokyo)

10:50- **Understanding of biological functions by synchrotron radiation research**

          Shuya Fukai (The University of Tokyo)

11:20- **Soft X-ray Nanofocusing with Ultraprecise Mirror**

          Hidekazu Mimura (The University of Tokyo)

11:50- **Poster short presentation**

12:10- **lunch**

13:00- **Poster session**

14:30- **Operando nano-spectroscopy for energy efficient, power generation and energy storage devices**

          Masaharu Oshima (SRRO, the University of Tokyo)

15:00- **New Frontier of Catalysis Science Opened by Development and Synergy of Operando Soft X-ray Spectroscopies**

          Susumu Yamamoto (ISSP, the University of Tokyo)

15:30- **Nano-metric Spin Texture Observed via Coherent Soft X-ray Scattering**

          Yuichi Yamasaki (The University of Tokyo)

16:00- **Coffee Break**

16:20- **Time-resolved Photoelectron spectroscopy on 2D electron systems for developing high-speed photonic and electronic devices**

          Hirokazu Fukidome (Tohoku University)

16:40- **Weak Ferromagnetism in α-Fe$_2$O$_3$ studied by MCD in SX-RIXS**

          Jun Miyawaki (ISSP, the University of Tokyo)

17:00- **Analysis of Structures and Electronic States by Microscopic High-resolution Two-Dimensional Photoelectron Spectroscopy**

          Munetaka Taguchi (Nara Institute of Science and Technology)

17:20- **Closing Address**   Shik Shin (ISSP, the University of Tokyo)

4. Seminar

Date: April 4, 2016
Title: Angle-Resolved Photoemission Spectroscopy at Diamond Light Source,
the example of quasi-one dimensional $Tl_2Mo_6Se_6$
Speaker: Dr. Moritz Hoesch（Diamond Light Source）

(ISSP Lectures by Visiting Professors)
Date: April 21, 2016
Title: Exotic Properties in Single-Layer Materials
Speaker: Dr. CHIANG, Tai Chang（University of Illinois at Urbana-Champaign & ISSP）

(LASOR Seminar)
Date: May 23, 2016
Title: Fast photostriction in a silicon single-crystal
Speaker: Dr. Yoshihito Tanaka（Graduate School of Material Science, University of Hyogo）

(ISSP Colloquiums)
Date: May 26, 2016
Title: Charge density waves (CDWs) in single-layer, multi-layer, and bulk titanium
diselenide - dimensional/confinement effects and the physics of CDWs
Speaker: Dr. CHIANG Tai Chang（University of Illinois at Urbana-Champaign & ISSP）

Date: June 16, 2016
Title: Oxygen Reduction Reaction over Carbon Based Cathode Catalysts in Proton Exchange
Membrane Fuel Cells - Catalysis by N-dopded Carbon without Transition Metals?-
Speaker: Dr. Yuta Nabae
（Department of Materials Science and Engineering, Tokyo Institute of Technology）

(LASOR Seminar)
Date: June 23, 2016
Title: Development and application of novel tools to study aqueous solutions using electrons
Speaker: Dr. Hiroharu Yui（Tokyo University of Science）

Date: July 20, 2016
Title: Magnetization dynamics in ordered alloy systems and its application to spintronic devices
Speaker: Dr. Takeshi Seki（Institute for Materials Research, Tohoku University）

(LASOR Seminar)
Date: July 26, 2016
Title: Electromagnon resonance in terahertz region
Speaker: Dr. Youtarou Takahashi（School of Engineering, the University of Tokyo）

(ISSP Lectures by Visiting Professors)
Date: October 19, 2016
Title: Study on Assembly and Functionality of Electron-Proton-Correlated Molecular Layers
Speaker: Dr. Hiroyuki S. Kato (Osaka University Graduate School of Science & ISSP)

Date: November 2, 2016
Title: Development and current status of high-spatial
Speaker: Dr. Hideaki Iwasawa (Diamond Light Source)

Date: March 21, 2017
Title: Exploration of novel two-dimensional materials
Speaker: Dr. Baojie Feng (ISSP, the University of Tokyo)

CO$_2$ HYDROGENATION ON THE Zn-DEPOSITED Cu(997) SURFACE STUDIED BY AMBIENT-PRESSURE X-RAY PHOTOELECTRON SPECTROSCOPY

Takanori Koitaya, Susumu Yamamoto, Yuichiro Shiozawa, Yuki Yoshikura, Masahiro Hasegawa, Jiayi Tang, Kaori Takeuchi, Kozo Mukai, Shinya Yoshimoto, Iwao Matsuda, and Jun Yoshinobu

The Institute for Solid State Physics, The University of Tokyo

Activation and hydrogenation of carbon dioxide (CO$_2$) are important topics for the use of abundant CO$_2$ as a chemical feedstock [1]. One of the promising ways for CO$_2$ utilization is methanol synthesis on Cu/ZnO catalysts. Metallic copper in the catalysts is considered to be an active site for the methanol synthesis [2]. However, zinc oxide in the catalyst is not just a support for metallic copper particles, but acts as a promotor for methanol synthesis [3]. In order to understand the synergetic effect between Cu and ZnO, it is necessary to reveal the chemical states of both adsorbates and substrates *under the reaction conditions*.

In the methanol synthesis (CO$_2$ + 3H$_2$ $\rightarrow$ CH$_3$OH + H$_2$O) and simultaneous reverse water-gas shift reaction (CO$_2$ + H$_2$ $\rightarrow$ CO + H$_2$O), water is formed in addition to methanol and CO molecules. Hence, the effect of water should be taken into account for elucidation of reaction mechanism of the methanol synthesis. Recent studies under well-defined experimental conditions revealed the importance of water on the methanol synthesis; the reactivity is significantly enhanced when a small amount of water exists in the feed gas [4-7].

In this study, reaction of CO$_2$ with hydrogen and water on the Zn-deposited Cu(997) surface was studied by *operando* ambient-pressure X-ray photoelectron spectroscopy (AP-XPS). The aim of this study is to reveal the roles of Zn and water in the CO$_2$ reaction under well-defined conditions. We used a Zn-deposited Cu single crystal as a model catalytic system. In addition, gas composition was precisely controlled using high purity gases. The oxidation state of Zn-deposited Cu surfaces and the stability of reaction products depend strongly on gas composition and sample temperature.

The experiments were performed using an AP-XPS apparatus at SPring-8 BL07LSU. The details of the AP-XPS system were described elsewhere [8]. Briefly, AP-XPS was carried out using a differentially pumped electron analyzer (SPECS, PHOIBOS150 NAP) with an ambient-pressure gas cell. The gas cell is equipped in an analysis chamber (base pressure = 3 × 10^{-10} mbar). XPS measurements can be done both under UHV and in near-ambient pressure up to 20 mbar. For ambient-pressure experiments, it is quite important to reduce the amount of impurity in the gas cell and the feed gases. In addition to bake-out of the gas cell in UHV, a sample stage in the gas cell was outgassed by heating to 800 K. The CO$_2$ gas (original purity = 99.995%) was purified by freeze-pump-thaw cycles, and the H$_2$ gas (original purity = 99.99999%) was also further purified using a cold trap at liquid nitrogen temperature. The D$_2$O (original purity = 99.99%) was purified by freeze-pump-thaw cycles.

AP-XPS measurements were done in the presence of 0.8 mbar CO$_2$, 0.4 mbar H$_2$, and 0.05 mbar D$_2$O gases. The C 1s and Zn 2p$_{3/2}$ spectra on the Zn(0.25 ML)/Cu(997) surface as a function of sample temperature are shown in Figures 1(a) and (b). The peaks of carbonate (CO$_3$) and neutral-carbon contamination (C^0) species adsorbed on the surface were observed at 299 K under the ambient-pressure condition, whereas a peak at 293.5-294 eV was attributed to gas-phase CO$_2$ molecules. In addition to these peaks, a peak at ~285.5 eV is found at 340-393 K, which has slightly higher binding energy than the C^0 species. From the peak energy, this peak can be attributed to carbon singly bonded to oxygen (C-O). The C-O species might be assigned to contamination or produced methoxy which was also observed on the Zn-deposited Cu film under CO$_2$ and H$_2$O gases [9].

When the Zn/Cu(997) sample was heated to 393 K in the moist condition, the CO$_3$ peaks

decreased in intensity, and a peak at 289.0 eV was observed above 393 K. This peak is assigned to formate (HCOO) species produced via CO_2 hydrogenation. Note that formate was observed only when water was added to the CO_2 + H_2 feed gas in the present experimental conditions. Hence, we conclude that water plays a key role in the hydrogenation of CO_2 into adsorbed formate. The deposited Zn was partly oxidized under the reaction condition by adsorbed species such as atomic oxygen, hydroxyl and formate (Fig. 1(b)). In contrast, the deposited Zn was completely reduced at 473 K under 0.8 mbar CO_2 and 0.4 mbar H_2 dry gas mixture without water. Thus, the surface oxidation state is significantly affected by gas-phase water. On the other hand, oxidation of copper was not detected in the Cu 2p spectra, indicating that the copper substrate is metallic even under the ambient reaction conditions.

At hydrogen partial pressure of 0.4 mbar, equilibrium coverage of atomic hydrogen should be negligible because of very low sticking probability of H_2 on Cu surfaces [10]. On the other hand, dissociation of water into hydroxyl can occur on Cu surfaces even under the UHV condition when atomic oxygen exists on the surface [11]. The difference in reactivity between H_2 and water indicates that a reactant in the CO_2 hydrogenation, i.e., a source of hydrogen, is not atomic hydrogen but probably hydroxyl species. Hence, one possible role of added water is to provide hydroxyl species on the surface.
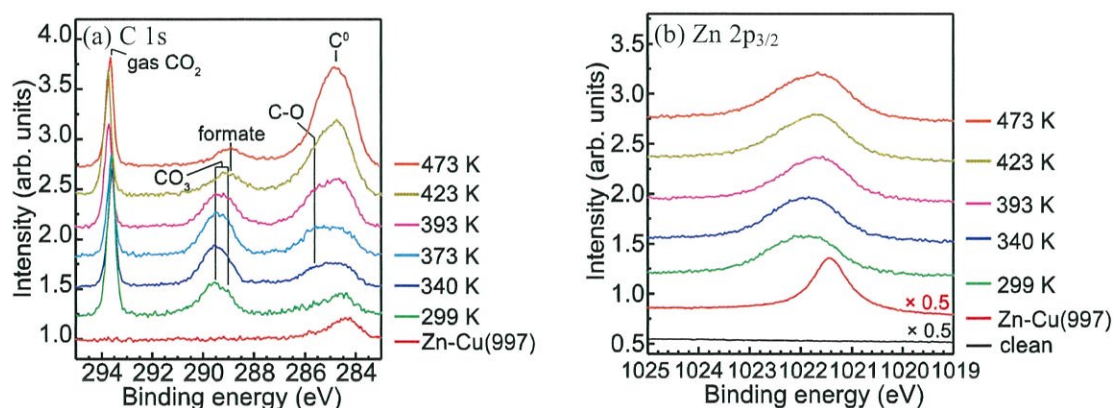

Figure 1. AP-XPS spectra of Zn(0.25 ML)/Cu(997) surface in the presence of 0.8 mbar CO_2, 0.4 mbar H_2, and 0.05 mbar D_2O: (a) C 1s ($h\nu$ = 630 eV) and (b) Zn $2p_{3/2}$ ($h\nu$ = 1100 eV). AP-XPS measurements were first performed at 299 K, then the sample was heated up to 473 K step by step under the ambient-pressure condition.

REFERENCES

[1] A. M. Appel *et al.*, Chem. Rev. **113**, 6621 (2013).

[2] N. Y. Topsøe and H. Topsøe, J. Mol. Catal. A **141**, 95 (1999).

[3] J. Nakamura, Y. Choi, and T. Fujitani, Top. Catal. **22**, 277 (2003).

[4] Y. F. Zhao, Y. Yang, C. Mims, C. H. F. Peden, J. Li, and D. H. Mei, J. Catal. **281**, 199 (2011).

[5] Y. Yang, C. A. Mims, R. S. Disselkamp, J. H. Kwak, C. H. F. Peden, and C. T. Campbell, J. Phys. Chem. C **114**, 17205 (2010).

[6] Y. Yang, C. A. Mims, D. H. Mei, C. H. F. Peden, and C. T. Campbell, J. Catal. **298**, 10 (2013).

[7] Y. Yang, D. H. Mei, C. H. F. Peden, C. T. Campbell, and C. A. Mims, ACS Catal. **5**, 7328 (2015).

[8] T. Koitaya *et al.*, Top. Catal. **59**, 526 (2016).

[9] X. Deng, A. Verdaguer, T. Herranz, C. Weis, H. Bluhm, and M. Salmeron, Langmuir **24**, 9474 (2008).

[10] L. Österlund, P. B. Rasmussen, P. Thostrup, E. Lægsgaard, I. Stensgaard, and F. Besenbacher, Phys. Rev. Lett. **86**, 460 (2001).

[11] Y. Q. Wang, L. F. Yan, and G. C. Wang, Phys. Chem. Chem. Phys. **17**, 8231 (2015).

Operando photoelectron nano-spectroscopy of energy efficient devices, power generation devices and energy storage devices using 3D-Nano-ESCA

[1]Masaharu Oshima and [2]Naoka Nagamura

[1]*Synchrotron Radiation Research Organization, The University of Tokyo, Tokyo, Japan,*

[2]*National Institute for Materials Science (NIMS), Tsukuba, Ibaraki, Japan*

We have developed soft X-ray scanning photoelectron emission microscopy (SPEM) with an angle-resolved electron analyzer (3D-nano-EASCA) with the spatial resolution of 70 nm [1] to investigate pin-point electronic structure in green nano-devices such as energy efficient devices like GaN HEMT, graphene FET and SiC MOSFET, power generation devices like fuel cells and photocatalysts for hydrogen generation, and energy storage devices like Li ion batteries (LIB). Furthermore, we modified 3D-nano-ESCA so that different voltages can be independently applied to five electrodes for gate, source, drain and ground in a sample holder connected to a semiconductor parameter analyzer.

The first example for energy efficient devices is GaN HEMT (High electron mobility transistor) which is expected as the next generation high-power high-frequency devices. This work has been done by Sumitomo Electric Co. and Tohoku University (Prof. Suemitsu and Prof. Fukidome) in collaboration with the University of Tokyo as the NEDO project. The *operando* nono-spectroscopy successfully revealed the mechanism of current collapse phenomena by analyzing Ga $2p$ photoelectron spectra in the channel region where the applied voltage is extended from the electrode. It is found that the current collapse may take place at the point where the local electric field is concentrated and surface states may trap electron carriers.

Furthermore, the nano-spectroscopy was applied to the SiC trench-MOSFET where one of the most important problems lies in the gate oxide/channel interface at the trench sidewall which is fabricated by reactive ion etching (RIE). This work was done in collaboration with Fuji Electric Co. and Tokyo City University (Prof. Nohira). The trench sidewall which was exposed by cleaving the trench structures with 0.6 μm width and 2 μm depth was analyzed by 3D-nano-ESCA to investigate chemical bondings and electronic structures (band bending), as shown in Fig. 1. [2] Based on these results, the RIE trench formation mechanism was discussed.

As for power generation devices, we have analyzed electronic structure of water splitting photocatalysts $La_2Ti_5CuS_5O_7$ (LTC) and $La_2Ti_5AgS_5O_7$ (LTA) as a p-type semiconductor photocathode generating H_2 gas in the Z-scheme photocatalysis. This work was done in collaboration with The University of Tokyo (Prof. Domen). It is revealed from Fig. 2 that shift of valence band spectra and core levels towards lower binding energy suggests successful hole doping probably into Cu $3d$ band by substituting Ti sites by Ga ions. [3]

Furthermore, ruthenen nano-sheet was analyzed by angle-resolved 3D-nano-ESCA in collaboration with Kyoto University (Prof. Matsubara). It is found that 3 ML ruthenen formed by reducing RuO_2 nano-sheet showed metallic behaviour, white 1 ML/2 ML ruthenen exhibited semiconducting behaviour with covalency. DFT calculation confirmed these findings by showing that AA stacking with coordination number 7 is more stable than AB stacking with coordination number 9. [4]

As for energy storage devices, we have also attempted to analyze local electronic structure of $LiCoO_2$ cathode materials for LIB after charging and discharging. This work has been done

DEVELOPMENT OF A SOFT X-RAY PHASE MODULATOR TO MEASURE THE ELEMENT-SPECIFIC COMPLEX PERMITTIVITY

Y. Kubota,[1] Y. Hirata,[1] J. Miyawaki,[1] S. Yamamoto,[1] H. Akai,[1] R. Hobara,[2] Sh. Yamamoto,[1] K. Yamamoto,[1] T. Someya,[1] K. Takubo,[1] Y. Yokoyama,[1] M. Araki,[1] M. Taguchi,[3] Y. Harada,[1] H. Wadati,[1] M. Tsunoda,[4] R. Kinjo,[5] A. Kagamihata,[5] T. Seike,[5] M. Takeuchi,[5] T. Tanaka,[5] S. Shin,[1] and I. Matsuda[1]

[1]*Institute for Solid State Physics, The University of Tokyo*
[2]*Department of Physics, The University of Tokyo*
[3]*Nara Institute of Science and Technology (NAIST)*
[4]*Department of Electronic Engineering, Tohoku University*
[5]*RIKEN SPring-8 Center*

Introduction

Permittivity is one of the most important quantities that characterize the material responses to external fields, such as electromagnetic waves. The determination of the permittivity of materials has been one of the highest priority tasks in science and technology. Its diagonal and off-diagonal components carry the non-magnetic and magnetic information regarding the response of the material, respectively, and it is the latter that has been significant in understanding spin polarization or magnetization. Their determination has been widely made using a probe light with a polarization modulation and the measurement of the magneto-optical effects. Such an experiment has been easily performed for visible light and hard X-rays [1, 2], but not for extreme extended-ultraviolet (EUV) ~ soft X-rays (SX) region because of the absorbance of light in matter. In this study, we developed a novel SX source for a segmented cross undulator enabling the polarization modulation of light to be performed continuously and magneto-optical measurements of a buried Fe nanofilm to be carried out at the Fe L-edge in the SX region. We succeeded in directly determining the complex components of the permittivity tensor.

Experimental

Continuous polarization modulation in the SX region was achieved from the segmented cross undulator, developed at SPring-8 BL07LSU [3]. The phase shifters control the phase retardation of the light from the undulators resulting in various polarized SX, furthermore, a continuous phase shift with a frequency p is obtained magnetically using an electromagnetic coil applied a sinusoidal alternating current (AC) [4]. The light polarization can be varied continuously from linear to right- or left-handed circular. When using this modulated beam in magneto-optical Kerr effect (MOKE) experiments, the ellipticity (η_K) appears in signals as the p component, whereas the $2p$ component depends on the Kerr rotation angle (θ_K). That is, by extracting the p and $2p$ components, η_K and θ_K are measurable simultaneously with high-sensitivity. A Ta (2 nm thick)/Cu (2 nm thick)/Fe (30 nm thick)/MgO heterostructure sample was used in the longitudinal MOKE (L-MOKE) experiment at room temperature. The Ta and Cu layers are capping layers to prevent the Fe layer from oxidizing. The incident angle of light onto the sample was about 80˚ with respect to the surface normal. Using a split-coil magnet, a magnetic field of strength ±0.3 T, under which the magnetization of the Fe nanofilm is saturated, was applied along the in-plane direction. Figure 1 shows the experimental set-up.

Results and discussion

We performed the simultaneous measurement of θ_K and η_K for the Fe nanofilm for the s-wave. The phase of the light polarization was modulated with settings the frequency p = 12.987 Hz.
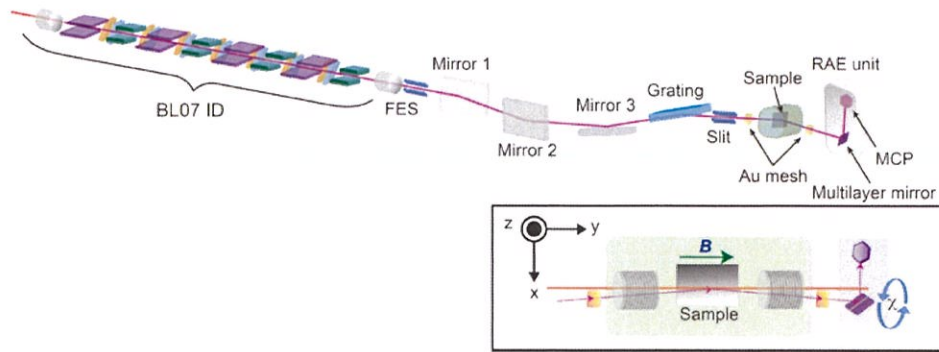
Fig. 1: Overview of the beamline at SPring-8 BL07LSU. A segmented cross-undulator (BL07 ID) consists of eight undulators and seven phase shifters. FES represents a front-end slit. The intensity of incident light and reflected light by a sample are monitored by two Au mesh. Inset shows a detail of the measurement chamber and the RAE unit.

Fine spectral features can be observed in the θ_K and η_K signals. Moreover, their spectra appear as derivatives of each other, which is consistent with the relationship expressed by the Kramers–Kronig relations [5].

The off-diagonal component of the permittivity tensor, which carries magneto-optical information, was determined using the experimental results of θ_K and η_K. For the first time, this result indicates that the present method is reliable in determining the off-diagonal component in the SX region.

Conclusion

We have described the development of a SX magneto-optical spectroscope that uses a new SX source from the segmented cross undulator at SPring-8 BL07LSU. This method offers various advantages for material science and technology. A complete dataset of real and imaginary parts of the complex permittivity tensor can be determined simultaneously with high-sensitivity. Thus, faint magnetic signals are able to be detected, moreover, the datasets are self-consistent with the Kramers–Kronig relations. This provides benefits when investigating new magnetic materials. By tuning the probe photon energy at the absorption edge, the data have element-selectivity, which is suitable for studying multi-element samples.

Acknowledgement

References

[1] K. Sato, Jpn. J. Appl. Phys. **20**, 2403 (1981).
[2] M. Suzuki *et al.*, Jpn. J. Appl. Phys. **37**, L1488 (1998).
[3] S. Yamamoto *et al.*, J. Synchrotron Radiat. **21**, 352 (2014).
[4] I. Matsuda *et al.*, Nucl. Instruments Methods Phys. Res. Sect. A Accel. Spectrometers, Detect. Assoc. Equip. **767**, 296 (2014).
[5] P. M. Oppeneer, in *Handbook of Magnetic Materials*, edited by K. H. J. Buschow (Elsevier, Amsterdam, 2001), Vol. 13.

High energy resolution resonant soft x-ray inelastic scattering study of LaCoO₃ thin films

Yuichi Yokoyama[A,B], Yuichi Yamasaki[C,D], Munetaka Taguchi[E], Yasuyuki Hirata[A,B], Kou Takubo[A], Jun Miyawaki[A], Yoshihisa Harada[A], Daisuke Asakura[F], Jun Fujioka[C], Masao Nakamura[D], Hiroshi Daimon[E], Masashi Kawasaki[C,D], Yoshinori Tokura[C,D], Hiroki Wadati[A,B]

[A]Synchrotron Radiation Laboratory, The Institute for Solid State Physics, The University of TokyoDepartment of Physics, [B]University of Tokyo, Tokyo 113-0033, Japan, [C]Department of Applied Physics and Quantum-Phase Electronics Center (QPEC), University of Tokyo, Hongo, Tokyo 113-8656, Japan, [D]RIKEN Center for Emergent Matter Science (CEMS), Wako 351-0198, Japan, [E]Nara Institute of Science and Technology (NAIST), 89165, Takayama, Ikoma, Nara 630-0192, Japan, [F]Research Institute for Energy Conservation, National institute of Advance Industrial Science and Technology (AIST), Umezono 1-1-1, Tsukuba 305-8568, Japan

Perovskite LaCoO₃ with Co³⁺ ($3d^6$) ion is considered to take high-spin (HS) state with $t_{2g}^4 e_g^2$, intermediate-spin (IS) state with $t_{2g}^5 e_g^1$, and low-spin (LS) state with t_{2g}^6. Since the energy difference between the HS and the LS state is the order of $k_B T$, the spin states of LaCoO₃ may change by external stimuli such as temperature or strain. In bulk single crystals, LaCoO₃ is a nonmagnetic semiconductor at the lowest temperatures, indicating the LS state and the population of the HS state gradually increases as the temperature increases [1]. On the other hand, LaCoO₃ epitaxial thin films are not nonmagnetic even at the lowest temperature. For example, LaCoO₃ thin films grown on (LaAlO₃)₀.₃ (SrAl₀.₅Ta₀.₅O₃)₀.₇ : LSAT(110) substrates exhibits spontaneous magnetization (T_c = 94 K), meaning that the spin state changes from LS state to IS and/or HS by epitaxial strain [2-3]. In LaCoO₃ thin films grown on LSAT(111), another type of spin ordering was reported [4]. Therefore, it is considered that the spin states of LaCoO₃ thin films can be controlled by the orientation of substrates. Then, we investigated the electronic structures directry by high energy resolution resonant soft x-ray inelastic scattering (RIXS).

The LaCoO₃ epitaxial thin films with 30 nm thickness on LSAT(110) and LSAT(111) were fabricated by pulsed laser deposition technique. The tensile strain of the thin films grown on LSAT(110) and LSAT(111) is ~ 1% and ~ 0.5%, respectively. The RIXS measurements of LaCoO₃ thin films and bulk single crystal were performed at BL07LSU HORNET, SPring-8. We used near Co L_3 edge (around 780 eV) as the excitation energy and performed the measurements at 300 K and 40 K. The energy resolution is approximately 300 meV. The incident angle of x-ray is 45°
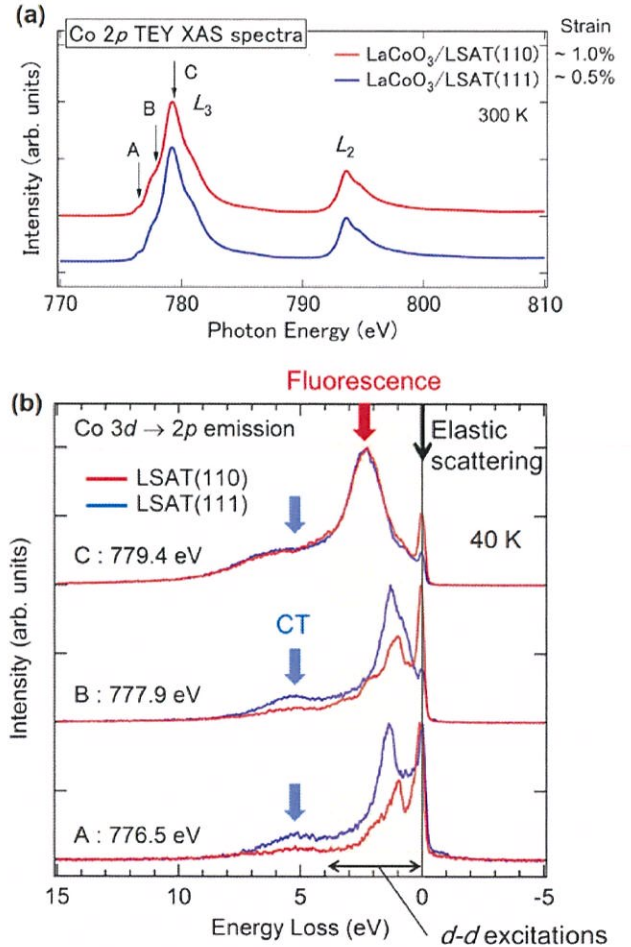

FIG. 1. (a) Co 2p TEY XAS spectra. (b) Co L3 edge RIXS spectra of LaCoO3 thin films.

relative to the sample surface, while the charge coupled device detector was positioned at 90° relative to the incident x-ray.

Figure 1(a) shows the Co $2p$ XAS spectra obtained by total electron yield (TEY). The peak ~ 779 eV corresponds to Co L_3 edge, while the peak ~ 794 eV corresponds to Co L_2 edge. Although the tensile strain is different between LSAT(110) and LSAT(111), the spectra is quite similar. Then, we selected the energy A, B, and C as the excitation energy of RIXS and investigated the electronic structures more precisely by RIXS. The Co L_3 edge RIXS spectra are shown in Fig. 1(b). In this figure, the black arrow shows the elastic scattering. The colored zone from 0 to 4 eV corresponds to the dd excitations. And the peak ~ 5 eV is charge-transfer (CT) excitations. From the spectra of A and B, the peaks of dd excitations are different between LSAT(110) and (111), indicating that the spin states change according to the magnitude of the tensile strain. On the other hand, in the spectra of C, the peaks of the

FIG. 2. Co L3 RIXS spectra excited by 776.5 eV and their comparison with the impurity Anderson model calculations.

dd excitations are not clear because of the larger fluorescence. So, we selected the excitation energy of A and compare with the impurity Anderson model calculations. Figure 2 shows the Co L_3 RIXS spectra at 300 K and 40 K excited the energy of A: 776.5 eV. In the bulk and the thin film on LSAT(111), the peak of LS state is observed at 40 K. By increasing the temperature to 300 K, the peak of HS state becomes stronger. On the other hand, a new peak at 0.9 eV is observed in the thin film on LSAT(110). Since the peak dose not correspond to the LS nor HS state, the peak means a new spin state. By comparing the theoretical calculations, the peak is considered to be the HS state in D_{2h} symmetry. We clarified the epitaxial strain induced new spin state realized by 1% tensile strain.
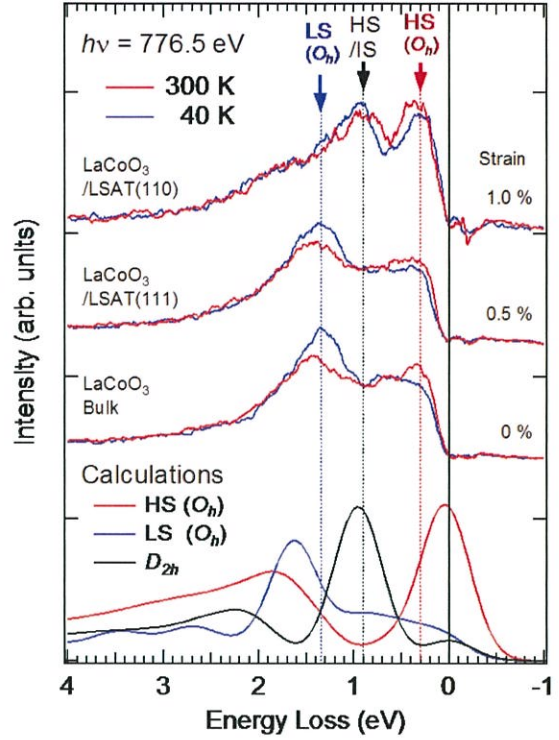
REFERENCES

[1] M. W. Haverkort et al., Phys. Rev. Lett. 97, 176405 (2006).
[2] J. Fujioka et al., Phys. Rev. Lett. 111, 027206 (2013).
[3] Y. Yamasaki et al., J. Phys. Soc. Jpn. 85, 023704 (2016).
[4] J. Fujioka et al., Phys. Rev. B 92, 195115 (2015).

PEUCULIAR INTERFACIAL DYNAMICS OF DIRAC ELECTRON SYSTEM

Hirokazu Fukidome[1], Takashi Someya[2], Susumu Yamamoto[2], Iwao Matsuda[2*]

[1]*Research Institute of Elecctrical Communication, Tohoku University*

[2]*Synchrotron Radiation Laboratory, The Institute for Solid State Physics, The University of Tokyo*

Graphene is proming for electronics and optoelectronics owing to such as giant carrier mobility and the opacity (2.3%) determined solely by the fine structure constant that describes coupling between light and relativistic electrons and that is traditionally associated with quantum electrodynamics rather than materials science. Unfortunately, however, graphene-based optoelectronic device properties, such as THz light emission driven the current injection of field-effect transistor device structure which uses the epitaxial graphene on a SiC substrate as the active layer, does not exhibit the ideal value estimated from the intrinsic properties.

Pump energy : 3.1 eV
Pump fluence: 1.3 mJ/cm²
Probe soft x-ray: 740 eV
Time res. : 50 ps
Pump laser: 3.1 eV, 208 kHz

① Graphene/buffer layer/ Si-terminatedSiC(0001)

② Graphene/ C-terminated SiC(000-1)

Fig. 1 Experimental system.

To raise up the optoelectronic device properties, it is necessary to the mechanism of carrier dynamics of graphene. In the previous device works, it was pointed out that the transport properties, such as the giant carrier mobility, of the epitaxial graphene on the C-terminted SiC(000-1) are superior to those on the Si-terminated SiC(0001). Someya et al. showed by using fs time-resolved angle-resolved photoelectron spectroscopy that population inversion, which was previously suggested not to occur, occurs for our high-quaility graphene on the C-terminated SiC(000-1), while it does not occur for graphene on the Si-terminated SiC(0001) [1,2]. However, the mechanism of the carrier dynamics still remains unclear because the interfacial dynamics between graphene and SiC has not been clarified yet.

To explore the mechanism, we have studied relaxation carrier dynamics of the graphene/SiC system excited by femtosecond laser (hν=3.1 eV), which was probed by soft x-ray time-resolved photoelectron spectroscopy of C 1s
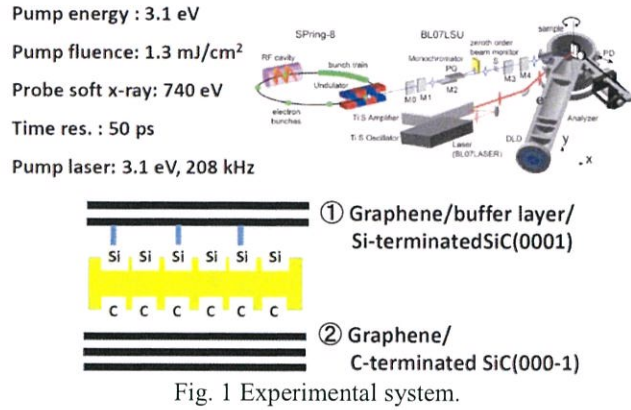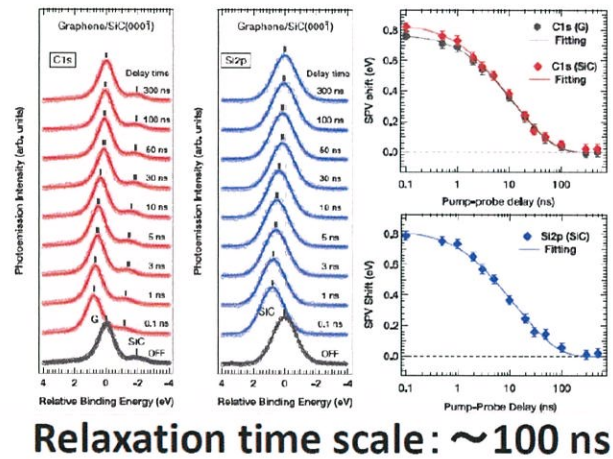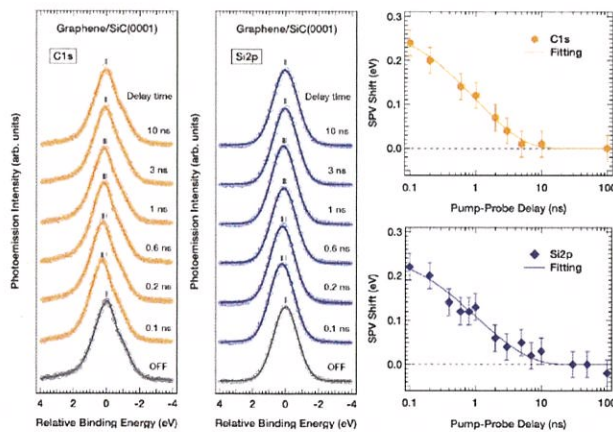

Relaxation time scale : ∼100 ns

Relaxation time scale : ∼10 ns

Fig. 2 Time-resolved C 1s and Si 2p spectra of graphene on (a) SiC(000-1) and (b) SiC(0001).

and Si 2p (Fig. 2).

We first studied the SiC surbstrate orientation dependence of carrier dynamics during surface photovoltage purmbed by the fs laser, as shown in Fig. 2. The relaxation time scale of the graphene on the C-terminated SiC(000-1) is longer than that on the Si-terminated SiC(0001).

On the reason for this difference in the relaxation time scale is the existence of the buffer layer situtated in graphene and Si-terminated SiC(0001). 1/3 of carbon atoms of buffer layer are bonded with surface Si atoms of the Si-terminated SiC(0001). On the rest of the Si-terminated SiC(0001) , there exists dangling bonds. It can be speculated that the dangling bonds induces carrier scattering, resulting in the degradation of transport properties.

In addition to the dangling bonds, the detailed analysis of our data indicates that there is another cause related with a peculiar band dispersion. The closeup view of the initial stage of the relaxation of graphene on the C-terminated SiC(000-1) (top right of Fig. 2) tells us that the Fermi level position of graphene does not coincide with that of the C-terminated SiC(000-1), while that of graphene coincides with that of the Si-terminated SiC(0001).

The cause of this is explained by the peculiar density of states of graphene. Thanks to the linear band dispersion of graphene, the density of states of conduction and valence bands linearly changes with energy, and becomes 0 at the Dirac point where the bottom of the conduction band touches with the top of the valence band. The Fermi level of graphene on the C-terminated SiC(000-1) is close to the Dirac point, i.e. negligible carrier doping. Therefore, even a small carrier doping drastically changes. On the other hand, graphene on the Si-terminated SiC(0001) is n-doped before the laser pump, so that the Fermi level position of graphene is not remarkable.

In conclusion, we have found the peculiar dynamics of graphene arising from the linear band dispersion. We believe that our finding surely affect the performances of the graphene-based optoelectronic devices.
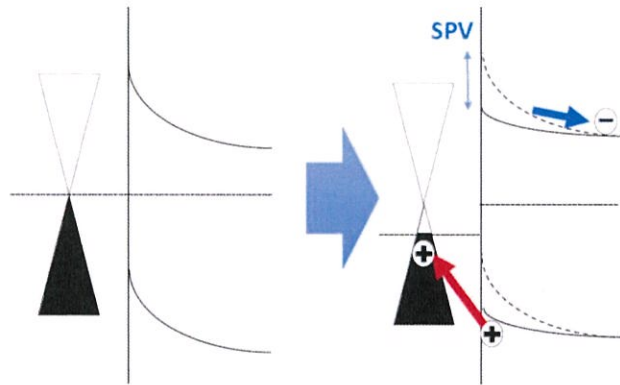
【Immediately after the pulse laser incidence】

Hole injection into graphene on C-face SiC(000-1), whose Fermi level is near the Dirac point (DOS→0), the C 1s graphene peak redshifts.

Therefore,

SPV(graphene)＝SPV(SiC)—E_F shift by hole doping

Fig. 3 The proposed mechanism for the initial non-equilibirum dynamics of graphene on the C-terminated SiC(000-1).

REFERENCES

[1] T. Someya, **H. Fukidome**, H. Watanabe, T. Yamamoto, M. Okada, H. Suzuki, Y. Ogawa, T. Iimori, N. Ishii, T. Kanai, K. Tashima, B. Feng, S. Yamamoto, J. Itatani, F. Komori, K. Okazaki, S. Shin, and I. Matsuda, Physical Review B 95. (2017) pp. 165303-1-7.

[2] T. Someya, **H. Fukidome**, Y. Ishida, R. Yoshida, T. Iimori, R. Yukawa, K. Akikuno, Sh. Yamamoto, S. Yamamoto, T. Yamamoto, T. Kanai, K. Funakubo, M. Suemitsu, J. Itatani, F. Komori, S. Shin, and I. Matsuda, Applied Physics Letters, 104. (2014), pp. 161103-1-161103-4.

DYNAMICS OF PHOTOEXCITED CARRIERS AT ORGANIC-OXIDE INTERFACE

Kenichi Ozawa[1], Susumu Yamamoto[2], Ro-Ya Liu[2], Yuto Natsui[3], Naoya Terashima[3], Hiroo Kato[3] and Iwao Matsuda[2]

[1]*Department of Chemistry, Tokyo Institute of Technology*

[2]*Institute for Solid State Physics, The University of Tokyo*

[3]*Department of Advanced Physics, Hirosaki University*

INTRODUCTION

Organic solar cells based on heterojunctions of p- and n-type organic molecular domains have recently been improved significantly in the light-to-electricity conversion efficiency [1]. Although the size of the molecular domains ranges from several ten nanometers to a few micrometers, a photoactive region is limited to a thin layer around the heterojunction with the width of several ten nanometers [2]. In this region, photoexcited excitons can reach the junction and undergo electron-hole separation owing to the energy level discontinuity. Electricity is generated when the electrons and holes are transported to a cathode and an anode, respectively, before they are quenched through charge recombination. Thus, it is important to understand details of charge separation and recombination dynamics especially at the organic/organic heterojunctions as well as the organic/electrode heterojunctions for pursuing solar cells with higher conversion efficiency.

In the present study, time-resolved soft X-ray photoelectron spectroscopy (TRXPS) has been used to examine carrier dynamics of a $C_{60}/TiO_2(110)$ system utilizing a ultraviolet (UV) laser pump and synchrotron radiation (SR) probe method. C_{60} and TiO_2 are used in an organic solar cell as an electron-transport p-type organic molecule and a cathode material, respectively. It is found that UV laser irradiation induces a spontaneous shift of the C 1s core level of C_{60}, whereas no such shift is observed in the Ti 2p core level of TiO_2. The excited state is swiftly quenched to the ground state within 1 ns, indicating a very fast decay of the UV-excited state.

EXPERIMENTAL

The TRXPS measurements were carried out at BL07LSU of SPring-8 (Proposal No. 2016A7503). The pulsed UV laser of the second harmonic generation of the Ti:sapphire laser was used to generate the photoexcited state. The photon energy, the pulse duration, the repetition rate and the power density were 3.06 eV, 35 fs, 208 kHz and 43 $\mu J/cm^2$/pulse, respectively. The photon energies of the SR light were 385 eV and 600 eV. The pulse duration of the SR light was 50 ps, which determines the time resolution of the system.

A commercially available rutile TiO_2 crystal with (110) orientation was used as a substrate. The surface was cleaned by cycles of Ar^+ sputtering and annealing in O_2 atmosphere. C_{60} (Kanto Kagaku, > 99%) was deposited on the clean TiO_2 surface by an evaporator (KOD-Cell, Kitano Seiki). The evaporation temperature was 435°C, and the deposition amount of C_{60} was evaluated from the attenuation magnitude of the Ti 2p peak intensity. The C_{60} coverage was adjusted to 1 monolayer by annealing of the surface after deposition.

RESULTS AND DISCUSSION

The energy of the pump UV laser used in the present study is 3.06 eV, which is larger than a band gap energy of rutile TiO_2 (3.0 eV) and an energy level difference between the highest occupied molecular orbital (HOMO) and the lowest unoccupied molecular orbital (LUMO) of C_{60} (2.3 eV [3]). Thus, valence electrons can be excited to unoccupied states in both C_{60} and TiO_2. However, our preliminary study has suggested that enough carriers are not excited to induce appreciably large surface photovoltages (SPVs) that are detectable by the present

measurement system if the laser power less than 0.1 mJ/cm²/pulse is irradiated on the clean TiO₂(110) surface (Fig. 1). This is also true for the C_{60}-covered surface. Fig. 2 shows Ti $2p_{3/2}$ spectra of the C_{60}-covered TiO₂(110) surface obtained before and 0.1-ns after irradiation of the UV pulse at 43 µJ/cm²/pulse. The peak positions are the same for both spectra, indicating that the SPV is not induced at this low power density.

On the other hand, the C 1s core level of C_{60} shows a slight but definite shift by UV irradiation. Fig. 3 shows C 1s spectra measured at various times after the UV pulse irradiation (delay times). When the C 1s spectrum is measured at 0.1 ns after UV irradiation, the peak moves towards the lower binding energy side by 15 meV. The magnitude of the shift is, however, diminished as the delay time is prolonged, and the shift is no more detected at 1 ns. This observation suggests that the photoexcited state is induced in the C_{60} layer by absorption of the UV laser but is swiftly deexcited within 1 ns.

The behaviour of the Ti 2p and C 1s spectra upon UV irradiation is different from that reported in the preceding study [4], in which the C_{60}/TiO₂(110) system was examined with a similar experimental condition employed in the present study. If the UV excited electron in the LUMO or higher state is transferred to the TiO₂ substrate, C_{60} is cationized so that the peak should have moved to the higher binding energy side [4]. Thus, the C_{60}-to-TiO₂ charge transfer seems to be absent. The spontaneous shift of the C 1s peak towards the lower binding energy side implies that the C 1s core holes created in the photoemission process are more efficiently screened by valence charge of C_{60} in the UV photoexcited state than in the ground state. A further study is needed to satisfactorily explain the origin of efficient core-hole screening as well as the discrepancy between the present and previous studies.

Fig. 1 UV laser power dependence of the SPV shift on clean TiO₂(110). The SPV was evaluated from the Ti $2p_{3/2}$ spectra and corresponds to the value at 1 ns after the UV pulse irradiation. The photon energy of the UV laser was 3.06 eV, and the repetition rate was 1 kHz.

Fig. 2 Ti $2p_{3/2}$ spectra of C_{60}-covered TiO₂(110) acquired before and 0.1-ns after the irradiation of the UV laser pulse (3.06 eV, 43 µJ/cm²/pulse and 208 kHz).

Fig. 3 C 1s spectra of C_{60}-covered TiO₂(110) measured at various times after the UV pulse irradiation (3.06 eV, 43 µJ/cm²/pulse and 208 kHz). Inset shows enlarged spectra before and 0.1-ns after the pulse irradiation.

REFERENCES

[1] P. Heremans *et at.*, ACC. CHEM. RES. **42**, 1740 (2009).
[2] B. A. Collins *et al.*, ADV. ENERGY MATER. **13**, 65 (2013).
[3] R. W. Lof *et al.*, PHYS. REV. LETT. **68**, 3924 (1992).
[4] K. Ozawa *et al.*, ORG. ELECTRON. **31**, 98 (2016).

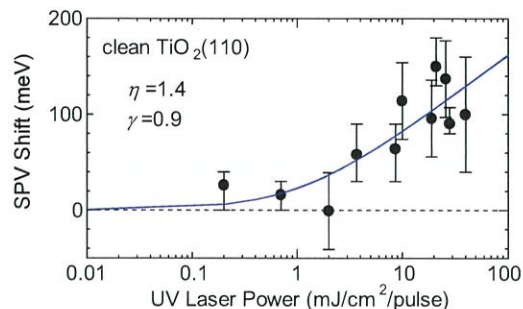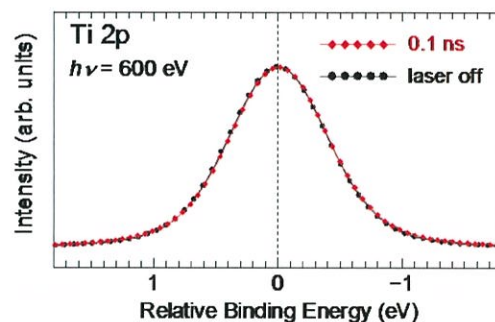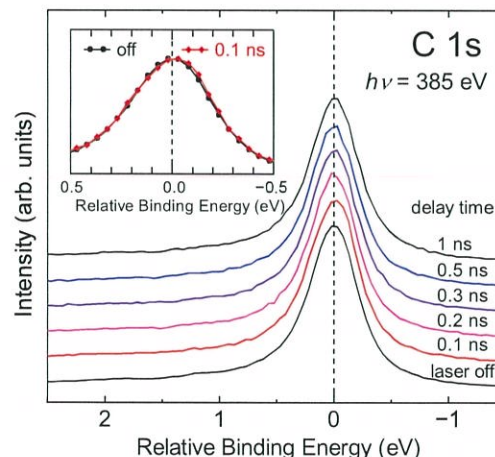# TIME RESOLVED X-RAY MAGNETO CIRCULAR DICHROISM OF FePt AND RESONANT SOFT X-RAY SCATTERING OF IrTe₂

Kou Takubo[*] Kohei Yamamoto, Yasuyuki Hirata, Yuichi Yokoyama, and Hiroki Wadati

[*]*The Institute for Solid State Physics, The University of Tokyo*

Control of electron, magnetic, and lattice states by optical excitations in electronically and magnetically ordered materials has attracted considerable attention due to their potential applications in electronic and magnetic recording media functioning on an ultrafast time scale. To capture their non-equilibrium dynamics with element selectivity, ultrafast time-resolved x-ray experiments have been carried out using a bunched synchrotron light source, recently.

We developed a time-resolved (Tr-) x-ray absorption spectroscopy (XAS) and resonant soft x-ray scattering (RSXS) measurement system [1], and measured Tr- x-ray magnetic circular dichroism (XMCD) at Fe $L_{2,3}$ edges of a magnetic material: FePt thin film in the partial electron yield (PEY) and total fluorescence yield (TFY) modes. FePt thin films have drawn intense research interest owing to their potential for high density recording applications by using their magnetism [2]. The static soft XMCD in the total electron yield (TEY) mode is the most functional and simple method. In the pump-probe experiments, however, the photo-current induced by the pump laser exceeds that by the probe x ray. On the other hand, the PEY mode, in which the emitted photoelectrons are measured, is rather surface sensitive but these spectra are known to usually be similar to those obtained in the TEY. The TFY mode, in which the fluorescence of an x-ray is measured, is rather bulk sensitive compared to PEY. Despite its bulk-sensitivity, the relationship between FY and the absorption coefficient is non-trivial and saturation effects become important in the TFY.

Figure 1 shows an overview of the experimental setup for Tr-XAS, Tr-XMCD, and Tr-RSXS measurements at BL07LSU of SPring-8. Tr-RSXS is performed at the $\theta < 90°$ side of the experimental chamber. The scattering is detected by the micro-channel plate (MCP) on the 2θ motion. On the other hand, XAS and XMCD in the PEY or TFY modes are measured at the $\theta > 90°$ side of the chamber. Emitted photoelectrons or x-ray fluorescence are caught by another MCP topped on the linear motion. The femtosecond Ti:sapphire laser with a wavelength of ~800 nm housed at the laser station of BL07LSU is introduced into the chamber. The laser irradiates samples 7° below the x-ray and photo-induced dynamics of the electronic and structural evolutions are examined by means of a pump-probed technique. The laser pulses with ~1 kHz repetition rate are synchronized with selected bunches of the synchrotron and delayed electronically. The signals of the MCP are amplified and gated on the oscilloscope which is triggered by the laser pulses.

Figure 2 shows the static XMCD spectra at the Fe $L_{2,3}$ edges for the FePt thin film in the TEY, PEY, and TFY modes. Intense XMCD was observed both at the $L_{2,3}$ edges, ~40% at 707 eV and ~6% at 720.2eV for the original μ^- XAS in TEY and PEY. A spectral difference between the TEY and PEY mode is barely observable. On the other hand, XMCD at
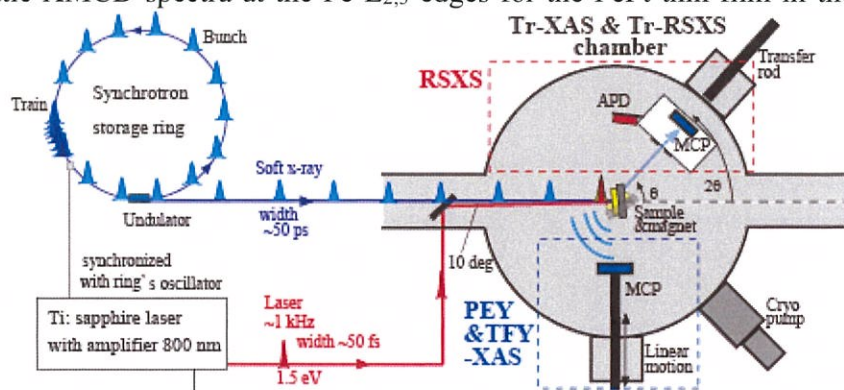

Fig.1 Tr-XMCD and Tr-RSXS measurements at BL07LSU of SPring-8.

the L_2 edge in the TFY mode is scarcely observed owing to the distortion caused by the saturation effect, although TFY has a bulk-sensitivity. Using the sum rules, the magnetic moments at the Fe site are estimated to be m_{spin}=2.63 μ_B and $m_{orbital}$=0.10 μ_B for TEY, and m_{spin}=2.74 μ_B and $m_{orbital}$=0.15 μ_B for PEY, respectively. Here, the number of the $3d$ electrons was assumed to be n_{3d}=6.6. These values are basically consistent with previous studies [2]. On the other hand, the magnetic moments are estimated to be m_{spin}=1.53 μ_B and $m_{orbital}$=0.08 μ_B for the TFY spectra, which exhibited a large discrepancy arising from their strong distortion.

The photo-induced dynamics of the FePt thin film were examined in the less-distorted PEY mode. The time-evolutions of the FePt thin film with 16 mJ/cm^2 laser irradiation are given in Fig. 3 (a) at $h\nu$=707.0 eV (L$_3$ edge) and (b) at 720.2 eV (L$_2$ edge), respectively. Almost similar time-evolutions are observed for the Fe L$_{2,3}$ edges. XMCD exhibits a reduction in its intensity by ~90% of the original value at both the L$_{2,3}$ edges ~30 ps after the pump pulse. Then the XMCD exhibits a slow recovery of the magnetization. The magnetization is not recovered to the original value even at t=1500 ps, which is completed before the next bunch arrives after ~342 ns.

Fig.2 Static XMCD spectra of the FePt thin film
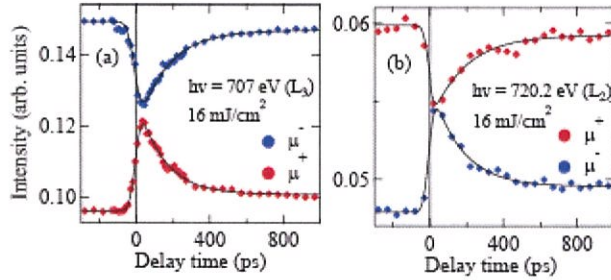
Fig.3 Time-evolutions of XMCD for the FePt thin film

We have also performed RSXS measurements of IrTe$_2$. IrTe$_2$ exhibits an exotic structural phase transition at T~260 K near its super conducting phase [4]. Fig. 4 shows a non-resonant superlattice reflection around Q=(1/5,0,4/5) at T=200 K. We plan to measure Tr-RSXS of IrTe$_2$ in future.
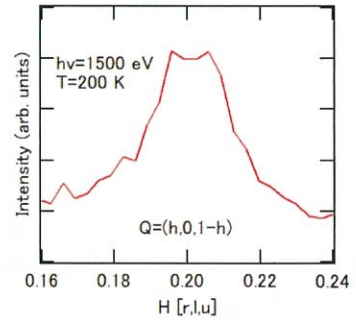
Fig.4 Superlattice reflection around Q=(0.2,0,0.8) of IrTe$_2$

In conclusion, we have studied the photo-induced magnetic dynamics of the FePt thin films at the Fe site using the Tr-XMCD. The ultrafast photo-induced demagnetization within 50 ps and its slow relaxation taking a few hundred ps are clarified. MCP has been used for Tr-XMCD both in the electron and fluorescence yield modes at the L$_{2,3}$ edges of the $3d$ transition-metals. The spectrum in the PEY mode is less distorted and basically similar to that obtained in the TEY mode. No difference of the change ratio is observed between the Fe L$_2$ and L$_3$ edges in the time-resolved measurement, taking advantage of the PEY method.
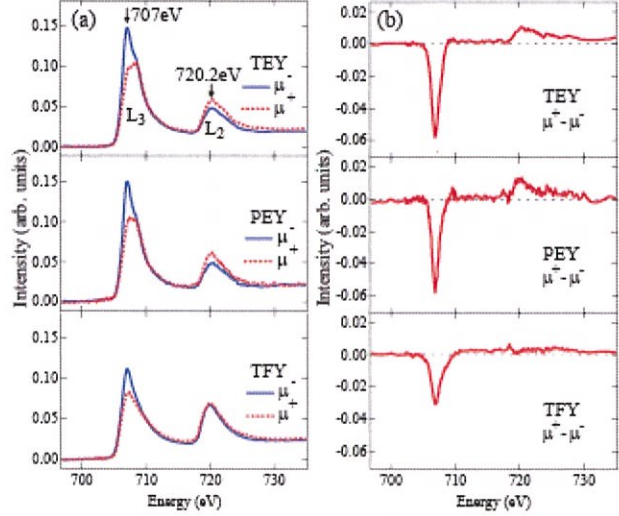
REFERENCES

[1] K. Takubo et al., Appl. Phys. Lett. **110**, 162401 (2017).
[2] T. Seki, H. Iwama, T. Shima, and K. Takanashi, J. Phys. D: Appl. Phys. **44**, 335001 (2011).
[3] M. M. Soares et al., Phys. Rev. B **90**, 214403 (2014).
[4] S.Pyon et al., J. Phys. Soc. Jpn. **81**, 053701 (2012).

RESONANT INELASTIC X-RAY SCATTERING STUDY ON BI2223 SUPERCONDUCTORS

H. Wang[1], J. Miyawaki[1,2], K Ishii[3], T. Tohyama[4], S. Adachi[2], T. Watanabe[5], S. Shin[1,2], and Y. Harada[1,2]

[1]Graduate School of Frontier Sciences, The University of Tokyo
[2]Institute for Solid State Physics, The University of Tokyo
[3]Synchrotron Radiation Research Center,
National Institutes for Quantum and Radiological Science and Technology
[4]Department of Applied Physics, Tokyo University of Science
[5]Graduate School of Science and Technology, Hirosaki University

Introduction

One of the ideal systems to study how to improve the superconducting critical temperature (T_c) is the Bismuth-based cuprates whose T_c becomes higher by varying the number of the superconducting CuO_2 layer n from 1 to 3 [1]. Among these layered materials, our research interests focus on a hole-doped $Bi_2Sr_2Ca_2Cu_3O_{10+\delta}$ (Bi2223) superconductor which has the highest $T_c = 110$ K and more notable three superconducting layers. Especially, the inner layer is different from the outer layers spatially; the carrier density is different between the inner and outer layers [2], which is consistent with the decrease of T_c with superconducting layers over 3. From the phase diagram of cuprates, superconductivity phase often appears in the vicinity of the charge density wave (CDW) phase, and CDW and superconductivity are supposed to interplay or compete with each other. Thus, Bi2223 provides us a unique opportunity to discuss the relationship between CDW and superconductivity. In addition, O K-edge resonant inelastic X-ray scattering (RIXS) has an advantage over the Cu L-edge in the hole-doped case, because the carriers (holes) are mainly on the oxygen sites, thereby making O K-edge RIXS more accessible to CDW.

Experimental

O K-edge RIXS on Bi2223 was carried out at the HORNET end-station of BL07LSU in SPring-8. The total energy resolution was set to be ~130 meV, and the scattering angle was fixed at 135°. In order to probe the quasi-elastic peak, σ polarization was used, where the electronic field of the linearly-polarized incident X-ray was perpendicular to the scattering plane. The incident angle was varied to measure the dispersion of the CDW. Measurement temperatures were from 30 K, which was well below the superconducting transition temperature T_c, to 250 K. The optimally hole-doped Bi2223 high-quality single crystal was grown with the floating-zone method. The Bi2223 crystal was cleaved in air before being loaded into the vacuum chamber.

Results and discussion

Figure 1 shows the momentum-transfer and temperature dependence of the intensity of the quasi-elastic peak along the nodal direction. The CDW signal in the quasi-elastic peak is expected at q~0.3 reciprocal lattice unit (r.l.u.), but due to the congenital defect of O K-edge wave length, the maximum momentum transfer obtained in our experimental setup was 0.265 r.l.u. However, at 150 K, which was above the $T_c = 110$ K, the clear jump of the intensity of the quasi-elastic peak were observed at $q = 0.265$ r.l.u. Since $q = 0.265$ r.l.u is smaller than the expected CDW period, the jump is ascribed to the tail of the CDW signal. Below T_c, no distinct increased intensity of the quasi-elastic peak was observed even at higher momentum transfer.

On the other hand, a dispersive excitation was unexpectedly observed at the energy range of 500–900 meV (Figure 2). Since a spin-flip excitation is forbidden at O K-edge, low energy paramagnons are highly unlikely to be found. At the same time, bimagnons are also unlikely to be assigned to the observed excitation, because the dispersion of the paramagnon does not generally reach up to 900 meV. Thus, we believe that the observed dispersion mainly comes from the contribution of charge excitations.

Conclusion

We observed CDW signals in O K-edge RIXS. The temperature dependence of CDW signals is the concrete evidence that superconductivity competes and kills CDW. Considering other antecedent challenges [3,4], what we found here confirms the idea that CDW is a universal phenomenon in cuprates. It is the distinctly important aims in the future to clarify the mechanism of CDW and whether it is related to the pseudogap and the high-energy charge excitation which we found in Bi2223.
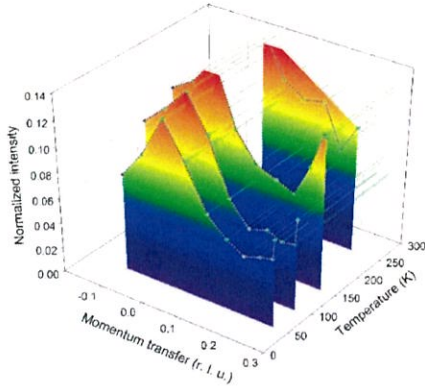

FIG. 1 Momentum- and temperature-dependence of the intensity of the quasi-elastic peak at O K-edge RIXS of Bi2223 along the nodal direction.
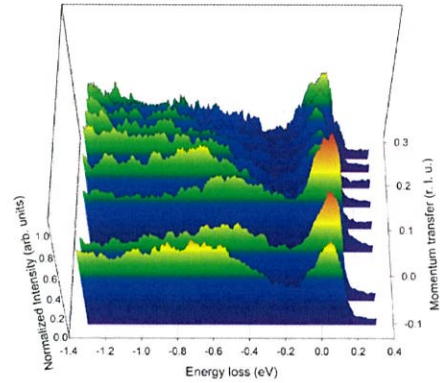

FIG. 2 Momentum-dependence of O K-edge RIXS spectra of Bi2223 along the nodal direction measured at 50 K.

References

[1] M. P. M Dean *et al.*, Phys. Rev. B **90**, 220506(R) (2014).
[2] S. Iwai *et al.*, JPS Conf. Proc. **1**, 012105 (2014).
[3] W. Tabis *et al.*, Nat. Commun. **5**, 5875 (2014).
[4] H. Y. Huang *et al.*, Sci. Rep. **6**, 19657 (2016).

INVESTIGATING THE ELECTRONIC STRUCTURE OF THE NITROGENASE ENZYME BY 2P3D RIXS

Benjamin E. Van Kuiken[1], Anselm W. Hahn[1], Serena DeBeer[1], Yi-Tao Cui[2], Jun Miyawaki[2], Yoshihisa Harada[2],

[1]*Max Planck Institute for Chemical Energy Conversion*

[2]*Synchrotron Radiation Laboratory, The Institute for Solid State Physics, The University of Tokyo*

Introduction

The goal of this experiment is to measure the low-lying excited states of iron-sulfur (FeS) compounds relevant to biological systems that perform nitrogen reduction using 2p3d resonant inelastic x-ray scattering (RIXS) spectroscopy. FeS clusters are a common component of proteins where Fe may be found as a monomer ligated to four cysteine residues or as a cluster of Fe atoms bridged by disulfide (S^{2-}) linkages. One of the most fascinating FeS clusters that has been discovered in nature is the iron-molybdenum cofactor of the nitrogenase, which possesses an active site comprised of a Fe_7MoS_9C (FeMoCo) cluster. While the structures of many FeS proteins including FeMoCo are well characterized, the electronic structure of these systems is notoriously complex. High metal-ligand covalency and exchange interactions between metal centers in multi–metal cluster lead to a dense manifold of low-energy ligand field (d-d) excited states that cannot be measured by traditional UV/Vis absorption spectroscopy. Consequently, 2p3d RIXS spectroscopy is an ideal candidate for investigating the low-lying excited states in these systems.

Experimental Methods

In this experiment, the soft X-ray RIXS is measured on a collection of FeS monomers $[Fe(SR)_4]^-$ and $[Fe(SR)_4]^{2-}$, dimers $LFe^{III}S_2Fe^{III}L$ and $LFe^{II}S_2Fe^{III}L$, and a cubane complex $Fe_3MoS_4L_4$. These spectra are compared with the spectra of ferric and ferrous iron chloride complexes $[Fe(II)Cl_4]^{2-}$, $[Fe(III)Cl_4]^{1-}$, $[Fe(II)Cl_6]^{4-}$, and $[Fe(III)Cl_6]^{3-}$. All data were measured at the HORNET spectrometer of BL07SLU at SPring8. Complexes were measured as
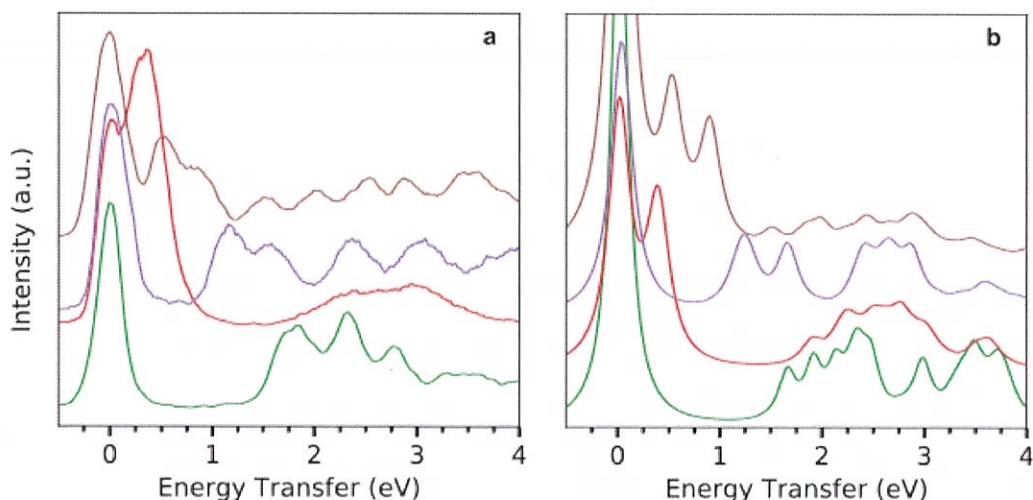

Figure 1. Experimental (a) and simulated (b) 2p3d RIXS spectra of iron chloride complexes where $[Fe(III)Cl_4]^-$, $[Fe(II)Cl_4]^{2-}$, $[Fe(III)Cl_6]^{3-}$, and $[Fe(II)Cl_6]^{4-}$ are shown in green, red, purple, and beige, respectively.

powders spread on sticky carbon tape that was fixed to a copper sample holder. Samples were kept at 30 K using a liquid He cryostat, and the samples were continuously moved during measurements to avoid beam damage.[1] All samples were excited at the maximum of the L_3-edge (~708 eV).

Results and Discussion

Figure 1 shows the 2p3d RIXS spectra of tetrahedral and octahedral iron chloride complexes.[2] Each spectrum exhibits multiple features between 0 and 4 eV on the energy transfer scale. These are d-d excitations. In the Fe(II) complexes $[Fe(II)Cl_4]^{2-}$ and $[Fe(II)Cl_6]^{4-}$ the lowest energy excitation corresponds to the spin-allowed $^5\Gamma$ to $^5\Gamma$ excitation. The rest

Figure 2. RIXS spectra of FeS complexes including spectra of monomers dimers and the cubane complex.

of the features arise from spin-forbidden transitions that are enabled by the strong spin-orbit coupling of the 2p core hole. Each experimental spectrum is simulated using a ligand field multiplet model shown in Figure 1b. The ligand field simulations allow one to extract the ligand field splitting 10Dq and the Racah parameters from the spectra, and the magnitude of 10Dq was found to be 0.7, 1.47, and 0.32 eV for $[Fe(III)Cl_4]^-$, $[Fe(III)Cl_6]^{3-}$, and $[Fe(II)Cl_4]^{2-}$, respectively. $[Fe(II)Cl_6]^{4-}$ was found to be structurally distorted by an axial compression, and a single 10Dq cannot be assigned.[2] The spectra of the Fe chlorides are in good agreement available optical measurements and highlight the ability of RIXS to probe the electronic structure of transition metal complexes.

Figure 2 shows the 2p3d RIXS spectra of FeS complexes. The most notable difference between the FeS complexes and chlorides is that the FeS spectra are broader. For example, if the spectra of the ferric tetrachloride (Figure 1a, green) is compared with the ferric tetrathiolate (Figure 2, green), it can be seen that the chloride complex contains three sharp features between 1.5 and 3 eV while there only a broad band in the FeS complex with the sharpest absorption centered at ~1.5 eV. This difference in the FeS and chloride spectra is attributed to the increase in metal-ligand covalency in going from chloride to thiolate ligands. The result is that the density of low-lying excited states is much higher in the case of the FeS complexes. The sharpest features in the FeS spectra are the intense transitions below 1 eV in $[Fe(II)(SR)_4]^{2-}$ and the mixed-valence dimer. This feature is quintet to quintet transition that is indicative of the presence of localized Fe(II). This feature is absent in the cubane complex $Fe_3MoS_4L_4$, which contains two Fe(III) and one Fe(II) atoms. This indicates that the Fe(II) in the cubane forms a delocalized mixed-valent pair. The qualitatively distinct FeS spectra show the power of 2p3d RIXS for mapping out dense manifolds of states in multi-atom transition metal clusters.
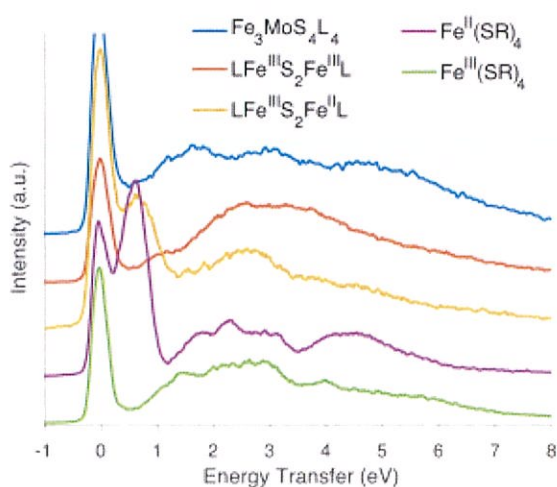
REFERENCES

[1] Van Kuiken, B. E. *et al*. Inorg. Chem. **55**, 11497-11501 (2016).
[2] Hahn, A. W. *et al*. Inorg. Chem. (2017), *in press*.

ELECTRONIC STATES REVEAL THE FUNCTION OF WATER ENCAPSULATED IN NANO-SPACES: SOFT X-RAY ABSORPTION/EMISSION STUDY

K. Yamazoe[1], D. Murakami[2], J. Miyawaki[1,3], Y.-T. Cui[3], M. Tanaka[2] and Y. Harada[1,3]*

[1]*Department of Advanced Materials Science, Graduate School of Frontier Sciences, The University of Tokyo*
[2]*Institute for Materials Chemistry and Engineering, Kyushu University*
[3]*The Institute for Solid State Physics, The University of Tokyo*
harada@issp.u-tokyo.ac.jp

Introduction

Water molecules in the vicinity of material surface play an important role on specific material functions[1]. For example, poly(2-methoxyethyl acrylate) (PMEA) is a bio-compatible polymer[2] widely used in the medical field where a great deal of researches have been focused on controlling the chemical structure of polymer to develop novel blood-compatible polymeric materials. Previous studies suggest the compatibility largely depends on the interaction between the polymer and water molecules[1,2]. Recently, Tsuruta *et. al.* has suggested that it is of particular importance to understand the hydrogen-bonding structure of water in polymer coating or polymer/water interfaces in order to develop functional polymer interfaces which show a resistance against nonspecific protein adsorption[1]. However, the water structure at the interface between those polymers and water is still under debate.

In this study, we used soft X-ray emission spectroscopy (XES). XES is an excellent tool for investigating the strength as well as symmetry of hydrogen-bonding of water molecules in polymer coating. Recently we successfully demonstrated that XES can be used to probe a slightly distorted but ordered hydrogen-bonding configuration of water confined in polyelectrolytes brush[3].

Experiment

PMEA was synthesized by free radical polymerization. Polymer thin films for XES experiment were prepared by twice spin-coating polymer solutions (0.2 wt/vol % methanol solution for PMEA) on a silicon carbide (SiC) substrates.

O 1s XES experiment of water in the polymer coating was performed at SPring-8 synchrotron radiation facility using the BL07LSU[4] HORNET station[5]. The SiC membrane with polymer coating was used to separate the flow of liquid or water vapour from high vacuum and to transmit incident and emitted soft X-rays. Water vapour was supplied by steam-generation equipment (HUM-1, Rigaku), and nitrogen was used as the carrier gas.

Results and Discussion

The XES spectra of water in PMEA coating (RH 80 %) and bulk liquid water are very similar as shown in Figure 1. This data suggests that the hydrogen-bonding structure of water in the PMEA is very similar to bulk liquid water. This interpretation is consistent with the study of Myalitsin *et al.* in which the peak position and the band structure of OH stretch vibration at the PMEA/water interface bear a striking resemblance to bulk liquid water[6]. We conclude that an unperturbed hydrogen-bonding structure of water at the PMEA/water interface plays an important role for bio-compatibility.

REFERENCES

[1] T. Tsuruta, Biomater. Sci., Polym. Ed. **21**, 1831 (2010).
[2] M. Tanaka *et al.* Polym. J. **45**, 701 (2013).
[3] K. Yamazoe *et al.* Langmuir **33** 3954 (2017).
[4] S. Yamamoto *et al.* J. Synchrotron Radiat. **21**, 352 (2014).
[5] Y. Harada *et al.* Rev. Sci. Instrum. **83**, 013116 (2012).
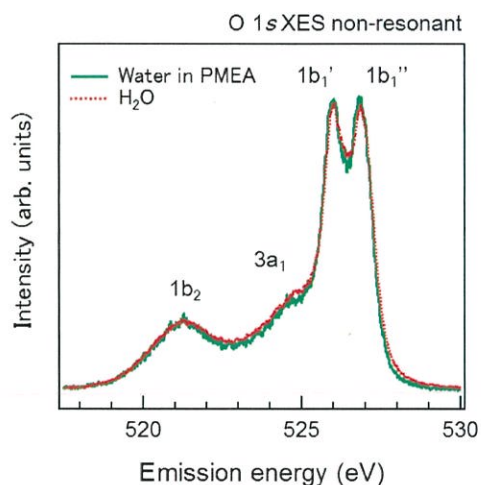[6] A. Myalitsin *et al.* 表面科学学術講演会要旨集 **36**, 38 (2016).

Figure 1. O 1s soft X-ray emission spectra of water in PMEA (RH 80 %) and liquid H_2O. The excitation energy is 550 eV, which is well above the ionization threshold. The XES spectra were normalized to have the same intensity of the $1b_1$' peak.

Study on electronic structure of Prussian blue analogues controlled by molecular adsorption

Takanobu Inoue[1], Jun Miyawaki[1,2,3], Yi-Tao Cui[3], Hiroko Tokoro[4], Yusuke Nakagawa[5], Shin-ichi Okoshi[5], Yoshihisa Harada[1,2,3]

[1]*Graduate School of Frontier Science, The University of Tokyo*

[2]*Institute for Solid State Physics, The University of Tokyo*

[3]*Synchrotron Radiation Research Organization, The University of Tokyo*

[4]*Division of Materials Science, Faculty of Pure and Applied Science, University of Tsukuba*

[5]*Department of Chemistry, School of Science, The University of Tokyo*

Prussian blue analogues, which make face-centered structure by cyano(CN)-bridged bimetal assemblies, have a variety of features and their developments are intensively promoted for various applications such as cathode material of rechargeable batteries. Their functional diversity derives from the combination of metals inserted in the CN-bridged framework. Among them, $(Co_xMn_{1-x})[Cr(CN)_6]_{2/3} \cdot zH_2O$ is known to show humidity-induced magnetization [1]. Its unique property is explained by different number of ligand coordination to the metal site neighboring a defect site by desorption/adsorption of H_2O molecules. However, microscopic origin of the magnetic property is not yet experimentally elucidated. In this study, in order to obtain the detailed $3d$ electronic states of metals which are responsible for its magnetic property, Co 2p X-ray absorption spectroscopy (XAS) was applied to the x=1 mother compound $Co[Cr(CN)_6]_{2/3} \cdot zH_2O$ to monitor changes in the Co $3d$ electronic states upon water and ethanol adsorption. In the XAS process, incident soft X-rays can resonantly excite the Co $2p$ core to the dipole allowed Co $3d$ empty states, which provides information about local coordination geometry and ligand hybridization of the Co $3d$ states.

XAS measurements of $Co[Cr(CN)_6]_{2/3} \cdot zH_2O$ powder and hexacyano complex $CsCo[Cr(CN)_6] \cdot H_2O$ powder, which has no defect in the CN-bridged framework, were carried out at SPring-8 BL07LSU, the University of Tokyo outstation. For the humidity dependence, an originally developed flow through cell for aqueous solutions was applied and the humidity was precisely controlled by flowing dry or humid N_2 gas through Teflon tubes using humidity controller HUM-1 from RIGAKU Co. Ltd.
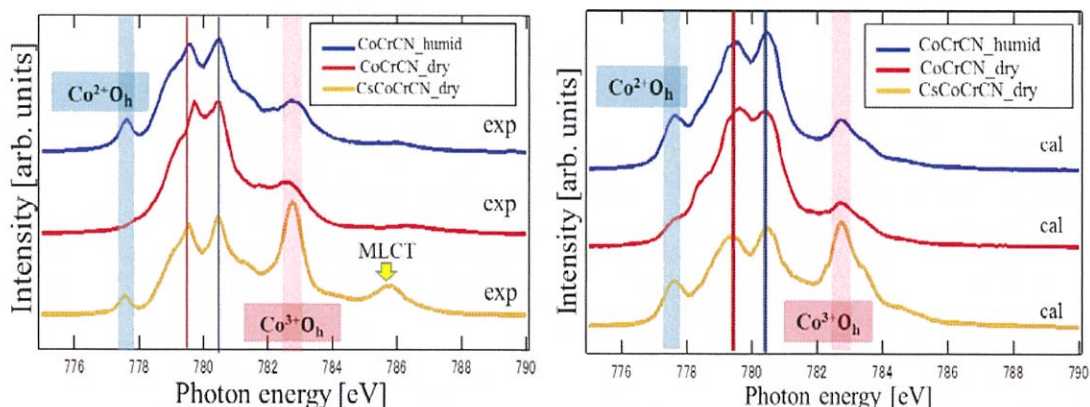

Figure 1 (*left: experiment, right: calculation*) Co 2p XAS spectra. Blue line: $Co[Cr(CN)_6]_{2/3} \cdot zH_2O$ humid condition, Red line : $Co[Cr(CN)_6]_{2/3} \cdot zH_2O$ dry condition, Orange line : $CsCo[Cr(CN)_6] \cdot H_2O$ dry condition.

Figure 1 shows Co 2p XAS spectra of humid $Co[Cr(CN)_6]_{2/3}\cdot zH_2O$ (blue), dried $Co[Cr(CN)_6]_{2/3}\cdot zH_2O$ (red), and defect-free $CsCo[Cr(CN)_6]\cdot H_2O$ (orange). Left panel shows the experimental results, while the right panel shows simulated XAS spectra by mixing calculated XAS spectra of CoO (Co^{2+} O_h), Co_3O_4 (Co^{2+} T_d), $SrCoO_{2.5}$ (Co^{3+} O_h) which have typical valence and coordination symmetry, using a cluster model calculation code CTM4XAS developed by F. M. F. de Groot [ref]. The overall profiles are well reproduced by the simulation, except for the experimentally observed peak around 786 eV, which may be ascribed to metal-to-ligand charge transfer (MLCT) excitation not included in the simulation. From this comparison the spectral change from dry to humid conditions can be quantitatively explained by a 25% increase of the component with Co^{2+} O_h symmetry (which is characterized by the peak around 777.5eV) and a 25% decrease of the one with Co^{2+} T_d symmetry, which is simply imagined by addition of two water molecules to the T_d symmetric (four coordinated) site to make the O_h symmetric site. We also found that certain amounts of Co^{3+} component are present in all the samples which was not expected in the previous study [2]. This may be partly due to radiation induced damage although the presence of the Co^{3+} states could explain the decrease of magnetization estimated from assuming only Co^{2+} states [1]. As demonstrated above, XAS is quite sensitive to the local coordination number and symmetry.

In summary, humidity dependence of the electronic structure of $Co[Cr(CN)_6]_{2/3}\cdot zH_2O$ and $Co[Cr(CN)_6]\cdot zH_2O$ was studied by Co 2p XAS. This technique can be extended to study adsorption-molecule dependence and detailed difference in hybridization with ligands, which will be a novel approach to discuss the relationship between the electronic structure and magnetization controlled by molecular adsorption.

References

[1] S. Ohkoshi, K. Aarai, Y. Sato and K. Hashimoto, Nat. Mater. **3**, 857 (2004).
[2] D. Bazina, L. Guczib, J. CATAL. **189**, 456 (2000).b

CHARGE EXCITATIONS RELATED TO CHARGE ORDER IN HOLE-DOPED CUPRATE SUPERCONDUCTORS

Kenji Ishii[1], Shun Asano[2], Masaki Fujita[2],
Shuichi Wakimoto[3], Jun Miyawaki[4], Yoshihsa Harada[4]

[1]*Synchrotron Radiation Research Center, National Institutes for Quantum and Radiological Science and Technology*
[2]*Intsitute for Materials Research, Tohoku University*
[3]*Materials Science Research Center, Japan Atomic Energy Agency*
[4]*Synchrotron Radiation Laboratory, The Institute for Solid State Physics, The University of Tokyo*

High-T_c superconducting cuprates are categorized into doped Mott insulators and interplay between charge and spin of electron governs their physical properties. Therefore both charge and spin excitations must be investigated on equal footing in order to understand the electron dynamics characterizing the cuprates. Resonant inelastic x-ray scattering (RIXS) is a suitable technique for the study of electron dynamics in the energy-momentum space. High-resolution RIXS at the Cu L_3-edge has been established as a tool to measure momentum-resolved spin excitations up to several hundreds meV [1]. In addition to the spin excitations, RIXS is sensitive to charge excitations and it is a unique and important advantage of RIXS. In the experiment in 2015, we found that RIXS at the O K-edge is useful for observing the charge excitations in the hole-doped cuprates and succeeded to observe momentum-dependent charge excitations in $La_{2-x}Sr_xCuO_4$ (x = 0.075 and 0.18) [2].

Recently, charge order in the cuprates attracts great interest as a competing phenomenon to the superconductivity and it is universally observed in the underdoped region of the hole-doped cuprates [3]. However, its energy scale has not been clarified yet and the origin is still under debate. Here we report a trial to search charge excitations related to the charge order in the hole-doped cuprates using O K-edge RIXS. Thanks to the extension of the scattering angle (2θ) up to 135° in the HORNET spectrometer, we are now able to access the reciprocal lattice point of the propagation vector of the charge order.

The experiment was performed at BL07LSU of SPring-8. Total energy resolution was 170 meV. We measured $La_{1.875}Ba_{0.125}CuO_4$ (LBCO x = 0.125) and $La_{1.75}Sr_{0.25}CuO_4$ (LSCO x = 0.25). Charge order below T_{co} = 50 K is established in the former while it is absent in the latter. The crystals were cleaved before the measurement and σ-polarized x-rays were irradiated on the *ab*-plane of the crystal. The *c*-axis was kept parallel to the horizontal scattering plane and momentum transfer in the CuO_2 plane (**q**) was scanned by rotating the crystal along the vertical axis. In the x-ray absorption spectrum (XAS) of $La_{2-x}Sr_xCuO_4$, two peaks are observed near the O *K*-edge [4]. The peak at lower energy is the O $2p$ state of doped holes (hole peak) and we tuned the incident photon energy to top of the peak of respective samples.

Figures (a) and (b) shows RIXS intensity maps at 30 K for LBCO x = 0.125 and LSCO x = 0.25, respectively. We could scan wider momentum space than the previous experiment by changing 2θ from 90° to 135°. The spectral weight at the sub-eV region shifts to higher energy with increasing **q**, showing positive dispersion. The magnitude of the dispersion becomes larger with increasing hole concentration. For example, the peak position at **q** = (0. 23, 0) is 0.66 eV for x = 0. 125 while it is 0.77 eV for x = 0. 25. Broad width of the spectral lineshpae indicates that the charge excitations in this energy range are damped by the strong Coulomb interaction between the charge. Theoretical calculation of the dynamical charge structure factor on oxygen orbitals in a three-band Hubbard model is consistent with the experimental observation of the momentum and doping dependence, and hence we confirm that the momentum-dependent spectral weight is ascribed to charge excitations. Comparing

the spectral weights at the same $|\mathbf{q}|$ of x = 0. 125, the peak of the (h,h) direction is located at higher energy than that of the (h,0) direction.

Figure (c) shows the spectra of charge-ordered LBCO x = 0.125 below (30 K) and above (100 K) T_{co}. Though charge order at $\mathbf{q} \sim (0.22,0)$ is confirmed by the enhanced elastic scattering at 30 K, we could not find any change in the inelastic part across T_{co}. It may indicates that effect of the charge order in hole-doped cuprates appears at lower energy than the experimental resolution. Judging from an optical study on the same material [5], effect of the charge order on the electronic excitations would appear below 0.1 eV.

Even thought the search of charge excitations related to charge order was unsuccessful, we could demonstrate the capability of O K-edge RIXS for the study of momentum-dependent charge excitations in the hole-doped cuprates. Combining the present work with the Cu L_3-edge RIXS of electron-doped $Nd_{2-x}Ce_xCuO_4$ [6], we proved that momentum-dependent charge in the sub-eV region exists commonly in doped cupratess and the broad spectral lineshape originating from the strong Coulomb interaction is a characteristic of the charge excitations in the doped Mott insulators.
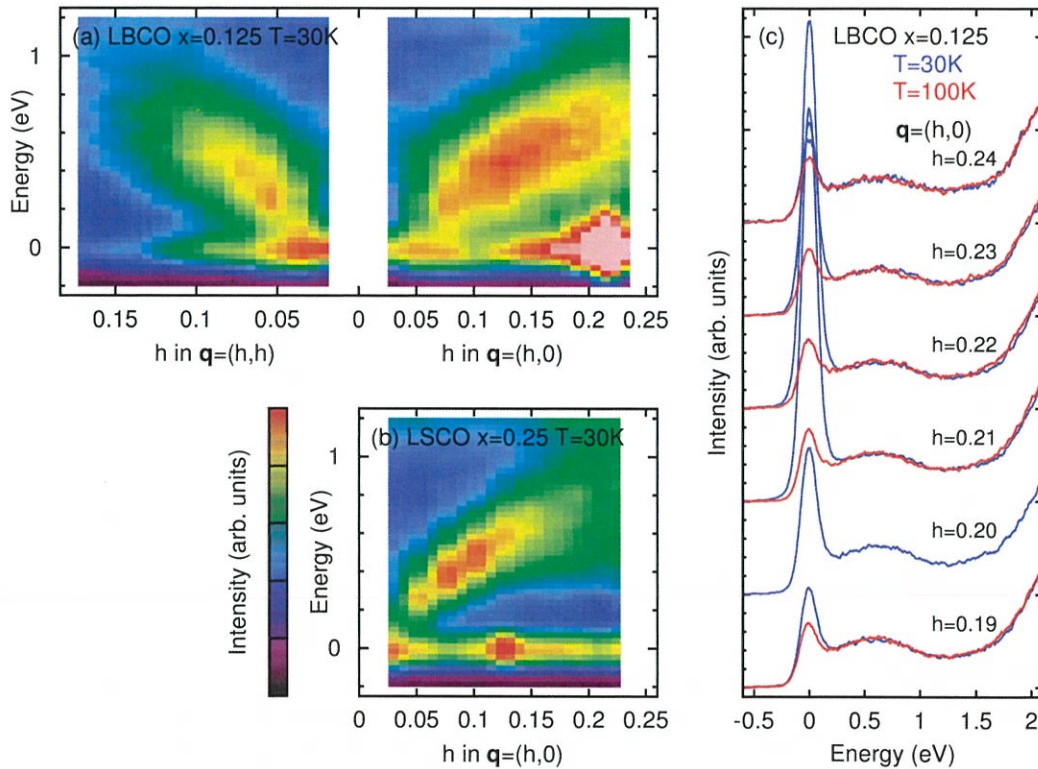
(a,b) Oxygen K-edge RIXS intensity maps of $La_{1.875}Ba_{0.125}CuO_4$ and $La_{1.75}Sr_{0.25}CuO_4$. (c) RIXS spectra of $La_{1.875}Ba_{0.125}CuO_4$ measured below (30 K) and above (100 K) the transition temperature of charge order (T_{co} = 50 K).

REFERENCES

[1] M. P. M. Dean, J. Magn. Mag. Mater. **376**, 3 (2015).
[2] K. Ishii *et al.*, ACTIVITY REPORT OF SYMCHROTRON RADIATION LABORATORY 2015.
[3] R. Comin *et al.*, Annu. Rev. Condens. Matter Phys. 7, **369** (2016).
[4] C. T. Chen *et al.*, Phys. Rev. Lett. **66**, 104 (1991).
[5] C. C. Homes *et al.*, Phys. Rev. Lett. 96, 257002 (2006).
[6] K. Ishii *et al.*, Nat. Commun. **5**, 3714 (2014).

Ni $L_{2,3}$-edge *operando* soft X-ray absorption spectroscopy of LiNi$_{0.5}$Mn$_{1.5}$O$_4$ cathode for Li-ion battery

Daisuke Asakura[1], Takaaki Sudayama[1], Hirofumi Matsuda[1], Jun Miyawaki[2,3], Yoshihisa Harada[2,3], and Eiji Hosono[1]

[1]*Research Institute for Energy Conservation, National Institute of Advanced Industrial Science and Technology*

[2]*Institute for Solid State Physics, The University of Tokyo*

[3]*Synchrotron Radiation Research Organization, The University of Tokyo*

LiNi$_{0.5}$Mn$_{1.5}$O$_4$ (LNMO) is a cathode material for Li-ion batteries (LIBs). The charge-discharge reaction mainly takes place at 4.7 V vs. Li/Li$^+$ which is higher than the redox potentials of typical cathode materials such as LiCoO$_2$, LiMn$_2$O$_4$ and LiFePO$_4$. The redox reaction in LNMO has been believed to take place at the Ni site as Ni^{2+} $\Leftrightarrow$ Ni^{4+}, although such a high oxidation state in Ni should be hardly observed. For Ni K-edge hard X-ray absorption spectroscopy, gradual edge shift accompanied with charging has been confirmed[1], suggesting oxidation reaction of Ni. However, the value of the oxidation state estimated from K-edge absorption spectra should have a large error bar. On the other hand, there are several reports for the Ni $L_{2,3}$-edge soft X-ray absorption spectroscopy (XAS)[2]. Similarly to the K-edge studies, oxidation reaction of the Ni has been observed, but the Ni^{2+} state remained at the charged state in most of the reports. Most likely, the observation of the Ni^{2+} state would come from *ex situ* sample preparation for the soft X-ray experiments. Thus, to accurately clarify the redox reaction, we conducted Ni $L_{2,3}$-edge *operando* XAS.

We have developed *operando* soft x-ray emission spectroscopy (XES) system for LiMn$_2$O$_4$[3] by using ultrahigh-resolution XES spectrometer, HORNET[4] at BL07LSU of SPring-8. The *operando* cell included the LiMn$_2$O$_4$ thin-film cathode, a Li-metal counter electrode and an organic electrolyte solution. In this study, we fabricated LNMO thin-film cathode and applied the same *operando* cell for the Ni $L_{2,3}$-edge *operando* XAS. The thin-film structure is Si$_3$N$_4$ (150 nm)/Al$_2$O$_3$ (5 nm)/Ti (20 nm)/Au (15 nm)/LNMO from the vacuum to the electrolyte side. The Al$_2$O$_3$ layer and Ti/Au multilayer were fabricated by RF sputtering and electron-beam deposition, respectively. The LNMO layer was fabricated by sol-gel method. In order to reduce beam damage on the LNMO thin film, the *operando* cell was slightly shifted to a defocused position from the focal point of the XES experiment. The charge-discharge experiment was carried out by a cyclic voltammetry with a scan speed of 0.5 mV/s.

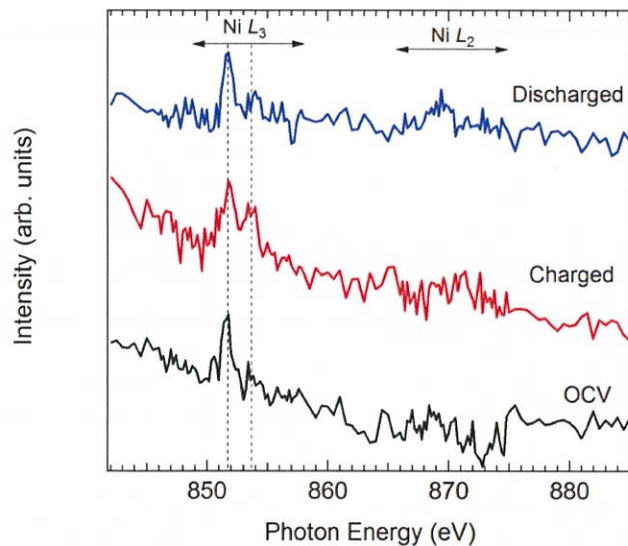Figure 1 shows the Ni $L_{2,3}$-edge *operando* XAS at the open-circuit voltage (OCV) before charging,

Fig. 1. Ni $L_{2,3}$-edge *operando* XAS for LNMO.

charged state at 4.9 V,   and discharged state at 3.0 V. Although the S/N ratio is quite low, the spectrum at the OCV has a main peak at 851.9 eV and a satellite structure centred at 853. 9 eV in the Ni L_3 region, which is attributed to the Ni^{2+} state. For the charged state, the intensity around the satellite is enhanced. In general, an Ni L_3-edge XAS spectrum for higher oxidation state (i.e. 3+ and 4+) than 2+ has a main peak around 2 eV above the main peak[5]. Thus, the Ni should be oxidized at the charged state. However, the peak at 851.9 eV is still high, indicating that a large amount of Ni^{2+} remains. We speculate that the oxidation reaction would be insufficient in this experiment. For the discharged state, the intensity around 853.9 eV became small similarly to the OCV spectrum. Thus at least the redox reaction of Ni should be reversible.

The insufficient oxidation reaction at the charged state might be dependent on the quality of the sample fabricated by a sol-gel method. In the near future, we will prepare an LNMO thin film made with a sputtering method and retry the *operando* XAS. The S/N ratio for XAS should be improved for the new sample, because the adhesion with the multilayer window and the density of LNMO on the window are enhanced by the sputtering method.

References

[1] For example, S. Mukerjee *et al*., Electrochim. Acta **49**, 3373 (2004).
[2] For example, D. Asakura *et al*., AIP Adv. **6**, 035105 (2016).
[3] D. Asakura *et al*., Electrochem. Commun. **50**, 93 (2015).
[4] Y. Harada *et al*., Rev. Sci. Instrum. **83**, 013116 (2012).
[5] Y. Nanba *et al*., Chem. Mater. **28**, 1058 (2016).

MAGNETIC FIELD DEPENDENCE OF RESONANT INELASTIC SOFT X-RAY SCATTERING OF MN$_2$VAL HEUSLER ALLOY WITH HALF METAL-TYPE ELECTRONIC STATE

Rie Y. Umetsu[1], Hidenori Fujiwara[2], Jun Miyawaki[3,4], Kodai Nagai[2], Yasuhiro Nakatani[2] and Shigemasa Suga[5]

[1] *Institute for Materials Research (IMR), Tohoku University*
[2] *Graduate School of Engineering Science, Osaka University, Osaka, Japan*
[3] *The Institute for Solid State Physics (ISSP), The University of Tokyo, Japan*
[4] *Synchrotron Radiation Research Organization, The University of Tokyo, Japan*
[5] *Institute of Scientific & Industrial Research, Osaka University, Osaka, Japan*

Introduction

Some of Mn- and Co-based Heusler-type alloys have been predicted to be half-metallic ferro- or ferri-magnets with the spin polarization of ~100 % around the Fermi energy (E_F) [1-3]. When the electrons are completely polarized around E_F, it is very efficient as a ferromagnetic electrode in various spin dependent devices. For fundamental investigation of the half-metallic materials, researchers have deeply thought how to show a real evidence of the characteristic electronic structure. In this work, we have first studied the detailed electronic structure and magnetic properties of the single crystals of Mn$_2$VAl and Co$_2$MnSi by 1) x-ray absorption spectroscopy (XAS) and 2) magnetic circular dichroism in XAS (XMCD). In addition, further information is obtained by resonant inelastic x-ray scattering (RIXS) measurements of Mn and V $2p$ core excitation for Mn$_2$VAl.

Experiments

a) Sample preparation

Mother ingots of Co$_2$MnSi and Mn$_2$VAl were prepared by induction melting in argon gas atmosphere, and single crystals were prepared by Bridgeman method. The obtained ingots were properly annealed for homogenization and control of the order degree. Crystal orientation was checked by the Laue method and the specimens were cut out in the stripe form with the length of 6 mm along the <100> with 1×1 mm^2 cross section.

b) XAS-MCD

Single crystalline samples were fractured *in situ* in ultrahigh vacuum in order to obtain the clean surface. XAS and XMCD measurements were performed at BL23SU in SPring-8. The spectra were recorded in total-electron-yield mode with an energy resolution better than 0.1 eV. Magnetic fields up to 2 T were applied along the incident photon beam direction by using a superconducting magnet. The measurement was performed at 20 K.

c) SX-RIXS

RIXS experiments were performed at the high-resolution soft x-ray emission station "*HORNET*" at BL07LSU in SPring-8. The specimen was fractured in advance in a separate globe box in Ar gas, and then transferred into the chamber without exposing the sample to the air atmosphere. The RIXS spectra were measured with circularly polarized light at 300 K. A permanent magnet with the field of 0.25 T was installed for MCD measurement [4].

Results

The experimental results of Mn and V $L_{2,3}$ XAS and XMCD spectra of Mn$_2$VAl are shown in Figs. 1(a) and 1(b), respectively [5]. Here, μ^+ (μ^-) denotes the XAS absorption intensity for parallel (antiparallel) alignment of the photon helicity and sample magnetization direction. There are fine structures in the XMCD ($\mu^- - \mu^+$) spectra for both Mn and V $L_{2,3}$ edges. The

spin and orbital magnetic moments were estimated by applying the magneto-optical sum-rule. Those for Mn were 0.27 and 0.005 μ_B/Mn/hole, and for V were -0.15 and 0.005 μ_B/V/hole, respectively. The values are consistent with that obtained by the theoretical calculation based on the density functional theory (DFT). In addition, if we assume $n_h = 5.20$ for Mn and $n_h = 7.39$ for V estimated from the DFT, the magnetic moments of Mn and V will be 2.86 and
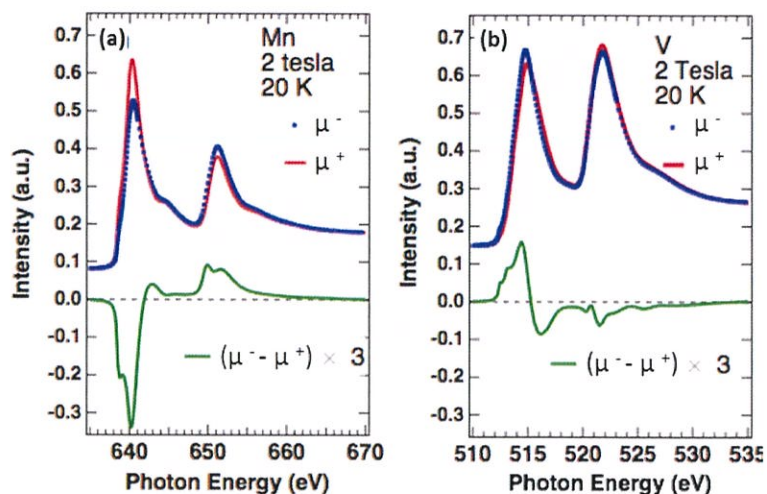
Figures 1. $L_{2,3}$ XAS and XMCD spectra of Mn_2VAl for Mn (a) and V (b) observed at 20 K under the applied magnetic field of 2 T [5].

-1.04 μ_B /f.u., respectively. As shown in the figures, the sign of the XMCD signals is opposite between Mn and V, reflecting ferrimagnetic coupling between them.

Figure 2 show the intensity mapping of the RIXS spectra on the V L-edge excitation by right circularly polarized light as a function of the incident photon energy (hν). The fluorescence components, that depend linearly on the incident photon energy, are observed as indicated by the reference dashed arrows. One can also recognize noticeable intensity around 2 eV of the energy loss corresponding to the d-d excitation. Since V atoms have O_h atomic configuration, the V $3d$ states are split into the t_{2g} and e_g states by the crystal field. From the first principles band calculation, splitting energy between the unoccupied e_g state and the occupied t_{2g} state of the $3d$ electrons on V atom is estimated to be about 3 eV, being in qualitative agreement with the experimental results.

References

[1] R.A. de Groot, F.M. Mueller, P.G.van Engen, K.H.J. Buschow, Phys. Rev. Lett. 50 (1983) 2024-2027.
[2] J.J. Kübler, A.R. Williams, C.B. Sommers, Phys. Rev. B 28 (1983) 1745-1755.
[3] S. Ishida, S. Akazawa, Y. Kubo, J. Ishida, J. Phys. F 12 (1982) 1111-1122.
[4] J. Miyawaki, S. Suga, H. Fujiwara, H. Niwa, H. Kiuchi, Y. Harada, J. Synchro. Rad. 24 (2017) 449-455.
[5] K. Nagai, H. Fujiwara, H. Aratani, S. Fujioka, H. Yomosa, Y. Nakatani, T. Kiss, A. Sekiyama, F. Kuroda, H. Fujii, T. Oguchi, A. Tanaka, J. Miyawaki, Y. Harada, Y. Takeda, Y. Saitoh, S. Suga, and R.Y. Umetsu, Phys Rev. B, submitted.
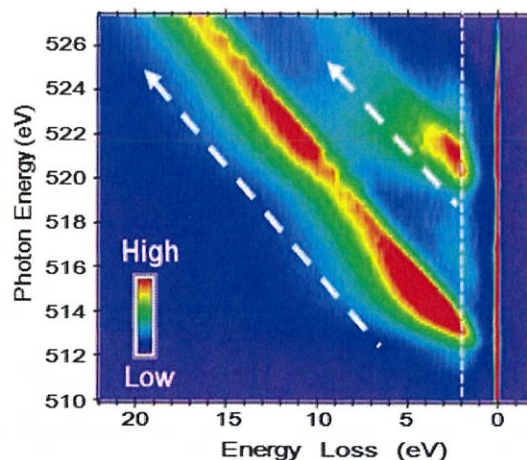
Figure 2. Intensity mapping of the RIXS spectra on the V L-edge excitations by right circularly polarized light as a function of the incident photon energy. The spectra were collected at 300 K and under applied magnetic field of 0.25 T.

DUAL GATE GRAPHENE TRANSISTOR TO REALIZE PINCH-OFF FOR THE REALIZATION OF THZ OPERATION

Keiichi Omika[1], Masato Okada[2], Fuminori Mitsuhashi[2], Yasunori Tateno[2], Tsuyoshi Kouchi[2], Naoka Nagamura[3], Masato Kotsugi[4], Koji Horiba[5], Maki Suemitsu[1], Masaharu Oshima[6], Hirokazu Fukidome[1]

[1]*Research Institute of Electrical Communication, Tohoku University*

[2]*Sumitomo Electric Industries,*

[3]*NIMS*

[4]*Tokyo University of Science*

[5]*KEK/PF*

[6]*University of Tokyo*

Graphene possesses excellent transport properties, such as the highest carrier mobility and saturation velocity. Therefore, a transistor utilizing graphene a channel (GFET) can realize a THz operation at a conventional gate length of 100 nm. We have succeeded in fabricating single-gate GFET whose carrier mobility is 100,000 cm^2/Vs. Furthermore, we obtained the excellent high-frequency charateristics of GFET (cutoff-frequency $\times$ gate-length = 0.04 THz·μm) [1]. However, this value does not the ideal value estimated from the intrinsic transport properties of graphene. Immaturity in fabrication and a contribution from parasitics regions, such as access regions, are the possible reasons for the degradation in the high-frequency characteristics.

In addition to these, the problem is that the pinch-off (drain current) is hardly obtained without fabricating nanoribbon or applying a perpendicular electric field which degrades the carrier mobility and the saturation mobility (Fig. 1).

Fig. 1 Determining factors for high-freqnency characteristics.

To achieve the pinch-off without degrading the carrier mobility and the saturation velocity, we have fabricated the dual-gate GFET (DG-GFET) and studied the operation mechanism of DG-GFET by using 3D nano-ESCA [2-4].

We have proposed DG-GFET, as schematically shown in Fig. 2 (Y. Tateno, H. Fukidome, M. Suemitsu, Japanese patent 2016-058449, US patent 14/844996). The main role of G2 is to suppress the hole production
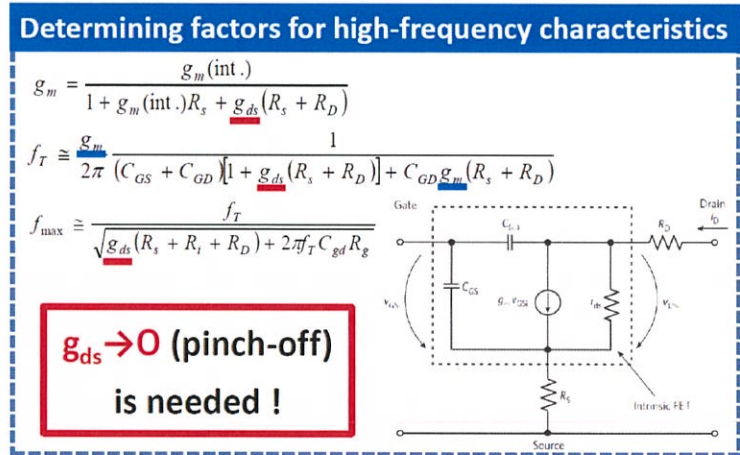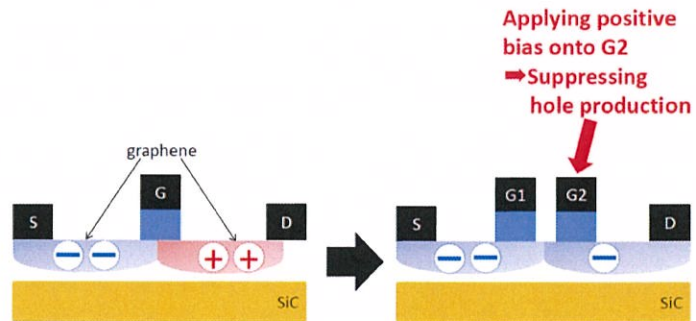

Fig. 2 Schematics of DG-GFET.

(Fig. 2, right), resulting the inhibition of the so-called ambipolar behaviour, which is frequently observed in the single-gate GFET. The simulation results (Fig. 3) demonstrates that DG-GFET exhibits the pinck-off (bottom of Fig. 3), while the pinch-off cannot be obtained for the single-gate GFET (top of Fig. 3)

In fact, DG-GFET fabricated by us exhibited the pinch-off, as shown in Fig. 4. Unfortunately, however, all the devices did not show the pinch-off. One of the possible reasons for this can be an unintentional doping into graphene.

To verify this, we have done the photoelectron nanospectrosopy using 3D nano-ESCA, as shown in Fig. 5. For this verification, we have used the DG-GFET which did not show good electrical characteristics. As a result, graphene in this sample is shown to be unintentionally n-doped. We did a further simulation, and we found that the unintentional doping degrades the DG-GFET device characterisitcs, such as pinch-off and gate-modulation.
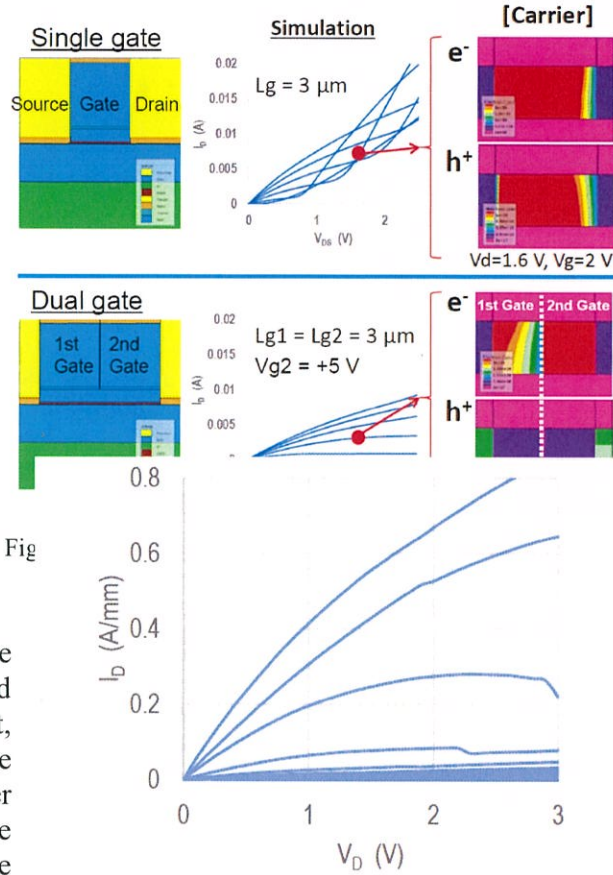
Fig. 4 The drain current (I_D) – Drain voltage (V_D) charcteristics of the DG-GFET fabricated by us.
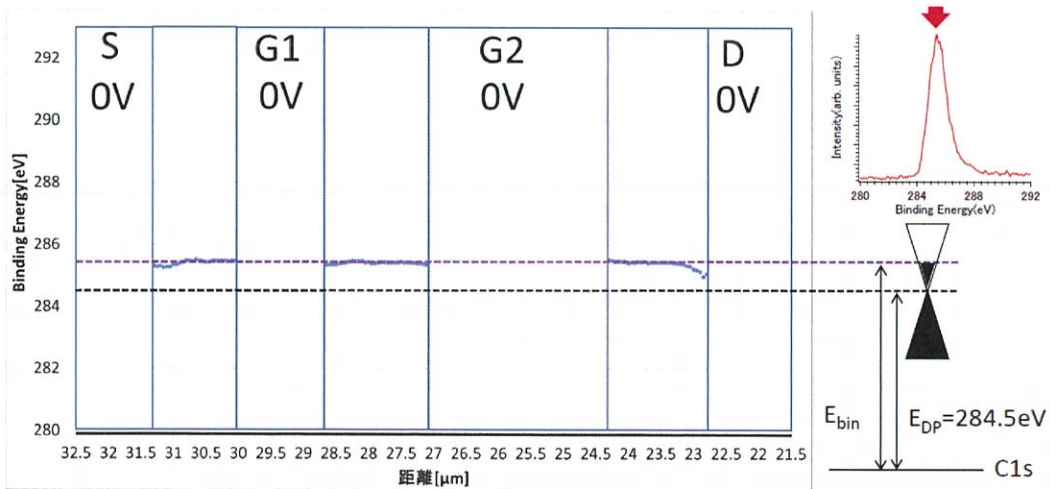

Fig. 5 3D nano-ESCA observation of DG-GFET (line profile of C1s core level).

In conclusion, we have successfully developed DG-GFET that overcome the weak point of GFET, and clarified the degradation mechanism of the DG-GFET device characteristics. From these results, the way to raise up the DG-GFET device characterstics is to suppress the unintentional doping during device processing.

REFERENCES

[1] M.-H. Jung, G.-H. Park, T. Yoshida, H. Fukidome, T. Suemitsu, T. Otsuji , and M. Suemitsu, Proc. IEEE, 101. (2013), pp.1603.
[2] N. Nagamura, K. Horiba, S. Toyoda, T. Kurosumi, T. Shinohara, M. Oshima, **H. Fukidome**, M. Suemitsu, K. Nagashio, and A. Toriumi, Appl. Phys. Lett., 102. (2013), pp. 246104.
[3] **H. Fukidome**, K. Nagashio, N. Nagamura, K. Tashima, K. Funakubo, K. Horiba, M. Suemitsu, and M. Oshima, Appl. Phys. Exp., 7. (2014), pp. 065101.
[4] R. Suto, G. Venugopal. K. Tashima, N. Nagamura, K. Horiba, M. Suemitsu, M. Oshima, and H. Fukidome, Mater. Res. Exp., 3 (2016) pp. 075004.

High energy resolution resonant soft x-ray inelastic scattering study of LaCoO₃ thin films

Yuichi Yokoyama[A,B], Yuichi Yamasaki[C,D], Munetaka Taguchi[E], Yasuyuki Hirata[A,B], Kou Takubo[A], Jun Miyawaki[A], Yoshihisa Harada[A], Daisuke Asakura[F], Jun Fujioka[C], Masao Nakamura[D], Hiroshi Daimon[E], Masashi Kawasaki[C,D], Yoshinori Tokura[C,D], Hiroki Wadati[A,B]

[A]Synchrotron Radiation Laboratory, The Institute for Solid State Physics, The University of TokyoDepartment of Physics, [B]University of Tokyo, Tokyo 113-0033, Japan, [C]Department of Applied Physics and Quantum-Phase Electronics Center (QPEC), University of Tokyo, Hongo, Tokyo 113-8656, Japan, [D]RIKEN Center for Emergent Matter Science (CEMS), Wako 351-0198, Japan, [E]Nara Institute of Science and Technology (NAIST), 89165, Takayama, Ikoma, Nara 630-0192, Japan, [F]Research Institute for Energy Conservation, National institute of Advance Industrial Science and Technology (AIST), Umezono 1-1-1, Tsukuba 305-8568, Japan

Perovskite LaCoO₃ with Co^{3+} ($3d^6$) ion is considered to take high-spin (HS) state with $t_{2g}^4 e_g^2$, intermediate-spin (IS) state with $t_{2g}^5 e_g^1$, and low-spin (LS) state with t_{2g}^6. Since the energy difference between the HS and the LS state is the order of $k_B T$, the spin states of LaCoO₃ may change by external stimuli such as temperature or strain. In bulk single crystals, LaCoO₃ is a nonmagnetic semiconductor at the lowest temperatures, indicating the LS state and the population of the HS state gradually increases as the temperature increases [1]. On the other hand, LaCoO₃ epitaxial thin films are not nonmagnetic even at the lowest temperature. For example, LaCoO₃ thin films grown on $(LaAlO_3)_{0.3}$ $(SrAl_{0.5}Ta_{0.5}O_3)_{0.7}$: LSAT(110) substrates exhibits spontaneous magnetization ($T_c = 94$ K), meaning that the spin state changes from LS state to IS and/or HS by epitaxial strain [2-3]. In LaCoO₃ thin films grown on LSAT(111), another type of spin ordering was reported [4]. Therefore, it is considered that the spin states of LaCoO₃ thin films can be controlled by the orientation of substrates. Then, we investigated the electronic structures directry by high energy resolution resonant soft x-ray inelastic scattering (RIXS).

The LaCoO₃ epitaxial thin films with 30 nm thickness on LSAT(110) and LSAT(111) were fabricated by pulsed laser deposition technique. The tensile strain of the thin films grown on LSAT(110) and LSAT(111) is ~ 1% and ~ 0.5%, respectively. The RIXS measurements of LaCoO₃ thin films and bulk single crystal were performed at BL07LSU HORNET, SPring-8. We used near Co L_3 edge (around 780 eV) as the excitation energy and performed the measurements at 300 K and 40 K. The energy resolution is approximately 300 meV. The incident angle of x-ray is 45°
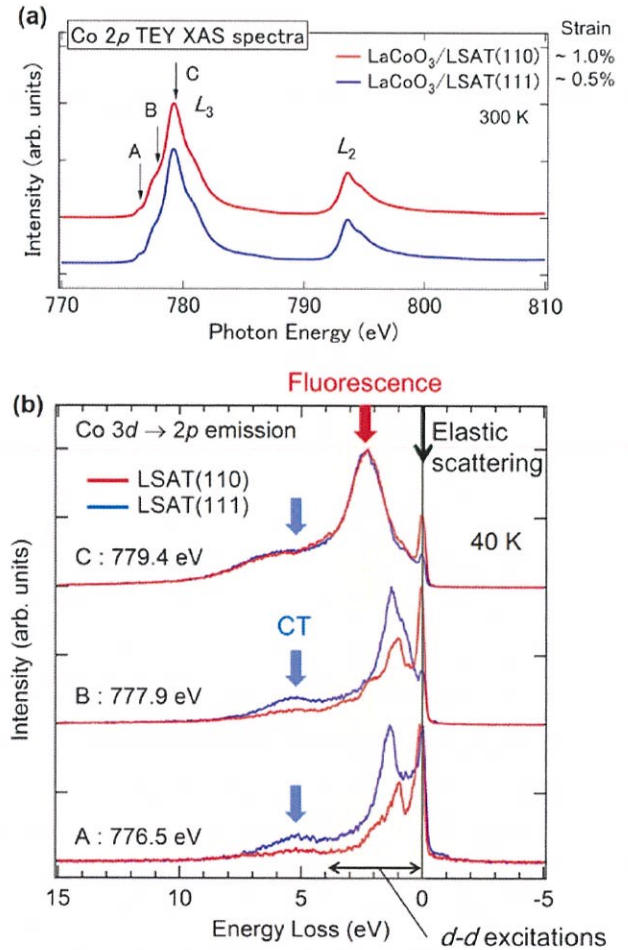

FIG. 1. (a) Co $2p$ TEY XAS spectra. (b) Co $L3$ edge RIXS spectra of LaCoO3 thin films.

relative to the sample surface, while the charge coupled device detector was positioned at 90° relative to the incident x-ray.

Figure 1(a) shows the Co 2p XAS spectra obtained by total electron yield (TEY). The peak ~ 779 eV corresponds to Co L_3 edge, while the peak ~ 794 eV corresponds to Co L_2 edge. Although the tensile strain is different between LSAT(110) and LSAT(111), the spectra is quite similar. Then, we selected the energy A, B, and C as the excitation energy of RIXS and investigated the electronic structures more precisely by RIXS. The Co L_3 edge RIXS spectra are shown in Fig. 1(b). In this figure, the black arrow shows the elastic scattering. The colored zone from 0 to 4 eV corresponds to the dd excitations. And the peak ~ 5 eV is charge-transfer (CT) excitations. From the spectra of A and B, the peaks of dd excitations are different between LSAT(110) and (111), indicating that the spin states change according to the magnitude of the tensile strain. On the other hand, in the spectra of C, the peaks of the

FIG. 2. Co L3 RIXS spectra excited by 776.5 eV and their comparison with the impurity Anderson model calculations.

dd excitations are not clear because of the larger fluorescence. So, we selected the excitation energy of A and compare with the impurity Anderson model calculations. Figure 2 shows the Co L_3 RIXS spectra at 300 K and 40 K excited the energy of A: 776.5 eV. In the bulk and the thin film on LSAT(111), the peak of LS state is observed at 40 K. By increasing the temperature to 300 K, the peak of HS state becomes stronger. On the other hand, a new peak at 0.9 eV is observed in the thin film on LSAT(110). Since the peak dose not correspond to the LS nor HS state, the peak means a new spin state. By comparing the theoretical calculations, the peak is considered to be the HS state in D_{2h} symmetry. We clarified the epitaxial strain induced new spin state realized by 1% tensile strain.
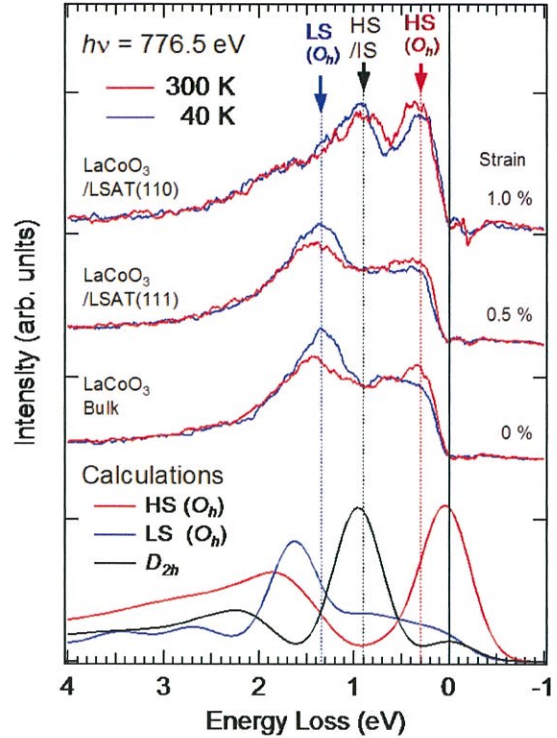
REFERENCES

[1] M. W. Haverkort et al., Phys. Rev. Lett. 97, 176405 (2006).
[2] J. Fujioka et al., Phys. Rev. Lett. 111, 027206 (2013).
[3] Y. Yamasaki et al., J. Phys. Soc. Jpn. 85, 023704 (2016).
[4] J. Fujioka et al., Phys. Rev. B 92, 195115 (2015).

Angular dependences of Fe $L_{2,3}$-edge soft X-ray absorption spectra for LiFePO$_4$ thin-film cathode for Li-ion battery

Daisuke Asakura[1], Takaaki Sudayama[1], Jun Miyawaki[2,3], Yoshihisa Harada[2,3], Hirofumi Matsuda[1], and Eiji Hosono[1]

[1]*Research Institute for Energy Conservation, National Institute of Advanced Industrial Science and Technology*

[2]*Institute for Solid State Physics, The University of Tokyo*

[3]*Synchrotron Radiation Research Organization, The University of Tokyo*

Olivine-type LiFePO$_4$ (LFP) is a typical cathode material for Li-ion batteries (LIBs). The robust poly-anion framework contributes to the stable charge-discharge reaction, resulting in a high cycle performance. The Li-ion diffusion in LFP is one-dimensional along the *b*-axis of the unit cell[1]. In the case of single-crystalline LFP, the Li-ion conduction should be highly oriented. On the other hand, the redox reaction in LFP is ascribed to Fe^{2+}/Fe^{3+} where the Fe t_{2g} orbital for the minority spin plays a major role on the redox reaction[2]. In order to fully understand the redox reaction and Li-ion diffusion in LFP, it is important to investigate whether the anisotropy of the t_{2g} orbital in the slightly deformed FeO$_6$ octahedron is related with the one-dimensional Li-ion diffusion.

Highly-oriented LFP thin films were successfully fabricated on Nb-doped SrTiO$_3$ (Nb:STO) (110) substrates by a sputtering method. Although further crystal-structure analyses for the thin films are needed, studying the angular dependence in X-ray absorption/emission spectra (XAS/XES) is helpful to discuss the anisotropy of the electronic structure. Moreover, *operando* soft X-ray XAS/XES measurements should be powerful to accurately detect the anisotropy for the t_{2g} orbital. We are now constructing an *operando* soft X-ray XAS/XES system for thin-film electrode with solid-state electrolyte. At this stage, we report the angular-dependent XAS results for the as-fabricated thin films.

The XAS experiments were carried out at BL07LSU of SPring-8 varying the polarization (horizontal/vertical) and the incidence angle of the X-rays to the sample (Fig. 1). The Fe $L_{2,3}$-edge XAS spectra were normalized at the pre-edge and post-edge regions.

Figure 2 shows the Fe $L_{2,3}$-edge total-electron-yield XAS spectra for LFP obtained for various geometries. Basically, all the spectra are attributed to the Fe^{2+} high-spin state as previously reported for LFP[3]. For the normal incidence (90°) (Fig. 2(a)), the line shape is almost similar between the horizontal and vertical polarizations while the area intensities of the L_3 and L_2 regions in the case of horizontal polarization are smaller than that in the case of vertical one. Comparing the result for 30° with that for 90° in the case of horizontal polarization (Fig. 2(b)), a clear difference is found at the L_3 main peak (708 eV) while the other parts are almost the same. The decrease of the main peak for the 30° geometry indicates that cross section
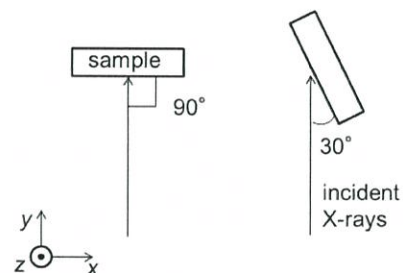

Fig. 1. A schematic picture of the Experimental geometry. The vertical and horizontal polarizations are along the *z*- and *x*-axes in the left figure, respectively.

of the t_{2g} orbitals along out-of-plane direction is smaller than that of the in-plane orbitals.

In the near future, we will perform further X-ray diffraction analyses to more-accurately ascribe the orientation of the thin film and measure the Fe L-edge resonant XES. The development of *operando* XAS/XES experiments with solid-state electrolyte will be continued.
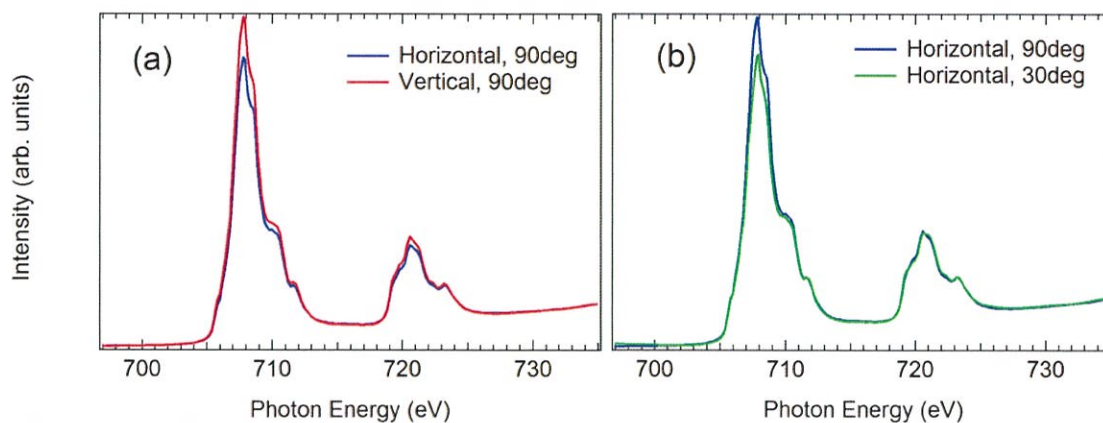

Fig. 2. (a) Polarization dependence for the normal incidence geometry and (b) incident X-ray angular dependence for the horizontal polarization of the Fe $L_{2,3}$-edge XAS results for LiFePO$_4$/Nb:STO(110) thin film.

References

[1] S.-i. Nishimura *et al.*, Nature Mater. **7**, 707 (2008).
[2] A. K. Padhi *et al.*, J. Electrochem. Soc. **144**, 1188 (1997).
[3] For example, X. Liu *et al.*, J. Am. Chem. Soc. **134**, 13708 (2012).

OBSERVATION OF PHOTO-INDUCED VALENCE TRANSITION IN $EuNi_2(Si_{1-x}Ge_x)_2$ WITH TIME-RESOLVED X-RAY ABSORPTION SPECTROSCOPY

Yasuyuki Hirata, Yuichi Yokoyama, Kohei Yamamoto, Kou Takubo, Hiroki Wadati
Synchrotron Radiation Laboratory, The Institute for Solid State Physics, The University of Tokyo

Kojiro Mimura
Department of Mathematical Sciences, Graduate School of Engineering, Osaka Prefecture Univeristy

Ultrafast optical control of charge and spin states in materials is one of the hottest topics of spintronics and information processing technologies. A number of studies on such control with a high intensity femtosecond visible-infrared laser have been reported. One example is all-optical helicity-dependent switching in Gd-Fe-Co intermetallics, where the magnetization is selectively reversed by the irradiation of circularly polarized laser.[1] Another is light-induced superconductivity (SC) in a stripe-ordered cuprate, $La_{1.675}Eu_{0.2}Sr_{0.125}CuO_4$ [2].

Here we focus on yet another type of phase transition: the valence transition in rare-earth intermetallics. The mixed valence transition in $EuNi_2(Si_{1-x}Ge_x)_2$ has been extensively studied, and a lot of interesting phenomena have been reported such as temperature-, magnetic field- and pressure- induced valence transitions [3-5]. For example, the mean valence of the Eu ion in $EuNi_2(Si_{0.21}Ge_{0.79})_2$ changes from nearly trivalent (~2.85) in the low temperature phase to nearly divalent (~2.25) in the high temperature phase, across the critical temperature (Tv) of ~ 84 K. Laser illumination can increase electron temperature up to ~ 1000K, which is expected to create novel electronic structures.

In order to unravel the valence dynamics of $EuNi_2(Si_{1-x}Ge_x)_2$, time-resolved x-ray absorption spectroscopy (TR-XAS) is the most powerful method because it can give us the information of valence states of constituent elements by using absorption edges. Figure 1 shows the preliminary results of static Eu $3d$-$4f$ XAS measurements with the total electron yield (TEY) method and the total fluorescence yield (TFY) method obtained in BL07LSU. From the comparison with atomic mutiplet calculations for the Eu^{2+} and Eu^{3+} free ions, we can identify the structure at1128-1129 eV is from Eu^{2+} and 1130-1131 eV is from Eu^{3+}. The TFY spectra were distorted due to the well-known saturation effects because this material does not have enough absorber, that is, elements with higher atomic number than Eu.
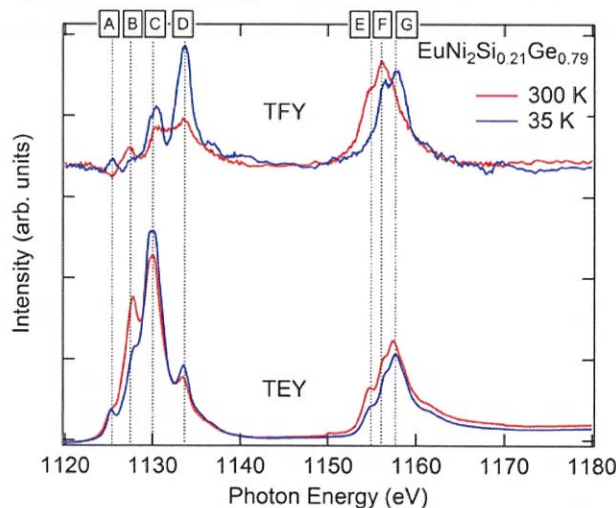

Figure 1. Static XAS spectrum of $EuNi_2(Si_{0.21}Ge_{0.79})_2$. with the total fluorescence yield (TFY) method and the total electron yield (TEY) method

We have performed TR-XAS measurement on $EuNi_2(Si_{1-x}Ge_x)_2$ with the partial electron yield (PEY) mode using the TR- resonant soft x-ray scattering system connected to the free-port station of BL07LSU.[6] A bulk polycrystalline $EuNi_2(Si_{0.21}Ge_{0.79})_2$ was fractured in vacuum and mounted on the sample manipulator. The femto-second Ti:Sapphire laser with the wavelength of 800 nm and the repetition rate of 1 kHz was irradiated on the sample as a pumping light. The photo-electrons produced on the sample by the probing soft x-ray with the energy of 1129 eV or 1131 eV were collected by a micro channel plate (MCP) detector. The measurement was done at the temperature $T = 30$ K.

Figure 2 shows the delay-time dependence of the normalized deviation of XAS intensity of Eu 3d-4f edge under the laser fluence of 10 mJ/cm^2. While XAS is suppressed by pumping laser with the probing x-ray energy of 1131 eV (a characteristic energy of Eu^{3+} ions), with the probing x-ray energy of 1129 eV (a characteristic energy of Eu^{2+} ions) XAS is enhanced by pumping laser. Both consistently suggest the photo-induced valence transition of Eu ion from 2.85+ to a lower valence. The rising time of the delay-scan coincides with the time resolution (50 ps), which indicates the time-scale of the valence transition is shorter than 50 ps.

In conclusion, we have carried out TR-XAS measurement on mixed-valent $EuNi_2(Si_{1-x}Ge_x)_2$ with PEY mode, and successfully observed the photo-induced valence transition. In the near future we will examine the laser fluence dependence of the transient response, the XAS energy spectrum at each delay-time, and the bulk-sensitive measurement with TFY mode to clarify the nature of the photo-induced valence transition. In order to reveal the rising behavior of the transition with the time-scale shorter than 50 ps, we also plan experiments using x-ray free electron lasers.
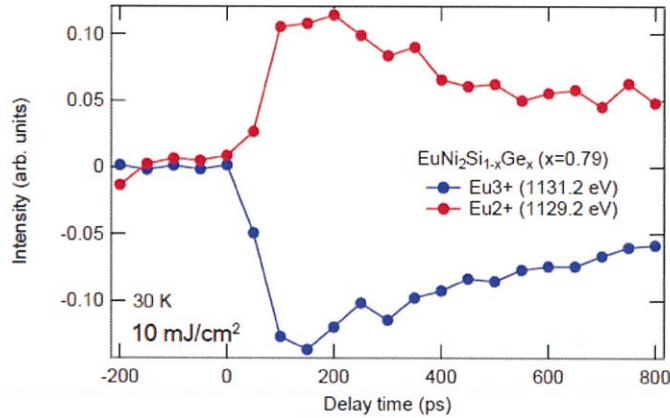
Figure 2. The delay-time dependence of the normalized deviation of the XAS intensity.

REFERENCES

[1] C. D. Stanciu *et al.*, Phys. Rev. Lett. 99, 047601 (2007).
[2] D. Fausti *et al.* Science 331, 189 (2011).
[3] H. Wada *et al.*, J. Phys.: Condens. Matter **9**, 7913 (1997).
[4] H. Wada *et al.*, Phys. Rev. B **59**, 1141 (1999).
[5] K. Yamamoto *et al.*, Physica B 378-380, 681 (2006).
[6] K. Takubo *et al.*, App. Phys. Lett. **110**, 162401 (2017).

ANALYSIS OF STRUCTURES AND ELECTRONIC STATES BY MICROSCOPIC HIGH ENERGY RESOLUTION PHOTOELECTRON DIFFRACTION

Hiroshi Daimon*, Hiroki Momono, Yusuke Hashimoto, Shun Fukami, Yudai Higa, Xin Liang Tan, Hiroyuki Matsuda, Munetaka Taguchi

*Graduate School of Materials Science, Nara Institute of Science and Technology

The main purpose of our study at BL07LSU is to develop and establish the experimental methods for structural and electronic states studies by using two-dimensional microscopic photoelectron diffraction spectroscopy, so-called DELMA [1-3]. We have so far developed a two-dimensional display-type ellipsoidal mesh analyzer (DELMA), which is composed of a wide acceptance angle electrostatic lens (WAAEL) unit, a transfer lens system and a high energy electron analyser (VG SCIENTA R4000) at SPring-8 BL07LSU [1]. In this year, we introduced a cryogenic two-stage 4K cryo-cooler and a new manipulator for a cooling system, making low temperature measurement of a photoelectron diffraction possible. Furthermore, we changed a trestle of DELMA to make it more stable. As a result, DELMA, which has been under development since 2009, is nearly complete and we have started a full-fledged electronic state measurements and the photoelectron holography measurements in low temperature regions (down to about 60 K).

In 2016B beam-time, the photoelectron diffraction measurements of magnetite Fe_3O_4 and a resonant photoemission spectroscopy measurement of Bi-based copper oxide high temperature superconductor $Bi_2Sr_2CaCu_2O_x$ (Bi-2212) were carried out.

For Fe_3O_4, a site resolved core-level x-ray photoelectron spectroscopy (XPS) measurement was attempted by using the photoelectron diffraction technique. The formula of magnetite is written as $Fe_A^{3+}[Fe_B^{3+}Fe_B^{2+}]O_4$ to reflect the fact that the A-sites are occupied by Fe^{3+} and the B-sites are occupied by equal number of Fe^{2+} and Fe^{3+}, thus resulting in an inverse spinel structure. The A-sites are tetrahedrally coordinated to oxygen and the B-sites are octahedrally coordinated to oxygen. Although a usual XPS measurement cannot separate these two sites, we attempted the site separation of XPS spectra with special attention to the forward focusing peaks (FFPs) present in the photoelectron diffraction pattern (see Figure 1). By selecting the characteristic FFPs directions and measuring the photon energy dependence of the FFPs intensity, we succeed in separating the each Fe contributions (A-site and B-site) from the x-ray photoelectron spectra of magnetite.

For Bi2212, the valence band measurement at the oxygen K absorption edge and its polarization dependence measurements were carried out. Usually, resonant photoelectron spectroscopy of a transition metal compound increases the spectral intensity in the vicinity of the Fermi level by resonating at the L or M absorption edge of the transition metal. However, since a lower Hubbard d-band exists at a high binding energy position considerably deeper than the Fermi level in the charge-transfer type insulator such as cuprates, it is impossible to increase the spectral intensity near the Fermi level. In order to overcome this problem, we tried to measure the electronic state near the Fermi level by resonating at the oxygen K absorption edge. Experiments were performed using x-rays of linearly polarized light at the incidence direction parallel (P-polarized) and perpendicular (S- polarized) to the CuO_2 plane. Surprisingly, we observed a large polarization dependence and obtained an unexpected result. When the P-polarized light (the electric vector is perpendicular to the CuO_2 plane) was incident, the intensity near the Fermi level increased (see Fig. 2). This fact indicates the existence of oxygen $2p_z$ orbital near Fermi level with significant weights.
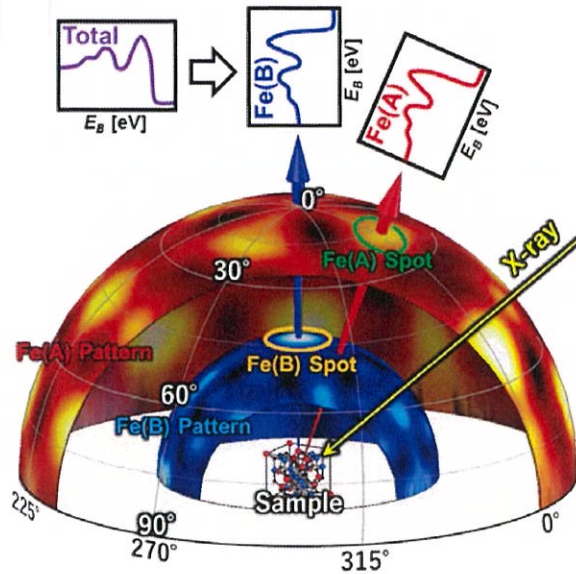
Figure 1.   Schematic view of the site resolved XPS for Fe₃O₄
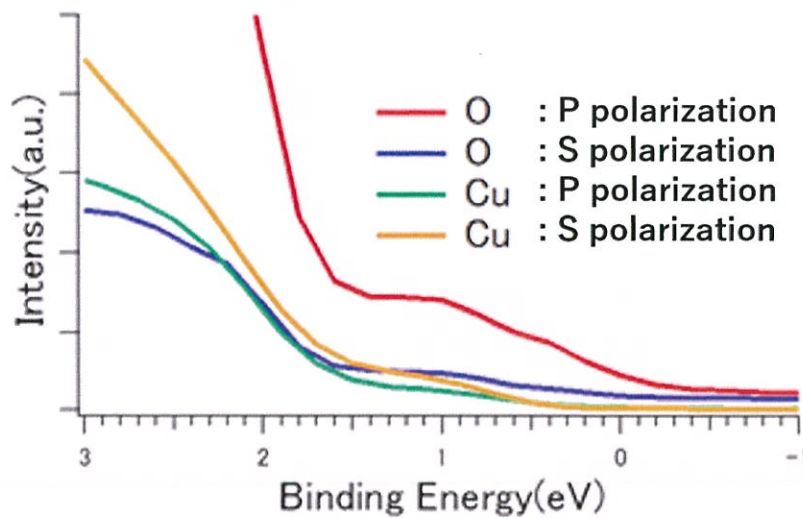
Figure 2. Resonant photoelectron spectra at O *K*-edge and Cu *L*-edge for Bi2212

REFERENCES

[1] L. Tóth, *et al.*, J. Vac. Soc. Jpn. **51**, 135 (2008).
[2] K. Goto, *et al.*, e-J. Surf. Sci. Nanotech. **9**, 311-314 (2011).
[3] L. Tóth, *et al.*, Nucl. Inst. Meth. Phys. Research Sec. A **661**, 98-105 (2012).

CARBONATE IONS
STUDIED IN HIGH-RESOLUTION RIXS

Victor Ekholm[1], Minjie Dong[1], Johan Gråsjö[1], Jun Miyawaki[3],
Yoshihisa Harada[3], Jan-Erik Rubensson[1]

[1]*Department of Physics and Astronomy, Box 516, SE-751 20 Uppsala, Sweden*
[2] *Department of Pharmacy, Uppsala University, Box 580, SE-751 23 Uppsala, Sweden*
[3]*RIKEN/SPring-8 Sayo-cho, Sayo, Hyogo 679-5148, Japan*

Resonant inelastic X-ray scattering spectra of carbonate ions in various environments were measured. It has earlier been demonstrated that RIXS spectra of carbonate ions (CO_3^{2-}) in aqueous solution can be measured at the oxygen K edge by means of selective excitation [1]. Here we use the high-energy resolution at the HORNET end station of BL07LSU [2] to investigate vibrational excitations. The carbonate ion is planar with D_{3h} symmetry, seemingly in conflict with the Lewis structure, which requires one short double and two longer single bonds. This conflict is solved by the concept of resonance between the three possible double bond sites. The symmetry may (dynamically) break in various chemical surroundings, and by electronic-vibronic coupling during the scattering process. The prospect that double bond dynamics during the fast scattering process were reflected in vibrationally resolved RIXS was one of the major motivations for the investigations.
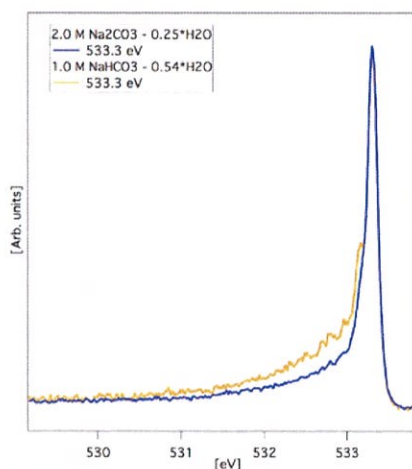

Fig. 1. RIXS spectra excited at the carbonate resonance just below the H_2O edge

In Fig. 1 we show vibrational progressions in the RIXS spectra of the CO_3^{2-} ion compared to the bicarbonate ion, HCO_3^-. It is immediately obvious that additional vibrational intensity is observed in the bicarbonate spectrum, as compared to the carbonate spectrum. Note that here the –C=O bond is selectively excited, and although O-H vibrations are found at larger energy losses, the hump at 533 eV in the bicarbonate spectrum is dominated by –C=O vibrations. We tentatively attribute the spectral difference to the difference in symmetry, and that the vibrations in the carbonate ion may be due to a symmetric stretch vibration.

A comprehensive data set was recorded showing, and we also compared the spectra to carbonate ions in Upsalite, a new mesoporous $MgCO_3$ material with properties that are investigated by several methods [3].

It is found that carbonate RIXS spectra show a drastic dependence on the chemical environment, both regarding the electronic and vibrational excitation. Variation of excitation energy and polarization of the incident radiation leads to a rich phenomenology, which is now being analyzed in collaboration with our theory partners.

REFERENCES

[1] Horikawa, Y., Yoshida, A., Takahashi, O., Arai, H., Tokushima, T., Gejo, T., & Shin, S. (2014). *Journal of Molecular Liquids*, *189*, 9–12. http://doi.org/10.1016/j.molliq.2013.06.021
[2] Yoshihisa Harada, Masaki Kobayashi, Hideharu Niwa, Yasunori Senba, Haruhiko Ohashi, Takashi Tokushima, Yuka Horikawa, Shik Shin, Masaharu Oshima. (2012). Review of Scientific Instruments 83:1, 013116.
[3] Forsgren J, Frykstrand S, Grandfield K, Mihranyan A, Strømme M (2013). PLoS ONE 8(7): e68486. doi:10.1371/journal.pone.0068486

Unraveling the synergic effect between Ni and Mn during the water oxidation reaction of nickel and manganese-based oxides by 2p3d RIXS

M. al Samarai [1], A. Hahn [1], O. Rüdiger [1], J. Miyawaki [2], Y. Harada [2], S. DeBeer [1]

[1] Max Planck Institute for Chemical Energy Conversion, Stiftstrasse 34−36, 45470 Mülheim an der Ruhr, Germany
[2] Institute for Solid State Physics, The University of Tokyo, Kashiwa, Chiba 277-8581, Japan

Introduction:

Splitting of water by utilization of sunlight is a clean and sustainable solution to reduce the environmental issues caused by the emission of fossil fuels. However, to realize an efficient solar induced water oxidation cycle, a highly active water oxidation catalyst is required. Within this context, in recent years, manganese-oxide-based systems have been widely investigated for photochemical reactions [1-4].

However, in order to meet the required specifications, there is an increased need to understand the catalytic background and improve the activity and stability of the catalysts. By increasing our knowledge about the morphology, dispersion, and electronic structure of elements involved in the catalytic active phase, we will be able to design and make better catalyst materials for the water oxidation reaction.

We planned to study the role of Ni during the operando electrochemical oxidation of water by the graphene supported Ni_6MnO_8 system by measuring the Ni 2p3d RIXS. This powerful technique in combination with 2p XAS can determine the accurate strength of the 3d spin−orbit coupling, distortions in symmetries, and superexchange interactions, leading to predictions of the strengths of these effects interactions.

Samples, experiment method, equipment used, experiment/measurement conditions

In the first stage of the beamtime Ni 2p3d TEY XAS of both NiO reference and the fresh (Dry) Ni_6MnO_8/ Graphene sample were measured. The NiO reference sample was placed on carbon-tape while the Ni6MnO8 catalyst sample was first dispersed in ethanol solution and after sonication step drop-casted on a Au-coated Si_3N_4 membrane. Measuring the aforementioned samples was necessary as it give us the opportunity to understand the moiety of the nickel oxide species in the active phase.

Au-coated Si_3N_4 membrane Thickness~ 150 nm   In-situ holder for Liquid phase experiments   Fully assembled In-situ holder
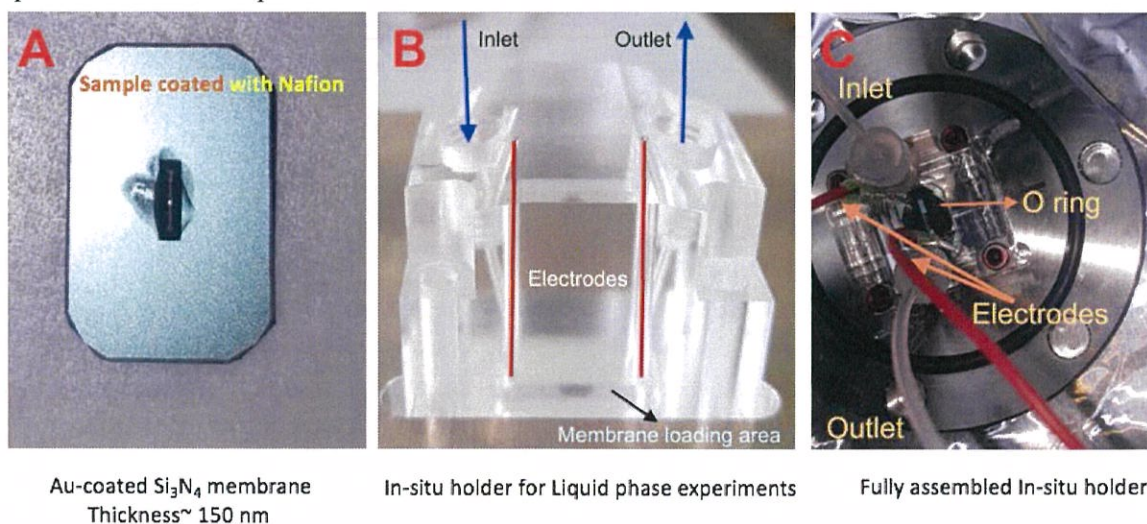
Figure 1: Overview of the applied Si_3N_4-membrane (A) and the assembled sample-holder used for the in-situ water oxidation experiments (B and C).

For the in-situ reaction the loaded Si_3N_4 membrane was loaded in a specially designed holder for liquid phase reactions as shown in Figure 1. The holder of this electrochemical cell is leak-tight and allows for both continuous flow of water while and application of current for electrochemical reaction.

During the subsequent steps the reactor was filled with the liquid cell is filled with 0.1 M KOH solution and the changes in the Ni-oxide compounds was measured by Ni 2p3d RIXS. During this in-situ reaction the fresh sample was firstly wetted without applying a potential (0 V), while during the subsequent steps the sample was gradually treated at higher potentials: 0.52 V, 1.25 V, and 1.65 V.

Results:

The obtained Ni L_3 spectra for the NiO and the fresh Ni_6MnO_8/Graphene are shown in Figure 2.

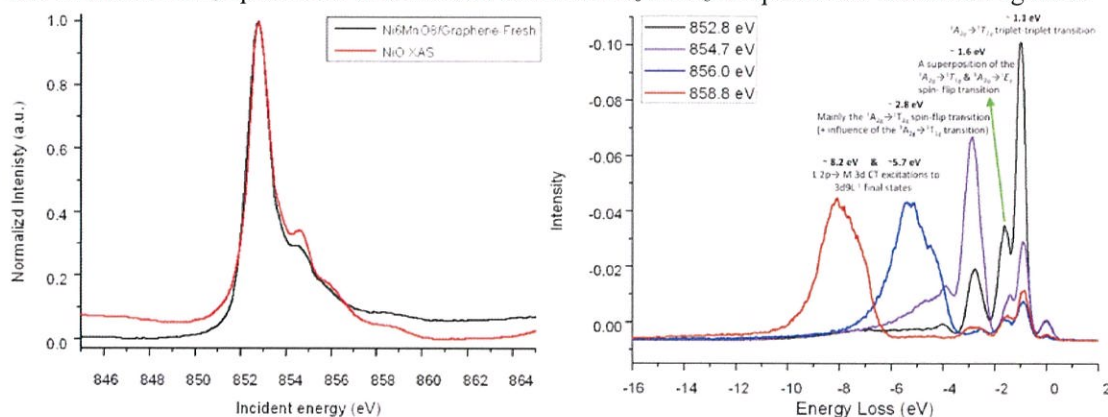**Figure 2: A) Ni L₃ edge XAS (TEY) of the NiO reference sample (in black) and Ni6MnO8/Graphene (in red). B) Ni 2p3d energy loss RIXS of the NiO reference sample with a summary of the assigned origins of the observed Energy loss features.**
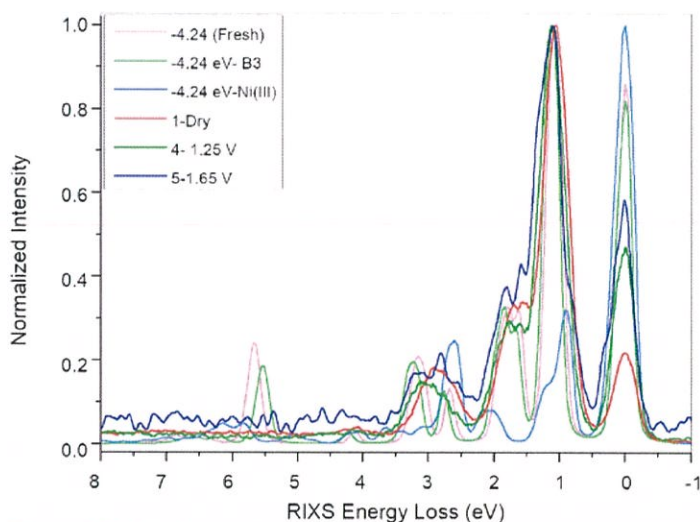
Figure 3: Multiplet simulation of Ni 2p3d RIXS for the 852.8 eV (-4.24 eV) emission slice. The first three spectra are the calculated counterparts of the three experimental spectra at the bottom of the figure legend.

Conclusions:

Nickel in the fresh(dry) Ni6MnO8/Graphene sample has a Ni(II) character in Oh symmetry resembling that of Ni in NiO compound. After the electrochemical oxidation, the Ni$^{(II)}$ component is partially transformed into Ni^{2+} species with larger CF (10Dq) parameter. Also, part of Ni(II) sites are oxidized to Ni(III). We suggest that the catalytic active species is a Ni(III) OOH species that is formed by application of potentials at basic pH conditions.

Time-resolved X-ray photoemission study on the WSe$_2$ surfaces

Ro-Ya Liu[1], Kenichi Ozawa[2], Naoya Terashima[3], Yuto Natsui[3], Baojie Feng[1], Suguru Ito[1], Wei-Chuan Chen[4], Cheng-Maw Cheng[4], Susumu Yamamoto[1], Tai-Chang Chiang[5], Iwao Matsuda[1]

[1]*Institute for Solid State Physics, The University of Tokyo, Japan*

[2]*Department of Chemistry and Materials Science, Tokyo Institute of Technology, Japan*

[3]*Department of Advanced Physics, Hirosaki University, Japan*

[4]*National Synchrotron Radiation Research Center, Taiwan*

[5]*Department of Physics, University of Illinois at Urbana-Champaign, USA*

Recently, two-dimensional devices based on transition metal dichalcogenides (TMDs) have attracted attentions and interests of the condensed matter community. WSe$_2$ is a member of a vast family of TMDs and it has a crystal structure of a periodic stack of the Se-W-Se trilayers in a 2H motif [1]. The material has been known to be suitable for the solar cell devices due to its high optical absorption coefficient in IR and visible light regions. Electron-hole carriers, generated by photon excitation, and its dynamics, such as the carrier density, surface photovoltage (SPV), carrier relaxation time …etc., are important references for designing the TMDs based solar cells and heterojunction transistor devices. However, the SPV effect in WSe$_2$ has not been examined in detail to find the critical factors in the opto-electronic performance. Moreover, the surface has left the possible optimization by atom/molecule adsorptions. Thus, it has been highly called for to extensively study surface/interface electronic states, carrier dynamics and their relationships. By measurements of time-resolved x-ray photoemission spectroscopy (TRXPS), we investigated the carrier dynamics at a surface of WSe$_2$ during the SPV change.

The TRXPS experiment was carried out at the synchrotron radiation (SR) beamline BL07LSU at SPring-8. The laser-pump and SR-probe method was performed with the pulse durations of ~ 35 fs and 50 ps for the laser and SR light pulse, respectively [2]. Pump light (h ν =1.55 eV) was generated by an amplified Ti:sapphire laser pulse with the repetition rate of 208 kHz. Photon energy of the pump just exceeds the indirect band gap (1.3 eV) and it was close to the optical absorption peak of the exciton (1.59 eV).

The SR light pulses (h ν =253 eV) were delivered by the several bunch mode (F-mode) with the time interval of 342 ns. In the present research, we made the TRXPS experiments on a surface of WSe_2 and also on surfaces after depositions of potassium (K) atoms and fullerene (C_{60}) molecules.

Figure 1 shows an example of the TRXPS data of the W $4f_{7/2}$ core-level on the K/WSe_2 surface. After the optical pumping, the energy position shifts to the lower binding energy and recovers to the original one after the delay time of ~ 10 ns. The temporal changes were also measured on the pristine and the C_{60}-covered WSe_2 surfaces. It was found, from the comparisons, that the SPV relaxation time becomes short by formation of the heterojunctions, K/WSe_2 and C_{60}/WSe_2. The electronic states of the overlayers likely become the new recombination centers of photo-excited carriers.
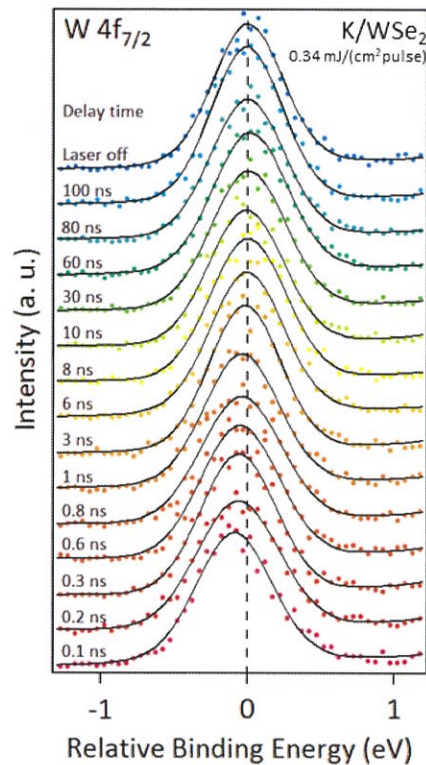

Fig. 1 A collection of the TRXPS spectra on the K/WSe_2 surface taken at different delay time

References

[1] A. Jakubowicz, D. Mahalu, M. Wolf, A. Wold, R. Tenne, Phys. Rev. B **40**, 2992 (1989)

[2] M. Ogawa, S. Yamamoto, Y. Kousa, F. Nakamura, R. Yukawa, A. Fukushima, A. Harasawa, H. Kondo, Y. Tanaka, A. Kakizaki, and I. Matsuda,. Rev. Sci. Instrum. **83**, 23109 (2012).

DETAILED ANALYSIS OF SPIN-POLARIZATION OF PHOTOELECTRONS FROM 1D BI/INSB(001) SURFACE STATES

Yoshiyuki Ohtsubo[1,2], Jun-ichiro Kishi[2], Ayumi Harasawa[3], Koichiro Yaji[3].
Shik Shin[3], Fumio Komori[3], Shin-ichi Kimura[1,2]

[1]Graduate School of Frontier Biosciences, Osaka University
[2]Department of Physics, Graduate School of Science, Osaka University
[3]The Institute for Solid State Physics, The University of Tokyo

Electronic states with Dirac-cone (DC)-like very steep dispersion is one of the hottest topics in solid state physics in these days [1, 2]. Among them, one-dimensional (1D) or quasi-1D (Q1D) DC-like states with spin polarization, such as surface states on vicinal Bi single crystals [3] gather much attention because the backscattering in the (Q)1D states is expected to be suppressed in higher efficiency than those of 2D DCs [4]. Such feature is attractive for future application to energy-saving and high-speed spintronic devices [5].

In this work, we have studied the Q1D surface electronic structure and its spin polarization of ultrathin Bi films grown on InSb(001) substrates. About this Q1D surface state, we have already reported its DC-like steep dispersion and spin polarization [6, 7]. This year, we observed the spin-polarized structure of photoelectrons from the Q1D states on Bi/InSb(001) more in detail in order to provide further insight for the future application to spintronics. The spin polarizations of photoelectrons were observed by the spin- and angle-resolved photoelectron spectroscopy using a laser (laser-SARPES) [8] at the Institute for Solid State Physics (ISSP). The InSb(001) substrate was cleaned by the repeated cycles of Ar sputtering and annealing and the following evaporation of Bi up to ~10 atomic layers resulted in the Q1D Bi/InSb(001) surface.

Figure 1 shows the spin-resolved momentum distribution curves (MDCs) along [110] (parallel to the DC-like steep dispersion). Spin polarizations along S_x ([1-10], Fig. 1 (a), (d), (g)) shows two separate peaks with its spin polarization orientations and inverts with respect to $k_{//[110]} = 0$ Å^{-1}. These peak positions correspond to the DC-like dispersion of the Q1D surface state observed by spin-integrated ARPES [6, 7]. These characteristics are the same in any $k_{//[1-10]}$ positions (wave vectors normal to the DC-like dispersion). Moreover, the same trend is observed even above the Fermi level (E_F) at room temperature as shown in Fig. 1 (j), (k). Thanks to the thermal broadening of the Fermi distribution function, we could observe the photoelectrons from the Q1D states above E_F. The spin-polarized MDC peaks also correspond to the band dispersions observed by spin-integrated ARPES and its spin polarization orientations along S_x is the opposite to those of the states below E_F. These features are consistent with the nearly 1D surface atomic structure as well as the surface-band dispersion [6, 7].

Along the other orientations (S_y : [110] and S_z : [001]), the polarizations are almost negligible at $k_{//[1-10]} = 0$ Å^{-1} but become evident at the other positions. However, the polarizations along S_y does not correspond to the surface band dispersion indicated by the peak positions of MDCs with S_x spin polarizations. On the other hand, Spin polarization towards S_z becomes prominent at $k_{//[1-10]} = -0.3$ Å^{-1} but almost negligible at $k_{//[1-10]} = +0.3$ Å^{-1}. These strange spin polarizations along S_y and S_z cannot be explained solely from the spin polarization of the initial states and it would be due to the photoexcitation process, so-called final-state effect. Recently, some reports were published telling that the spin polarization of photoelectrons from surface states strongly depends on the polarization (in other words, parity) of the incident photons [9, 10]. As shown in Fig. 1 (l), we changed the polar angle of the substrate for different $k_{//[1-10]}$ points. So, the in-plane (out-of-plane) component of the electric field of the incident photons becomes dominant for positive (negative) wavenumbers. The drastic change of the S_z spins might be due to these different incident electric field.

In summary, we have studied the spin polarization texture of the photoelectrons from the Q1D surface states on Bi/InSb(001) in detail by using laser-SARPES. The spin-polarization structure along S_x indicated the Q1D spin-polarized structure along the steep DC-like dispersion of the surface states. The spin polarizations along the other directions (S_y and S_z) were sensitive to the photoemission experimental geometries, suggesting that the spin polarizations along these orientations are due to the photoemission final-state effect.

These results were summarized together with the results obtained last year and have been already submitted [7].
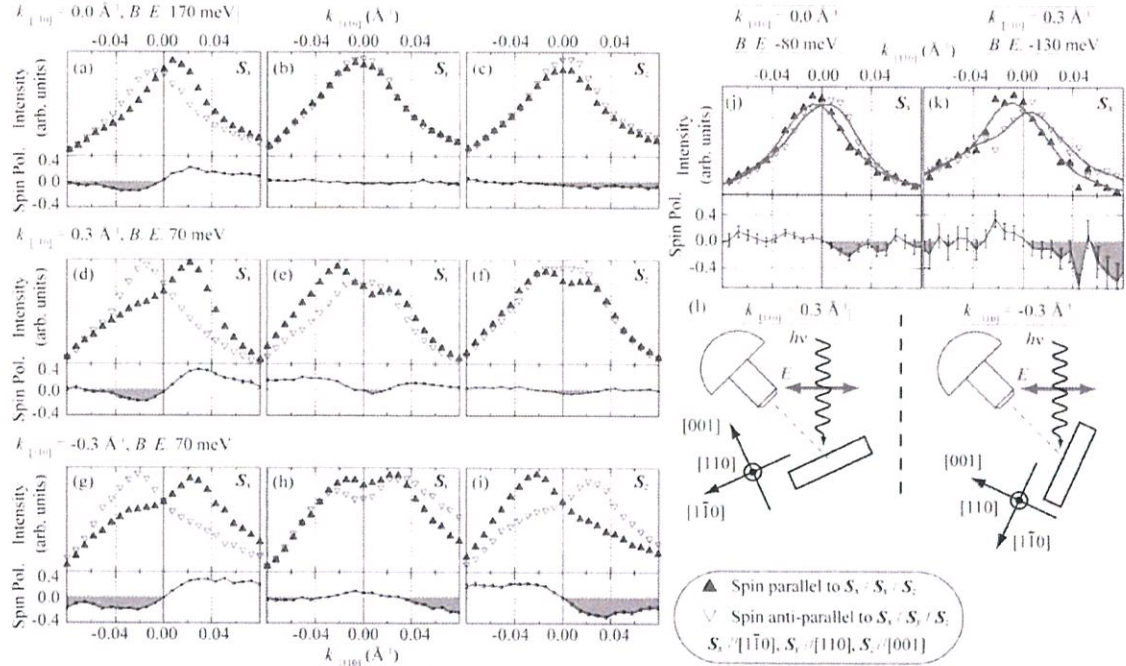

Figure 1: Spin-resolved momentum distribution curves (MDCs) along the DC-like steep dispersion ([110]) of the Bi/InSb(001) surface state at room temperature with a linearly polarized laser ($h\nu$ = 6.994 eV). Binding energies and the wave vectors normal to the DC-dispersion ([1-10]) are shown. Solid curves in (j) and (k) are smoothed curves of MDCs provided as visual guides. (l) Schematics of the laser-SARPES experimental geometries.

REFERENCES

[1] A. K. Geim and K. S. Novoselov, Nature Mat. **6**, 183 (2007).

[2] M. Z. Hasan and C. L. Kane, Rev. Mod. Phys. **82**, 3045 (2010).

[3] J. W. Wells *et al.*, Phys. Rev. Lett. **102**, 096802 (2009).

[4] G. Autès *et al.*, Nature Mat. **15**, 154 (2016).

[5] A. Manchon *et al.*, Nature Mat. **14**, 871 (2015).

[6] "Spin polarization of 1D surface state on Bi/InSb(001)" J. Kishi *et al.*, Activity Report of Synchrotron Radiation Laboratory 2015

[7] J. Kishi *et al.*, *submitted.* (arXiv: 1704.05258 (2017)).

[8] K. Yaji *et al.*, Rev. Sci. Instrum. **87**, 053111 (2016).

[9] C. Jozwiak *et al.*, Nature Phys. **9**, 293 (2013).

[10] K. Yaji *et al.*, Nature Commun. **8**, 14588 (2017).

OBSERVATION OF INTRINSIC ELECTRONIC STATES OF HALF-METALLIC FERROMAGNETS STUDIED BY BULK-SENSITIVE HIGH-RESOLUTION SPIN-RESOLVED PHOTOEMISSION SPECTROSCOPY

Hirokazu Fujiwara,[1] K. Terashima,[2] M. Sunagawa,[1] T. Nagayama,[1] K. Yaji,[3] A. Harasawa,[3] K. Kuroda,[3] T. Wakita,[2] Y. Muraoka,[1,2] and T. Yokoya[1,2]

[1]*Graduate School of Natural Science and Technology, Okayama University, Okayama 700-8530, Japan*

[2]*Research Institute for Interdisciplinary Science, Okayama University, Okayama 700-8530, Japan*

[3]*Institute for Solid State Physics, University of Tokyo, Kashiwa, Chiba 277-8581, Japan*

Half-metallic ferromagnet is a key material for spintronics devices because of its 100 % spin polarization of the density of states (DOS) at the Fermi level (E_F).[1] Chromium dioxide, CrO_2, has the highest spin polarization obtained by point-contact Andreev reflection measurements at low temperature.[2] However, magnetoresistance studies using magnetic tunneling junctions reported that the spin polarization exponentially decreases with increasing temperature and, as a result, CrO_2 behaves as 'normal' ferromagnetic metal above 50–100 K.[3,4] The magnitude of the spin depolarization is much greater than that of magnetization measured by SQUID.[5] As one of the reasons of the precipitous depolarization, it is suggested that an electron-magnon interaction broadens bandwidth of minority spin states above E_F and the tail of the minority spin states comes across E_F, which can permit spin-flip scattering of the conducting majority spin electrons.[6] The minority spin state appearing at E_F by the electron-magnon interaction is so-called *non-quasiparticle* (NQP). Although the indication of existence of the NQP states have been suggested in several tunneling magnetoresistance studies,[7] there is no direct evidence for the NQP in half-metallic ferromagnets at present. In this study, in order to demonstrate the existence of the NQP states, we performed high-resolution spin-resolved photoemission spectroscopy (SRPES) on CrO_2 films.

CrO_2 (100) epitaxial films ($T_C \sim 390$ K) grown on rutile-type TiO_2 (100) substrates were prepared by a chemical vapor deposition method.[5] The CrO_2 films were removed from the quartz tube and then immediately placed under high vacuum for the spin-resolved PES measurements. All of the spin-resolved PES data were acquired by the laser-based spin- and angle-resolved photoemission spectroscopy (ARPES) apparatus at the Institute for Solid State Physics at the University of Tokyo. The photon energy and energy resolution were 6.994 eV and 30 meV, respectively. We magnetized the samples along the magnetic easy axis ([001] direction) by bringing the samples close to a magnet at room temperature.

Figure 1 (a) shows temperature dependence of the obtained spin polarization. At 10 K, we observed 100 % spin polarization near E_F, showing the half-metallicity of the CrO_2 film. The spin polarization decreases toward higher binding energy, which reflects the secondary electron-like background of the minority spin state as shown in Fig. 1(b).

With increasing temperature, we observed depolarization which makes the spectral shape between 500 meV binding energy and E_F more parallel to the horizontal axis, as seen in Fig. 1 (a). The energy dependence of spin polarization at 300 K fits nicely with that obtained by measurements using Xe I light ($hv = 8.44$ eV).[9] From analogy with the previous study using Xe I light, the temperature-dependent depolarization arises in the whole spin-polarized energy range to decrease the macroscopic magnetization.

Finally, we mention an indication of depolarization just at E_F. In Fig. 1 (a), we find tendency that spin polarization drops from a binding energy of several 10 meV toward E_F

above 120 K. The temperature dependence of the spin polarization at E_F shows precipitous decrease with increasing temperature, as shown in Fig. 1 (c). This kind of depolarization can be a possible reason for the rapid reduction of the magnetoresistance incomprehensible from the temperature dependence of the magnetization. The energy scale of the depolarization is consistent with that of the NQP state,[6] indicating that one of origin of the depolarization is appearance of the NQP state at and above E_F.

In summary, we have performed high-resolution SRPES on CrO_2 films and observed two energy scales of the temperature-dependent depolarization, which may shed light on the characteristic many-body interaction in half-metals.
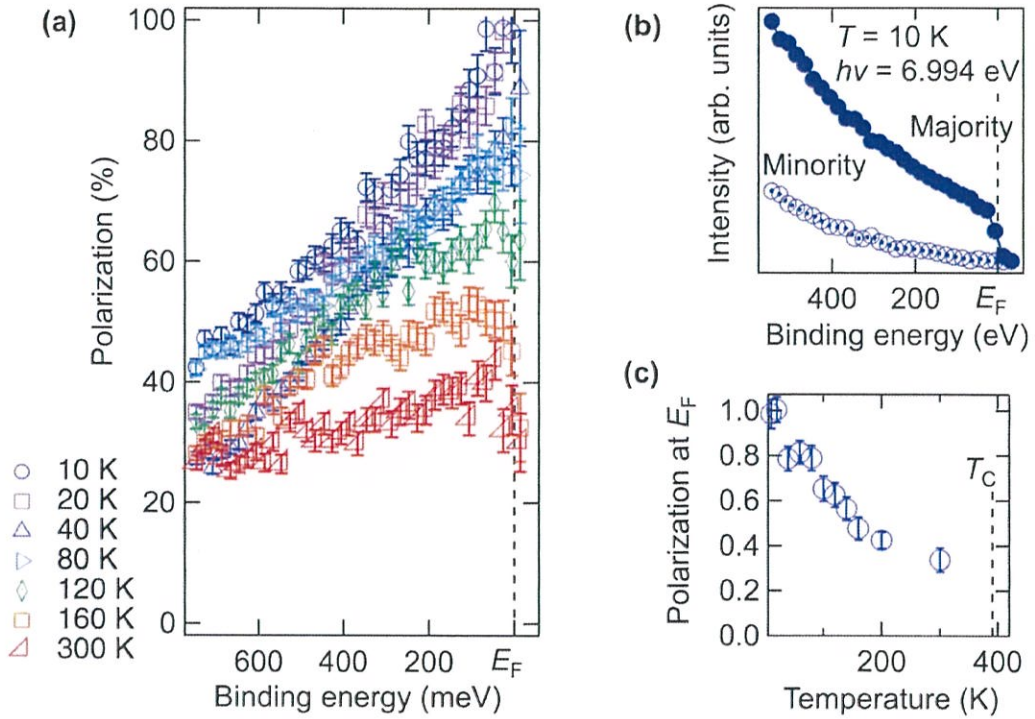

Figure 1 (a) Temperature dependence of the spin polarization as a function of binding energy of CrO_2. The statistical error bars are estimated from $1/(S_{eff}I_{total}^{1/2})$. (b) SRPES spectrum measured at 10 K. Filled and empty circles correspond to the majority and minority spin, respectively. (c) Temperature dependence of spin polarization at E_F. Each value represents the average values in the region between 20 meV and E_F.

REFERENCES

[1] R. A. de Groot *et al.*, Phys. Rev. Lett. **50**, 2024 (1983).
[2] R. J. Soulen Jr. *et al.*, Science **282**, 85 (1998).
[3] J. M. D. Coey *et al.*, Phys. Rev. Lett. **80**, 3815 (1998).
[4] S. M. Watts *et al.*, Phys. Rev. B **61**, 9621 (2000).
[5] K. Iwai *et al.*, J. Appl. Phys. **108**, 043916 (2010).
[6] L. Chioncel *et al.*, Phys. Rev. B **75**, 140406(R) (2007).
[7] L. Chioncel *et al.*, Phys. Rev. Lett. **100**, 086402 (2008).
[8] R. Cheng *et al.*, Appl. Phys. Lett. **79**, 3122 (2001).
[9] H. Fujiwara *et al.*, Appl. Phys. Lett. **106**, 202404 (2015).
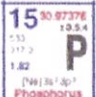
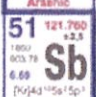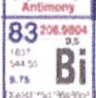# SPIN-RESOLVED ARPES ON THE GREY ARSENIC SURFACE

Y. Ishida, P. Zhang, K. Yaji, S. Shin

LASOR, The Institute for Solid State Physics (ISSP), The University of Tokyo

In 2008, it was experimentally established [1] that non-magnetic insulators can be classified into two categories; namely, into a topologically trivial insulator and a topologically non-trivial insulator. The classification owes to the fact that a topological number Z_2 can be assigned to each of the insulators. Z_2 takes the number of either 0 or 1 depending on the structure of the electronic bands of bulk. The insulators endowed with the non-trivial $Z_2 = 1$ exhibit novelty on their surface: The surface of a topological insulator (TI) inevitably harbours spin-polarized metallic states that show Dirac-conical dispersions. Thus, detection of the novel surface states by using angle-resolved photoemission spectroscopy (ARPES) methods has become the standard in judging the topological nature of the insulators.

Pnictogens are the chemical elements in group 15 of the periodic table. Elemental crystals of pnictogens form into semimetals, and their topological classification has been undertaken by several research groups; see Table 1: Black phosphorus is said to be topologically trivial [2]; antimony is categorized as a TI [3]; and bismuth may be topologically non-trivial, as claimed by some groups recently [4]. Meanwhile, grey arsenic remained untouched, presumably because of the obsession that arsenic is toxic. Once crystallized, however, grey arsenic itself is not poisonous unless it is heated up to temperatures above 130°C in air.

Table 1: Topological classification of the pnictogen elemental semimetals.

Spin-resolved ARPES (SARPES) can directly assess the spin polarization of the bands: Thus, the technique is routinely adopted for the topological classification of the non-magnetic insulators. The laser-SARPES apparatus developed at ISSP [5] realizes the highest energy resolution of 1.3 meV and achieves a high throughput, thanks to the combination of the bright-and-monochromatic 7-eV laser-based light source and V-LEED detection system for resolving the spin polarizations of the photoelectrons. The use of the 7-eV probe is also advantageous for achieving a high momentum resolution, because the band structures in momentum (k) space are magnificently replicated in the angular distribution of the photoelectrons compared to the cases where probes of higher photon energies are adopted.

In the present project, we investigated the surface of a grey arsenic single crystal by using the laser SARPES apparatus. First, we found a pair of spin-polarized surface bands on the (111) face of grey arsenic (Figs. 1a and 1b). The pair forms two concentric Fermi surfaces

that enclose the surface Gamma point (Fig. 1c). The pair mimics the bands of two-dimensional free electrons subjected to the Rashba-type interaction. In fact, we observe that the bands show the expected polarization (Fig. 1d), and they can be nicely fit by the free electron bands subjected to the Rashba-type interaction (Fig. 1e): The best fit is obtained with the mass being 0.07 times that of a bare electron and the splitting of 0.0054 Å^{-1} along k.

Combined with information of the band structures in the unoccupied side obtained by using time-resolved ARPES and the first principles calculation, we concluded that the spin-split surface bands discovered on As(111) occur due to reasons of the topology of the bulk band structure: That is, grey arsenic is a TI. Thus, we came to the picture that there is a boundary between phosphorous and arsenic in the group 15 elements, below which the elemental semimetals become topologically non-trivial. For further reading, see Ref. [6].
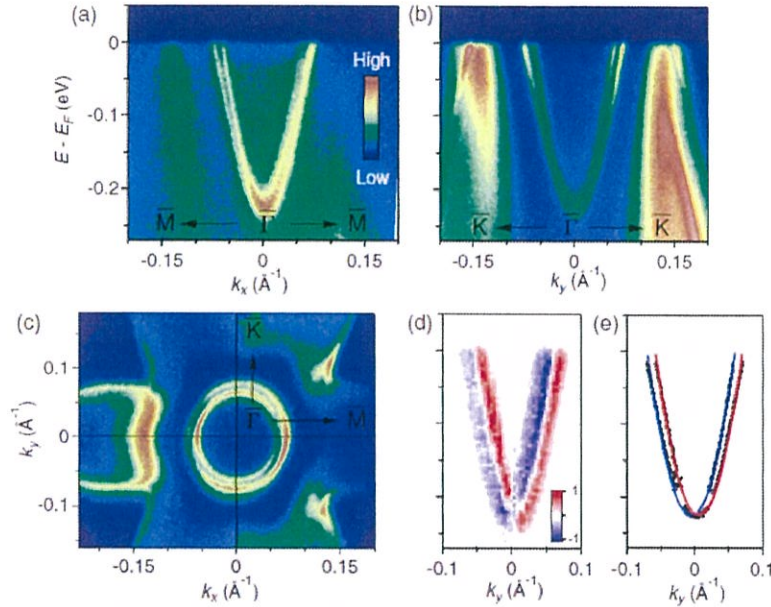

Fig. 1: Band structures of the 111 face of grey arsenic recorded by the laser SARPES apparatus. Band dispersions along k_x (a) and k_y (b). (c) Fermi surface mapping. (d) Spin polarization of the bands recorded by SARPES. (e) Fits of the dispersions to those of nearly-free electrons spin-split by the Rashba-type interactions.

REFERENCES

[1] D. Hsieh, D. Qian, L. Wray, Y. Xia, Y. S. Hor, R. J. Cava, M. Z. Hasan, *Nature* **452**, 970 (2008).

[2] Jimin Kim, Seung Su Baik, Sae Hee Ryu, Yeongsup Sohn, Soohyung Park, Byeong-Gyu Park, Jonathan Denlinger, Yeonjin Yi, Hyoung Joon Choi, Keun Su Kim, *Science* **349**, 723 (2015).

[3] D. Hsieh, Y. Xia, L. Wray, D. Qian, A. Pal, J. H. Dil, J. Osterwalder, F. Meier, G. Bihlmayer, C. L. Kane, Y. S. Hor, R. J. Cava, M. Z. Hasan, *Science* **323**, 919 (2009).

[4] Y. Ohtsubo, L. Perfetti, M. O. Goerbig, P. Le Fevre, F. Bertran, A. Taleb-Ibrahimi, *New J. Phys.* **15**, 033041 (2013); S. Ito, B. Feng, M. Arita, A. Takayama, R.-Y. Liu, T. Someya, W.-C. Chen, T. Iimori, H. Namatame, M. Taniguchi, C.-M. Cheng, S.-J. Tang, F. Komori, K. Kobayashi, T.-C. Chiang, and I. Matsuda, *Phys. Rev. Lett.* **117**, 236402 (2016).

[5] K. Yaji, A. Harasawa, K. Kuroda, S. Toyohisa, M. Nakayama, Y. Ishida, A. Fukushima, S.Watanabe, C. Chen, F. Komori, S. Shin, *Rev. Sci. Instrum.* **87**, 053111 (2016).

[6] P. Zhang, J.-Z. Ma, Y. Ishida, L.-X. Zhao, Q.-N. Xu, B.-Q. Lv, K. Yaji, G.-F. Chen, H.-M. Weng, X. Dai, Z. Fang, X.-Q. Chen, L. Fu, T. Qian, H. Ding, S. Shin, *Phys. Rev. Lett.* **118**, 046802 (2017).

LASER-SARPES STUDY ON THE INTERBAND HYBRIDIZATION OF SPIN-ORBIT COUPLED SURFACE STATES IN THIN FILMS

Ryo Noguchi[1], Kenta Kuroda[1], T. Kondo[1], M. Sakano[1], K. Yaji[1], A. Harasawa[1], K. Kobayashi[2], F. Komori[1], and S. Shin[1]

[1]The Institute for Solid State Physics, The University of Tokyo
[2]Department of Physics, Ochanomizu University

Introduction:

The Rashba effect leads to spin-splitting in electronic structures at the surface or the interface of solids due to the broken inversion symmetry collaborated with spin-orbit coupling (SOC). In the conventional Rashba model, an eigenstate of the SO-induced spin-splitting is treated with an assumption of a fully spin-polarized state which protects electrons from backscattering. However, in real materials, the assumption can be usually broken because the SO coupling mixes different states with different orbitals and orthogonal spinors in a quasiparticle eigenstate. This SO entanglement can permit the spin-flip electron backscattering and moreover play a significant role in an emergence of the large spin-splitting. Therefore, it is essentially important to experimentally explore the SO coupling not only in the lifting spin degeneracy but also in the SO-entangled wavefunction as eigenstates.

Here, we report a direct investigation on the SO entanglement in the Rashba surface states of Bi/Ag(111) surface alloy by using a combination of polarization variable laser with spin- and angle-resolved photoemission spectroscopy (laser-SARPES). In contrast to the previous experiments [1, 2], our laser-SARPES deconvolves the orbital wavefunction and the coupled spin, and the surface wavefunctions are directly imaged into momentum-space through orbital-selection rule. It is shown that the interband SO coupling modifies the spin and orbital character of the surface states, leading to a large deviation from the conventional Rashba model [3].

Experimental:

Laser-SARPES was performed at newly home-built laser-SARPES machine at ISSP with high-flux 6.994-eV laser light. The laser-SARPES machine is based on two high efficient VLEED spin-polarimeters and the hemispherical analyzer with photoelectron deflector function (ScientaOmicron DA30L). This spectrometer can resolve spin polarization components of photoelectrons for in-plane ($P_{x,y}$) and out-of-plane (P_z) orientation. The spin polarized photoelectrons were excited by p- and s-polarized light (ε_p and ε_s, respectively). During the measurement, the sample temperature was kept around 15 K, and instrumental energy and angular resolutions were set below 20 meV and 0.7°, respectively [4].

Results:

A schematic of electronic structure of Bi/Ag(111) is shown in Fig. 1(a). The sp_z-derived bands and the higher-lying p_{xy} bands, dispersing downwards in energy with a large Rashba spin-splitting, are observed as shown in Fig. 1(b). Figure 1(c) summarizes the linear polarization dependence in Bi/Ag(111). Considering the orbital selection rule in the dipole excitation, ε_p selectively detects *even*-parity orbital with respect to the mirror plane, while ε_s is sensitive to the *odd*-parity orbital. For the result obtained by ε_p, we observe the strong intensity for the sp_z and inner p_{xy} bands [the left panel in Fig. 1(c)]. The data particularly displays the band crossing of the outer sp_z and inner p_{xy} bands around $k_x=0.15$ Å^{-1}, where the spectral intensity of the outer sp_z is strongly suppressed. Surprisingly, with the light polarization ε_s, the dispersion of the outer sp_z is clearly observed even at lager $k_x>0.15$ Å^{-1} together with the outer p_{xy} band [the middle panel in Fig. 1(c)]. The right panel of Fig. 1(c) shows the differential intensity map. The

magenta-green colour contrast reflects the contribution of the *even-* and *odd*-orbital components in the surface wavefunction. It is immediately found that the orbital character of sp_z band changes the orbital character at the band crossing.

To get further insight into the influence of the interband SO coupling, we carried out laser-SARPES measurements collaborated with the orbital selection rule of ε_p and ε_s. Figure 1(d) shows spin-polarization and intensity maps obtained by ε_p and ε_s. For ε_p, the inner and outer sp_z-bands around $\bar{\Gamma}$ point in the both materials show negative and positive spin-polarization, respectively, displaying a conventional Rashba-type spin-texture. The observed spin polarization is found to be large up to nearly 80%. Most remarkably, we find that the sign of the spin polarization sensitively depends on the linear polarization. This can be seen particularly around k_x=0.12 Å^{-1} in Bi/Ag(111). The spectral weight of the spin-up is considerably larger than the spin-down for ε_p and achieves nearly +80% spin-polarization. For ε_p, the intensity relation turns opposite and the resulting spin-polarization is found to be -70%. Since the linear polarization is sensitive to different orbital symmetry, our laser-SARPES unambiguously reveals that the spin direction strongly depends on the orbital character. We now show that the total spin
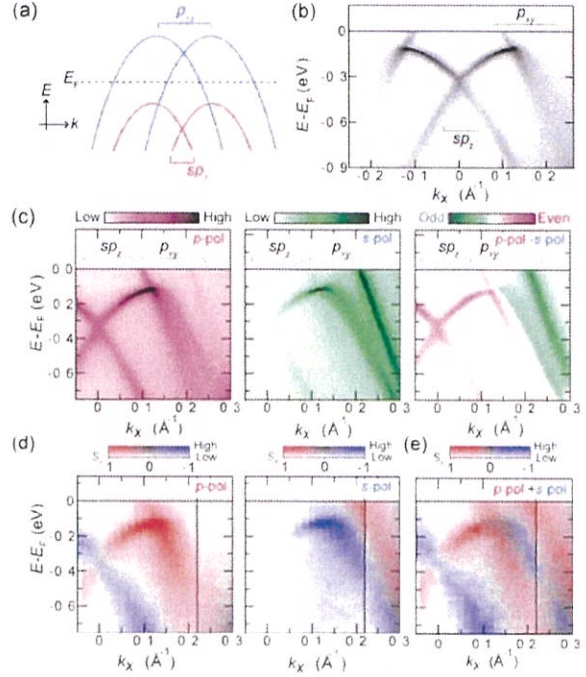

Fig. 1: (a) Schematic of the energy dispersion of Rashba spin-split bands in Bi/Ag(111). (b) ARPES intensity map with *p*-polarization along $\bar{\Gamma}$ - $\bar{K}$ line of the surface Brillouin zone. (c) The magnified ARPES intensity maps with (left) *p*- and (middle) *s*-polarization, and (right) the differential intensity maps, which are obtained by $I_p - I_s$ where I_p and I_s are the photoelectron intensity obtained by *p*- and *s*-polarized light without intensity normalization. (d) Orbital-selective spin-polarization and photoelectron intensity maps obtained by (left) *p*- and (right) *s*-polarized light with the two-dimensional color codes. Spin quantum axis is set along *y*. (e) The total spin polarization (P_{total}) mapping.

information (P_{total}) can be traced back only by using a combination of the spin mapping with ε_p and ε_s lasers. Owing to selective detection of the pure orbital-symmetry in our experimental set-up, the orbital-dependence in the spin polarization is eliminated by integrations of spin-polarization maps [Fig. 1(e)] as follows:

$$P_{total} = \frac{(I_{\{\uparrow,p\}}+I_{\{\uparrow,s\}})-(I_{\{\downarrow,p\}}+I_{\{\downarrow,s\}})}{(I_{\{\uparrow,p\}}+I_{\{\uparrow,s\}})+(I_{\{\downarrow,p\}}+I_{\{\downarrow,s\}})}$$

where $(I_{\{\uparrow,p\}}, I_{\{\uparrow,s\}})$ and $(I_{\{\downarrow,p\}}, I_{\{\downarrow,s\}})$ are the spin-up and spin-down intensities obtained by $(\varepsilon_p, \varepsilon_s)$. The mapping of P_{total} clearly demonstrates the complex spin texture of the sp_z band under interband hybridization, which is comparable to the theoretical predictions. This technique demonstrates a general advantage to investigate the unconventional spin textures in strong SO-coupled states although the results could be influenced by the cross-section for ε_p and ε_s and the photoemission calculation to consider photon energy dependence is required.

REFERENCES

[1] C. R. Ast, et al., Phys. Rev. Lett. **98**, 186807 (2007).
[2] F. Meier *et al.*, Phys. Rev. B, 77, 165431 (2008).
[3] R. Noguchi *et al.*, Phys. Rev. B **95**, 41111 (2017).
[4] K. Yaji *et al.*, Rev. Sci. Instrum., **87**, 053111 (2016).

MAPPING OF SPIN-ORBITAL ENTANGLEMENT IN THE NOVEL SUPERCONDUCTOR Sr_2RuO_4 BY USING LASER SPIN-RESOLVED ARPES

K. Kuroda[1], S. Akebi[1], M. Nakayama[1], M. Sakano, K. Yaji[1], A. Hasawa[1], H. Taniguchi[2],
Y. Maeno[2], S. Nakatsuji[1], S. Shin[1] and T. Kondo[1]
[1]The Institute for Solid State Physics, The University of Tokyo
[2]Deparatment of Physics, Kyoto University

Introduction:

Since the great discovery of superconductivity in Sr_2RuO_4, many theoretical and experimental efforts have been paid for examining spin-triplet chiral p-wave superconductivity [1-3]. However, some recent experiments have not supported this, in which spin-triplet superconductivity alone was insufficient to explain the experimental facts [4, 5]. This contradiction mostly comes from the inclusion of low-energy fine-electronic structure and its wavefunction character due to spin-orbit coupling (SOC). It can be easily imagined that SOC can play a fundamental role beyond simple models for Cooper pairing mechanism, since the energy scale of the SOC of nearly 100 meV in Sr_2RuO_4 is much larger than the scale of T_c ~0.2 meV. In the presence of SOC, the quantum states with different orbitals and spins are generally mixed and the eigenstate wavefunction is strongly modified. This spin-orbital (SO) entanglement thereby results in the breakdown of singlets and triplets for Cooper paring, although the both are generally used to treat novel superconductivity. Recently, the SO entanglement and its momentum dependence have been theoretically predicted in bulk Sr_2RuO_4 [6].

In this work, by using spin- and angle-resolved photoemission spectroscopy combined with 7-eV laser (Laser-SARPES), we have obtained the first experimental evidence of the SO entanglement in the eigenstate wavefunctions in Sr_2RuO_4. We have recently shown that 7-eV excitation energy selectively detects the electronic structures at the top most (001) cleaved surface [7] and thereby the data we present here show the surface states. Our findings therefore hold importance not only for understanding mechanism of superconductivity but also possible topological edge states that might be detected below T_c on the side surfaces [8].

Experimental:

Laser-SARPES experiments were performed at newly home-built laser-SARPES machine at ISSP with high-flux 6.994-eV laser light [9]. The laser-SARPES machine is based on two high efficient VLEED spin-polarimeters and the hemispherical analyzer with photoelectron deflector function (ScientaOmicron DA30L). This spectrometer can resolve spin polarization components of photoelectrons in three-dimension for in-plane ($P_{x,y}$) and out-of-plane (P_z) orientation. The clean surface of Sr_2RuO_4 was *in situ* cleaved at below 20 K. During the measurement, the sample temperature was kept below 20 K, and instrumental energy and angular resolutions were set below 20 meV and 0.7°, respectively. All data was taken before sample degradation within 24 hours.

Results:

We start with a brief explanation for overall shape of Fermi surface obtained by our laser photon energy as shown in Fig. 1(a). The three-bands, α-band, γ-band and β-band, form the
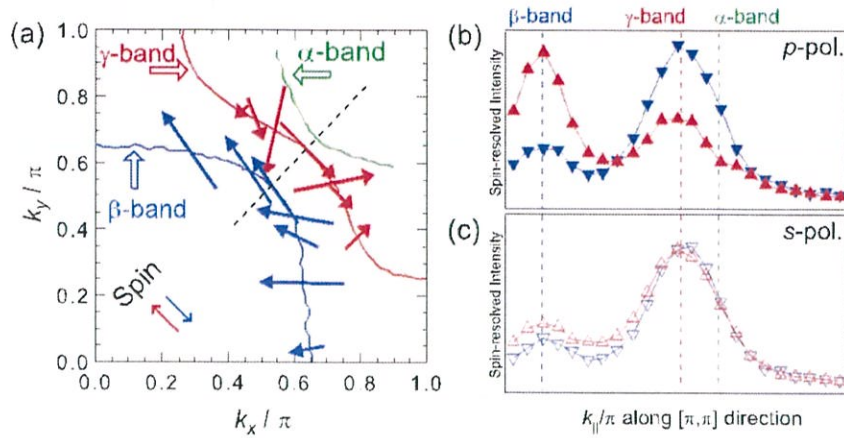
Fig. 1: (a) Shape of the Fermi surfaces for (001) cleaved surface state of Sr_2RuO_4 (open arrows, solid lines: α-, β- and γ-bands are shown green, red and blue lines, respectively). Our laser photon energy enables us to selectively detect only the surface signals [7]. (c) and (d) The spin-resolved momentum-distribution curves (MDCs) by using p- and s-polarization set up, respectively. These MDCs are obtained at $k_\parallel$ cut along (π, π) direction as denoted by dashed line in Fig. 1(a). The red and blue triangles respectively show the spin-up and spin-down states, and the resolved spin axis is perpendicular to the momentum cut [see the inset in Fig.1 (a)]. The obtained momentum dependence of the spin direction and its size is shown by closed arrows in Fig. 1(a).

Fermi surface indicated by open arrows (α-, β- and γ-bands are shown green, red and blue lines, respectively). We observe clear the evidence of the SOC along (π, π) $k_\parallel$ direction [dashed line in Fig. 1(a)], where these three bands are located close to each other. Figures 1(b) and (c) present spin-resolved momentum-distribution curves along this $k_\parallel$ cut [the resolved spin axis is shown in the inset of Fig. 1(a)]. We clearly observe the large photoelectron spin-polarization for β- and γ-bands for p-polarization [Fig. 1(b)]. This photoelectron spin-polarization is shown to be originated from the photoemission matrix element effect, since the large spin-polarization is absent in the both bands for s-polarization [Fig. 1(c)]. Interestingly, we find clear $k_\parallel$ dependence [see closed arrows in Fig. 1(a)]. Most remarkably, the direction of the photoelectron spin-polarizations is always opposite for β- and γ-bands [e.x. see Figs. 1(a)]. Moreover, it is worth noting that the orientation is insensitive to the experimental geometry. These results strongly indicate that the observed spin-polarization and its $k_\parallel$ dependence present the SO entanglement in initial state wavefunctions.

References:

[1] K. Ishida et al., Nature **396**, 658 (1998).
[2] T. M. Riseman et al., Nature **396**, 242 (1998).
[3] K. D. Nelson et al., Science **306**, 1151 (2004).
[4] S. Kittaka et al., Phys. Rev. B **80**, 174514 (2009).
[5] S. Yonezawa et al., Phys. Rev. Lett. **110**, 077003 (2013).
[6] C. N. Veenstra et al., Phys. Rev. Lett. **112**, 127002 (2014).
[7] T. Kondo et al., Phys. Rev. Lett. **117**, 247001 (2016).
[8] S. Kashiwaya et al., Phys. Rev. Lett. **107**, 077003 (2011).
[9] K. Yaji et al., Rev. Sci. Instrum., **87**, 053111 (2016).

ELECTRONIC STATES AND ELECTRON-PHONON COUPLING IN 1D NANORIPPLED GRAPHENE ON MACROFACET OF 6H-SiC

Fumio Komori[1,*], Koichiro Ienaga[1], Takushi Iimori[1], Koichiro Yaji[1], Toshio Miyamachi[1], Shuhei Nakashima[1], Yukio Takahashi[1], Kohei Fukuma[2], Shingo Hayashi[2], Takashi Kajiwara[2], Anton Visikovsliy[2], Kazuhiko Mase[3,4] Kan Nakatsuji[5], and Satoru Tanaka[2]

[1]*Institute for Solid State Physics, The University of Tokyo, 5-1-5 Kashiwanoha, Kashiwa, Chiba 277-8581, Japan*
[2]*Department of Applied Quantum Physics and Nuclear Engineering, Kyushu University, Fukuoka 819-0395, Japan*
[3]*Institute of Materials Structure Science, High Energy Accelerator Research Organization, Tsukuba 305-0801, Japan*
[4]*Department of Materials Structure Science, SOKENDAI (The Graduate University for Advanced Studies), 1-1 Oho, Tsukuba 305-0801, Japan*
[5]*Department of Materials Science and Engineering, Tokyo Institute of Technology, Yokohama 226-8502, Japan*

Modulation of the graphene electronic states by one-dimensionally (1D) periodic potential at a nanoscale has been theoretical predicted, such as an energy gap at the Dirac point and anisotropic dispersion relation [1]. We prepared a nano-rippled graphene on a vicinal SiC(0001) substrate, and measured its band structure by angle resolved photoelectron spectroscopy (ARPES). For the same sample, the interaction between Dirac electrons and phonon system was studied using inelastic scanning tunneling spectroscopy (IESTS). We found spatially-dependent inelastic tunneling with the period of the nano-ripple structure. This clarified the structure of nano-rippled graphene used in this research. [2]

The ARPES measurement was carried out using the ARPES spectrometers with a He discharge tube at Kashiwa, ISSP, and with linearly-polarized light of 49 eV in BL13B of Photon Factory at KEK. Besides ARPES measurements, IESTS at 80 K were performed at ISSP. The nano-rippled graphene was fabricated by thermal decomposition of a SiC (0001) substrate with a slope of 4° in an Ar atmosphere. The graphene that was carried in the atmosphere to the ARPES chambers was annealed in an ultrahigh vacuum for the cleaning the surface before the measurements.

Figure 1 shows the STM image and the LEED image. As shown in Fig. 1 (a), the surface consists of terrace and macrofacets of 27°. A part of the terrace consists of graphene as shown in Fig. 1 (b) and so called a buffer layer with a 6√3 x 6√3 superstructure. In the macrofacet part, graphene with one-dimensional undulation in the facet direction can be seen. In the
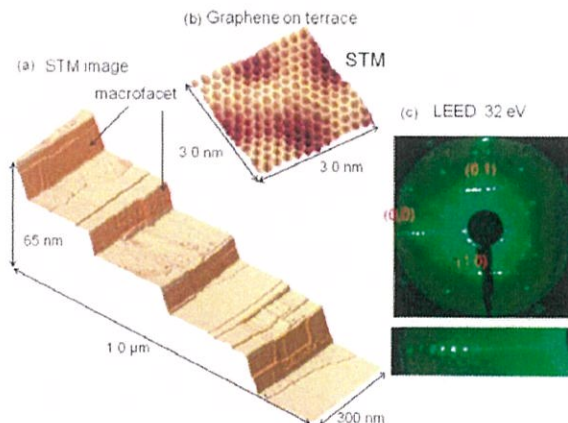

Fig. 1 STM images (a,b) and LEED pattern (c) of the sample surface. A repeated macrofacet and terrace structure is formed on the substrate as in (a). One-dimensionally nano-rippled structure can be seen on the macrofacet surface, On a part of the terrace, single-layer graphene with surface modulation due to the buffer layer at the subsurface was formed as in (b). In LEED pattern. (c), satellite graphene spots due to the nano-rippled graphene structure appear around the integer spots of graphene on the macrofacets. Magnified image of the satellite spots is shown in the lower part in (c).

LEED image, satellite spots were observed, reflecting of the undulated macrofacet as shown in Fig. 1 (c). The enlarged STM image of the macrofacet part is shown in Fig. 2. There is a periodic undulation on the macrofacet with graphene atomic structure, which indicates continuous graphene covering the macrofacet. The modulation period is 3.4 nm, which is coincident with the period obtained from the satellite spot interval of the LEED image shown in Fig. 1 (c).
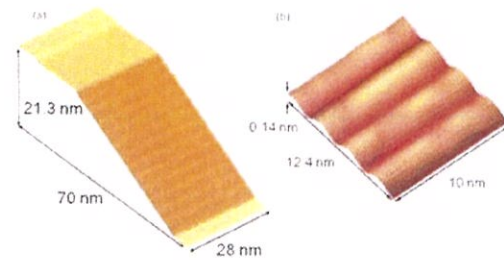

Fig. 2 Magnified STM images including a macrofacet (a) and with atomic resolution (b).

Figure 3 shows the ARPES image of the Dirac band from this facet. As shown in Fig. 3 (a) at 21.2 eV, satellite band signals were observed reflecting the one-dimensional super periodicity of the graphene on the macrofacet. The Dirac point of this graphene is 0.8 eV below Fermi energy, and the amount of doping is smaller than that of the graphene on the terrace. A band gap was not clearly observed, and the electron velocity was not significantly different from that on the terrace. When measured at 40.8 eV, signals from the second-layer graphene were also clearly observed as shown in Fig. 3 (b).

Furthermore, in the STS measurement, we observed inelastic tunneling signals due to phonons in the vertical direction of the graphene plane. This signal intensity periodically oscillates in the 1D undulation direction of graphene. This means that the intensity of the inelastic scattering due to the electron-phonon interaction oscillates in the tilting direction of the macrofacet. Since the STM image of the graphene surface looked uniform, we concluded that the intensity oscillation is attributed to the second layer graphene under the surface.

As a result, we propose a structural model of the graphene shown in Fig. 4. There are graphene nanoribbons and buffer layers at the interface with the SiC substrate. The tunneling electrons are easy to move from the surface graphene to the second layer nanoribbon in the former part, but in the latter, electrons are difficult to move because of the long interlayer distance. Due to this difference, the probability that tunnel electrons interact with the phonon system is larger in the latter.

In conclusion, one-dimensional nano-rippled graphene was fabricated on macrofacet of 6H-SiC substrate. Graphene Dirac band was confirmed by ARPES measurement. We proposed a structural model of this graphene by ARPES and STM / STS measurements.

REFERENCES

[1] C.-H. Kim *et.al.*, *Nature Phys.* **4**, 213 (2008).
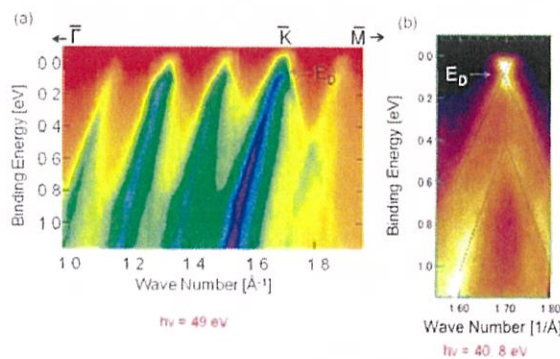[2] K. Ienaga *et al.*, *Nano. Lett.* **17**, 3527 (2017).

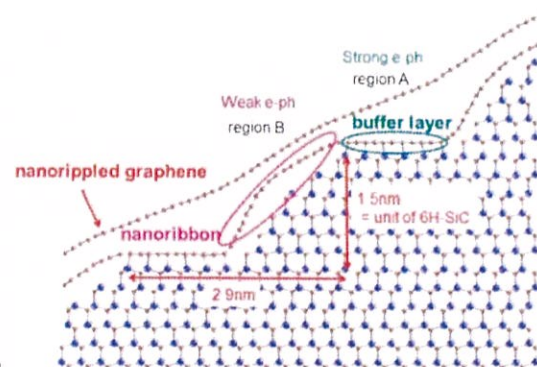Fig. 3 ARPES spectra using 49 eV (a) and 40.8 eV (b).

Fig. 4 A proposed model of the graphene on the macrofacet.

Staff

Director: SHIN Shik, Professor

KOMORI Fumio, Professor

MATSUDA Iwao, Associate Professor
HARADA Yoshihisa, Associate Professor
WADATI Hiroki, Associate Professor
YAMAMOTO Susumu, Research Associate
YAJI Koichiro, Research Associate
MIYAWAKI Jun, Research Associate
HIRATA Yasuyuki, Research Associate
FUKUSHIMA Akiko, Technical Associate
SHIBUYA Takashi, Technical Associate
HARASAWA Ayumi, Technical Associate
KUDO Hirofumi, Technical Associate

Technical Assistant: FUJISAWA Masami
KOSEGAWA Yuka
ARAKI Mihoko

Secretary: AIHARA Yumiko
HARADA Misa
YOSHIZAWA Motoko
TSUTSUMI Yumiko
IKEDA Kuniko

Graduate Student: YAMAMOTO Shingo
KUBOTA Yuya
RO-Ya-Liu
SOMEYA Takashi
YAMAZOE Kosuke
YOKOYAMA Yuichi
ITOH Suguru
ITAMOTO Haruki
INOUE Takanobu
YAMAMOTO Kohei
WANG Hao

Contract Researcher: TAKUBO Kou
CUI Yitao
FENG Baojie
TANG Jiayi
AKADA Keishi (2016.12~)

Publication List(2016)

---Harima---
Resonant Inelastic X-ray Scattering Study of Entangled Spin-Orbital Excitations in Superconducting PrFeAsO0.7
T. Nomura, Y. Harada, H. Niwa, K. Ishii, M. Ishikado, S. Shamoto, and I.Jarrige
Physical Review B, 94, 035134 (2016)

Phonon-Dressed Two-Dimensional Carriers on the ZnO Surface
R. Yukawa,K. Ozawa,S. Yamamoto,H. Iwasawa,K. Shimada,E. F. Schwier,K. Yoshimatsu,H. Kumigashira,H. Namatame,M. Taniguchi,and I. Matsuda
Physical Review B, 94, 165313 (2016)

Investigation of Photo-carrier Generation Processes of Organic Solar Cells Using Time Resolved X-ray Photoelectron Spectroscopy
T. Sakurai, S. Wang, W. Fu, K. Ozawa, R. Yukawa, S. Yamamoto and I. Matsuda
Extended Abstracts of the 2016 International Conference on Solid State Devices and Materials (SSDM), 277-278 (2016)

軟 X 線分光による Operando 電子状態解析
朝倉大輔、細野英司
Electrochemistry, 84, 529-533 (2016)

Operando Soft X-ray Emission Studies of Lithium-Ion Batteries
Daisuke ASAKURA, Eiji HOSONO and Yoshihisa HARADA
表面科学 (Journal of the Surface Science Society of Japan), 37, 66-71 (2016)

Characterization of Nitrogen Species Incorporated into Graphite using Low Energy Nitrogen Ion Sputtering
Hisao Kiuchi, Takahiro Kondo, Masataka Sakurai, Donghui Guo, Junji Nakamura, Hideharu Niwa, Jun Miyawaki, Maki Kawai, Masaharu Oshima and Yoshihisa Harada
Physical Chemistry Chemical Physics, 18, 458-465 (2016)

Ligancy-Driven Controlling of Covalency and Metallicity in a Ruthenium Two-Dimensional System
Satoshi Toyoda, Katsutoshi Fukuda, Koji Horiba, Masaharu Oshima, Kazuhiro Kumagai, Yu Kumagai, Fumiyasu Oba, Yoshiharu Uchimoto, and Eiichiro Matsubara
Chemistry of Materials, 28, 5784-5790 (2016)

X-ray and Electron Spectroscopy of Water

Thomas Fransson, Yoshihisa Harada, Nobuhiro Kosugi, Nicholas A. Besley, Bernd Winter, John J. Rehr, Lars G. M. Pettersson, and Anders Nilsson
Chemical Reviews, 116, 7551-7569 (2016)

Lewis Basicity of Nitrogen-Doped Graphite Observed by CO_2 Chemisorption
Hisao Kiuchi, Riku Shibuya, Takahiro Kondo, Junji Nakamura, Hideharu Niwa, Jun Miyawaki, Maki Kawai, Masaharu Oshima and YoshihisaHarada
Nanoscale Research Letters, 11, 127 (2016)

Redox Potential Paradox in NaxMO2 for Sodium-Ion Battery Cathodes
Yusuke Nanba, Tatsumi Iwao, Benoit Mortemard de Boisse, Wenwen Zhao, Eiji Hosono, Daisuke Asakura, Hideharu Niwa, Hisao Kiuchi, Jun Miyawaki, Yoshihisa Harada, Masashi Okubo and Atsuo Yamada
Chemistry of Materials, 28, 1058-1065 (2016)

What Determines the Lifetime of Photoexcited Carriers on TiO_2 Surfaces?
Kenichi Ozawa , Susumu Yamamoto , Ryu Yukawa, Roya Liu, Masato Emori, Koki Inoue, Taku Higuchi, Hiroshi Sakama, Kazuhiko Mase, and Iwao Matsuda
The Journal of Physical Chemistry C, 120, 29283-29289 (2016)

Capturing Transiently Charged States at the $C60/TiO_2(110)$ Interface by Time-Resolved Soft X-ray Photoelectron Spectroscopy
Kenichi Ozawa, Susumu Yamamoto, Ryu Yukawa , Kazuma Akikubo ,
Masato Emori , Hiroshi Sakama , Iwao Matsuda
Organic Electronics, 31, 98-103 (2016)

Tailoring Photovoltage Response at $SrRuO_3/SrTiO_3$ Heterostructures
Ryu Yukawa, Susumu Yamamoto, Kazuma Akikubo, Kaori Takeuchi,   Kenichi Ozawa, Hiroshi Kumigashira and Iwao Matsuda
Advanced Materials Interfaces, 3, 1600527 (2016)

Observation of Nanoscopic Charge-Transfer Region at Metal/MoS2 Interface
Ryota Suto, Gunasekaran Venugopal, Keiichiro Tashima, Naoka Nagamura, Koji Horiba, Maki Suemitsu, Masaharu Oshima and Hirokazu Fukidome
Material Research Express, 3, 075004 (2016)

Real-Time Observation of Reaction Processes of CO_2 on Cu(997) by Ambient-Pressure X-ray Photoelectron Spectroscopy
Takanori Koitaya, Susumu Yamamoto ,Yuichiro Shiozawa, Kaori Takeuchi, Ro-Ya Liu, Kozo Mukai, Shinya Yoshimoto, Kazuma Akikubo, Iwao Matsuda and Jun Yoshinobu
Topics in Catalysis, 59, 526-531 (2016)

Intermediate Honeycomb Ordering to Trigger Oxygen Redox Chemistry in Layered Battery Electrode
Benoit Mortemard de Boisse, Guandong Liu, Jiangtao Ma, Shin-ichi Nishimura, Sai-Cheong Chung, Hisao Kiuchi, Yoshihisa Harada, Jun Kikkawa, Yoshio Kobayashi ,Masashi Okubo and Atsuo Yamada
Nature Communications, 7, 11397 (2016)

Hybridization and Electron-Phonon Coupling in Ferroelectric $BaTiO_3$ Probed by Resonant Inelastic X-ray Scattering
Fatale, S.; Moser, S.; Miyawaki, J.; Harada, Y.; Grioni, M.
Physical Review B, 94, 195131 (2016)

Pt-free carbon-based fuel cell catalyst prepared from spherical polyimide for enhanced oxygen diffusion
Y. Nabae, S. Nagata, T. Hayakawa, H. Niwa, Y. Harada, M. Oshima, A. Isoda, A. Matsunaga, and K. Tanaka
Sci. Rep. 6, 23276 (1-7) (2016)

Electronic Structure of Pt and Pt-Co Nanoparticles with O_2 and O_2/H_2O Adsorption Revealed by In Situ XAFS and Hard X-Ray Photoelectron Spectroscopy
Yitao Cui, Yoshihisa Harada, Tatsuya Hatanaka, Naoki Nakamura, Masaki Ando, Toshihiko Yoshida, Eiji Ikenaga, Kenji Ishii, Daiju Matsumura, Rui Li, Masaharu Oshima
ECS Transactions, 72, 131-136 (2016)

Combined Experimental and Computational Analyses on the Electronic Structure of Alluaudite-type Sodium Iron Sulfate
G. Oyama, H. Kiuchi, S. Cheong Chung, Y. Harada, A. Yamada
J. Phys. Chem. C, 120, 23323-23328 (2016)

Time-resolved soft X-ray core-level photoemission spectroscopy to 880℃ using pulsed laser and synchrotron radiation, and switched heating current
T. Abukawa, S. Yamamoto, R. Yukawa, S. Kanzaki, K. Mukojima, I.Matsuda
Surface Science 43, 656 , [published online 14 October 2016] (2017)

Generation of metallic eg-derived band at $Cs/SrTiO_3$ interface observed by polarization-dependent photoemission spectroscopy
Kazuma Akikubo, Iwao Matsuda, Didier Schmaus, Guillaume Marcaud, Susumu Yamamoto, Ro-Ya Liu, Ryu Yukawa, Mathieu G. Silly, Fausto Sirotti, and Marie D'Angelo
Thin Solid Films 603, 149 (2016)

Thickness-dependent physical properties of $La_{1/3}Sr_{2/3}FeO_3$ thin films grown on $SrTiO_3$ (001) and (111) substrates
M. Minohara, M. Kitamura, H. Wadati, H. Nakao, R. Kumai, Y. Murakami, and H. Kumigashira
J. Appl. Phys. 120, 025303-1-6 (2016)

Photoinduced Demagnetization and Insulator-to-Metal Transition in Ferromagnetic Insulating $BaFeO_3$ thin films
T. Tsuyama, S. Chakraverty, S. Macke, N. Pontius, C. Schussler-Langeheine, H. Y. Hwang, Y. Tokura, and H. Wadati
Phys. Rev. Lett. 116, 256402-1-5 (2016)

Interface electronic structure at the topological insulator–ferrimagnetic insulator junction
Y Kubota, K Murata, J Miyawaki, K Ozawa, M C Onbasli, T Shirasawa, B Feng, Sh Yamamoto, R-Y Liu, S Yamamoto, S K Mahatha, P Sheverdyaeva, P Moras, C A Ross, S Suga, Y Harada, K L Wang and I Matsuda
Journal of Physics: Condensed Matter, 29, 5, 055002, (2016)

Investigation of the enhanced photocathodic activity of La5Ti2CuS5O7 photocathodes in H2 evolution by synchrotron radiation nanospectroscopy
Enju Sakai, Naoka Nagamura, Jingyuan Liu, Takashi Hisatomi, Taro Yamada, Kazunari Domen and Masaharu Oshima
Nanoscale Communication, 45, (2016)

Polarization dependence of resonant magneto-optical Kerr effect measured by twotypes of figure-8 undulators
Y.Kubota, Sh.Yamamoto, T.Someya, Y.Hirata, K.Takubo, M.Araki, M.Fujisawa, K.Yamamoto, Y.Yokoyama, M.Taguchi, S.Yamamoto, M.Tsunoda, H.Wadati, A.Shin, I.Matsuda
Journal of Electron Spectroscopy and Related Phenomena (2016)

時間分解軟 X 線光電子分光法：半導体表面における光励起キャリアの実時間観測
山本　達、松田　巌
表面科学 37，　　1, 9-13, (2016)

Light and SEM observation of opal phytoliths in the mulberry leaf
O. Tsutsui, R. Sakamoto, M. Obayashi, S. Yamakawa, T. Handa, D. Nishio-Hamane and I. Matsuda, Flora, 218, 44-50 (2016)

オペランド軟 X 線発光分光によるリチウムイオン電池の研究

朝倉大輔、細野英司、原田慈久　表面科学, 37, 2, 66-71 (2016)

Material/element-dependent fluorescence-yield modes on soft X-ray absorption spectroscopy of cathode materials for Li-ion batteries
D.Asakura, E.Hosono, Y.Nanba, H.Zhou, J.Okabayashi, C.Ban, P.A.Glans, J.Guo, T.Misokawa, G.Chen, A.J.Achkar, D.G.Hawthron, T.Z.Regier, H.Wadati
AIP Advences, 6, 35105 (2016)

新型スピントロニクスと悪魔の階段
和達大樹
パリティ, 31, 5, 48-51 (2016)

In situ hard x-ray photoelectron study of O2 and H2O Adsorption on Pt Nanoparticles
Y.Cui, Y.Harada, E.Ikenaga, R.Li, N.Nakamura, T.Hatanaka, M.Ando, T.Yoshida, G.L.Li, M.Oshima
The Journal of Physical Chemistry C, 120, 10936-10940 (2016)

Direct evidence of metallic bands in a monolayer boron sheet
Baojie Feng, Jin Zhang, Ro-Ya Liu, Takushi Iimori, Chao Lian, Hui Li, Lan Chen, Kehui Wu, Sheng Meng, Fumio Komori, and Iwao Matsuda
Physical Review B, Rapid Communications, 94, 041408 (2016)

Asymmetric structure of germanene on an Al(111) surface studied by total-reflection high-energy positron diffraction
Y.Fukaya, I.Matsuda, B.Feng, I.Mochizuki, T.Hyodo, S.Shamoto
2D Materials, 3, 3, 035019 (2016)

Proving Nontrivial Topology of Pure Bismuth by Quantum Confinement
S.Ito, BJ.Feng, M.Arita, A.Takayama, RY.Liu, T.Someya, WC.Chen, T.Iimori, H.Namatame, M.Taniguchi, CM.Cheng, SJ.Tang, F.Komori, K.Kobayashi, TC.Chiang, I.Matsuda
Phys.Rev.Lett, 117, 236402 (2016)

Resonant Soft X-Ray Scattering Studies of Transition-Metal Oxides
Hiroki Wadati
Springer Tracts in Modern Physics 269, 159-196 (2017)

---E-labo---
High-resolution three-dimensional spin- and angle-resolved photoelectron spectrometer using vacuum ultraviolet laser light
Koichiro Yaji, Ayumi Harasawa, Kenta Kuroda, Sogen Toyohisa, Mitsuhiro Nakayama, Yukiaki Ishida, Akiko Fukushima1 Shuntaro Watanabe, Chuangtian Chen, Fumio Komori and Shik Shin
Rev. Sci. Instrum. 87, 053111 (2016)

One-dimensional metallic surface states of Pt-induced atomic nanowires on Ge(0 0 1)
Koichiro Yaji, Sunghun Kim, Izumi Mochizuki, Yasuo Takeichi, Yoshiyuki Ohtsubo, Patrick Le Fèvre, François Bertran, Amina Taleb-Ibrahimi, Shik Shin and Fumio Komori
J. Phys.: Condens. Matter 28, 274001 (2016)

Coherent control over three-dimensional spin polarization for the spin-orbit coupled surface state of Bi 2 Se 3
Kenta Kuroda, Koichiro Yaji, M. Nakayama, A. Harasawa, Y. Ishida, S. Watanabe, C.-T. Chen, T. Kondo, F. Komori, and S. Shin
Phys. Rev. B 94, 195134 （2016）

Spin texture in type-II Weyl semimetal WTe 2
Baojie Feng, Yang-Hao Chan, Ya Feng, Ro-Ya Liu, Mei-Yin Chou, Kenta Kuroda, Koichiro Yaji, Ayumi Harasawa, Paolo Moras, Alexei Barinov, Walid Malaeb, Cédric Bareille, Takeshi Kondo, Shik Shin, Fumio Komori, Tai-Chang Chiang, Youguo Shi, and Iwao Matsuda
Phys. Rev. B 94, 165162 （2016）

Direct mapping of spin and orbital entangled wave functions under interband spin-orbit coupling of giant Rashba spin-split surface states
Ryo Noguchi, Kenta Kuroda, K. Yaji, K. Kobayashi, M. Sakano, A. Harasawa, Takeshi Kondo, F. Komori, and S. Shin
Phys. Rev. B 95, 041111(R) (2017)

Topologically Entangled Rashba-Split Shockley States on the Surface of Grey Arsenic
Peng Zhang, J.-Z. Ma, Y. Ishida, L.-X. Zhao, Q.-N. Xu, B.-Q. Lv, K. Yaji, G.-F. Chen, H.-M. Weng, X. Dai, Z. Fang, X.-Q. Chen, L. Fu, T. Qian, H. Ding, and S. Shin
Phys. Rev. Lett. 118, 046802 (2017)

Spin-dependent quantum interference in photoemission process from spin-orbit coupled states

Koichiro Yaji, Kenta Kuroda, Sogen Toyohisa, Ayumi Harasawa, Yukiaki Ishida, Shuntaro Watanabe, Chuangtian Chen, Katsuyoshi Kobayashi, Fumio Komori & Shik Shin
Nature Communications 8, 14588 (2017)

Observation of spin-polarized bands and domain-dependent Fermi arcs in polar Weyl semimetal MoTe2
M. Sakano, M. S. Bahramy, H. Tsuji, I. Araya, K. Ikeura, H. Sakai, S. Ishiwata, K. Yaji, K. Kuroda, A. Harasawa, S. Shin, and K. Ishizaka
Phys. Rev. B 95, 121101(R) (2017)